Accepted Manuscript

Petroleum Geoscience

Combined geophysical and tectono-stratigraphic models to characterise Jurassic syn-rift petroleum systems in the Shushan Basin, northern Egypt

Ahmed I. Albrkawy & Tiago M. Alves

DOI: https://doi.org/10.1144/petgeo2024-095

To access the most recent version of this article, please click the DOI URL in the line above. When citing this article please include the above DOI.

This article is part of the Geoscience driving the North Africa and Eastern Mediterranean Energy Hub collection available at: https://www.lyellcollection.org/topic/collections/east-mediterranean

Received 20 November 2024
Revised 17 October 2025
Accepted 1 December 2025

Supplementary material at https://doi.org/10.6084/m9.figshare.c.8187067

Combined geophysical and tectono-stratigraphic models to characterise Jurassic syn-rift petroleum systems in the Shushan Basin, northern Egypt

Ahmed I. Albrkawy[a,b], Tiago M. Alves[a]

a: 3D Seismic Lab, School of Earth and Environmental Sciences, Cardiff University, Main Building, Park Place, Cardiff, CF10 3AT, United Kingdom.

b: Geology Department, Faculty of Science, Suez Canal University, Egypt.

Abstract

Northern Egypt and its Western Desert region are hydrocarbon provinces recording important Mesozoic extension. Yet, Jurassic and older syn-rift strata are still poorly characterised in these two areas, and particularly so in the onshore Shushan Basin. This work uses seismic-reflection data tied to borehole and geochemical data to investigate three (3) main Jurassic syn-rift seismic and depositional megasequences in the Shushan Basin: i) a Lower Jurassic retrogressive megasequence, ii) a Middle Jurassic prograding megasequence, and iii) an Upper Jurassic retrogressive megasequence. These megasequences, defined for the first time in this work, accompanied Late Triassic-Early Cretaceous tectonic extension, with deposition occurring in proximal environments such as rivers, lakes and deltas. Terrigenous organic matter was preserved over long periods of time in such environments, within clay-rich source intervals, as confirmed via organic geochemical analyses. Significantly, the presence of kerogen of Types II and III, and a total organic content of up to 3.91%, suggest good hydrocarbon source-rock potential in specific Jurassic intervals. One-dimensional burial models suggest that, with sufficient burial, these source intervals generated oil and

gas with a recorded maximum yield in the Early Miocene. As a corollary, this work indicates that conventional and unconventional hydrocarbon exploration targets exist in the Shushan Basin. Results show Middle Jurassic shale-rich intervals to be prime tight-gas targets, while Upper Jurassic carbonate units are promising conventional reservoirs in both the central and southern parts of the basin. The high formation temperatures recorded show that geothermal options are also feasible for deep wells, expanding the economic importance of northern Egypt.

Keywords: SE Mediterranean region; Shushan Basin; seismic attributes; rock-eval pyrolysis; reservoir modelling; depositional megasequences.

1. Introduction

The Shushan Basin is located in the Western Desert of northern Egypt, approximately 150 km south of the Mediterranean coast (**Fig. 1**). It developed as a series of Late-Palaeozoic-Early Mesozoic horsts and grabens that were part of a broader SE Mediterranean domain, itself shaped by the opening of the Mesozoic Tethys Ocean and subsequent tectonic inversion (Mansour et al., 2020; Yousef et al., 2023). Regional tectonic models indicate that continental rifting in northern Egypt began in the Late Palaeozoic and continued episodically through the Mesozoic, prior to the closure of the eastern Tethys Ocean near the Syrian Arc system (Schlumberger, 1984; Youssef, 2003; Barrier, 2014; Ghalayini, 2018). A better knowledge of the Jurassic syn-rift stratigraphy in the Shushan Basin is thus important to characterise the hydrocarbon and geoenergy potentials of North Africa (El Nady, 2013; Hassan et al., 2022; Mousa et al., 2024). It will also improve our knowledge on the syn-rift tectonic episodes affecting the southern part of the Tethys Ocean, namely how Mesozoic sedimentary basins developed in this region, and when syn-rift tectonic movements were initiated (Mansour et al., 2021; Hassan et al., 2023).

The Sushan Basin lies within a prolific hydrocarbon-producing province of northern Egypt, yet exploration has only targeted Cretaceous plays, historically. Jurassic strata in this region remain poorly studied when compared to the Cretaceous and Paleogene intervals. Significant discoveries such as the Obaiyed Field in 1994, a major gas condensate accumulation, have nevertheless highlighted the petroleum potential of Jurassic strata in the Western Desert (Strating et al., 2005; Dolson et al., 2001). Exploration wells have confirmed the existence of viable Jurassic petroleum systems across the region, particularly in hydrocarbon source intervals that extend into similar syn-rift basins such the Matruh Basin to the north of the study area (**Fig. 1**). Thermal maturity models indicate that these source intervals entered the oil window by the Late Cretaceous, and led to the generation of both oil and gas (Cheng, 2020; Attiya et al., 2023, El-Shorbagy et al., 2023). Recently, El Dally et al. (2023) applied 3D basin and petroleum-system modelling to the Shushan Basin to demonstrate that the Mid-Jurassic Khatatba Formation reached the oil window by the Turonian (Late Cretaceous), suggesting substantial gas potential in deeper Jurassic intervals. While El Dally et al. (2023) study was solely focused on basin-scale models of source-rock maturity, the present work provides new tectono-stratigraphic evidence that refines the depositional framework of the Shushan Basin, highlighting reservoir-source relationships within Jurassic successions. Importantly, by shifting the focus of exploration campaigns to deeper reservoirs and unconventional targets, this work opens up new opportunities for the production of gas as a transitional fuel, and geothermal heat as a renewable source of energy (Hakimi et al., 2023; Zaher et al, 2018; Elmasry et al., 2023).

This work delves into the thus far poorly studied Jurassic strata of the Shushan Basin by using multiple data sets and approaches. Located c. 150 km to the south of northern Egypt's coast, the Shushan Basin was first developed as a series of Late Palaeozoic-Early Mesozoic horsts and grabens, which controlled its depositional history (**Fig. 1**). This work addresses the geological, petrophysical, geochemical, and mechanical characters of syn-rift Jurassic strata in this basin. It ends by concluding on the Shushan Basin's ability to produce and store hydrocarbons in particular stratigraphic intervals. In summary, this work addresses three (3) main research questions:

a) What is the relationship between Jurassic depositional cycles in the Shushan Basin and their reservoir and source rock potentials?

b) What is the impact of Late Mesozoic-Early Cenozoic tectonics on the quality of Jurassic reservoirs in the region?

c) What particular syn-rift intervals are posed for future natural gas and geothermal energy production?

New seismic reflection profiles from the Shushan Basin delineate key structural trends and thickness variations. Geochemical analyses identify potential source rock intervals, assess kerogen type using hydrogen index (HI) and oxygen index (OI), and evaluate maturity by using T_{max} and vitrinite reflectance. Petrophysical logs allow for facies recognition, porosity trends, and indirect reservoir quality assessment. Basin modeling provides estimates of burial history, temperature evolution, and hydrocarbon generation timing.

2. Geological setting

The evolution of the Eastern Mediterranean region documents multiple rifting episodes associated with the progressive opening of the Mesozoic Tethys Ocean. Magmatic anomalies recognised by Granot (2016) in putative oceanic crust offshore Egypt led to the Neotethys Ocean being considered as forming contemporaneously with the amalgamation of the Pangaea Supercontinent in the latest Palaeozoic-Triassic. Later, Segev et al. (2018) integrated geological and geophysical data to suggest that the Levant Basin formed approximately 100 Myr later, during the Cretaceous. Its opening was triggered by the ‘Levant-Nubia' mantle plume that induced responsible for a sequence of wide-spread ocean island basalt volcanism in eastern Egypt, Lebanon, and southwest Syria (Segev et al., 2025). Based on these and other authors, one should therefore assume that the Eastern Mediterranean experienced two key rift phases: one that led to the opening of the Herodotus basin (in the Palaeozoic or Triassic), and one that resulted in the opening of the Levant

basin (Cretaceous). This broader tectonic evolution provides the regional context for the development of the northern Egypt and its associated rift basins, including the Shushan Basin.

At the regional scale of analysis, northern Egypt is part of the Afro-Arabian shield, which is itself divided into five (5) distinct structural zones (**Fig. 1**). These zones are, from south to north: i) the Craton or Nubian-Arabian Shield with Precambrian rocks outcropping near Egypt's southern border, ii) the Stable Zone (or Shelf) recording mild tectonic deformation and filled by thin Mesozoic fluvial strata (Schlumberger, 1984; Said, 2017), iii) the Unstable Zone (or Shelf), in which the study area is located, characterised by Palaeozoic to Cenozoic strata that are up to 6,300 m thick (Schlumberger, 1984; Keeley, 1989; Abdelazeem et al., 2021), and iv) an Hinge Zone extending along the northern coastline of Egypt, responsible for important Cenozoic tectonic subsidence and gravity sliding in the Nile Delta (Tassy et al., 2015). The Nile Delta Cone comprises thick Pliocene-Holocene strata, including slope-channel systems that were developed over a steep Hinge Zone (Keeley, 1994; Dolson et al., 2005).

Three (3) main extensional episodes controlled the development of the northern Egyptian basins from the Carboniferous to the Early Cretaceous (Keeley, 1989; Stampfli et al. 2001; Garfunkel 2004; Bosworth et al. 2008, Elkhodary and Youssef, 2013; Bakheit et al, 2014). These phases produced a series of syn-rift depocentres that were first shortened and mildly uplifted in the Late Cretaceous, as part of the Syrian Arc system, and later during Miocene rifting of the Red Sea. Such a mild tectonic inversion is documented by the reactivation and folding of older syn-rift structures in the Shushan, Matruh, and Natrun basins, amongst others (El-Shazly et al., 1966; Halsey and Gardener, 1975; Kuss et al., 2000; Wescott et al., 2011; Moustafa, 2013; Ibraheem et al., 2018; Gaber, 2022). Syrian Arc tectonics started in the Late Cretaceous and lasted until the Early Eocene (EGPC, 1992; Sarhan and Basal, 2020; Elhossainy et al., 2022; Albrkawy et al., 2025).

In more detail, the published literature stresses the existence of three (3) main Mesozoic hydrocarbon source intervals in northern Egypt, which are described below.

2.1 Middle Jurassic source rocks - Khatatba Formation

Jurassic strata in the northern Western Desert can exceed 1,500 m in some areas and comprise, in the Shushan Basin, three (3) main stratigraphic units (**Fig. 2**). The oldest unit, the Lower Jurassic Ras Qattara Formation is composed of coarse-to fine-grained clastics. The Khatatba Formation (Middle Jurassic) comprises fine- to coarse-grained fluvial and deltaic deposits. The Masajid Formation (Upper Jurassic) is a predominant carbonate interval but interfingers with shales through most of the Western Desert (Schlumberger, 1984; Albrkawy et al., 2025) (**Fig. 2**).

The Khatatba Formation (Middle Jurassic) is the main hydrocarbon source rock of northern Egypt. In the Shushan Basin, it is sub-divided into four (4) members which, from top to bottom, are named the Zahra, Upper Safa, Kabrit, and Lower Safa members (**Fig. 2**). Both the Lower and Upper Safa members contain intervals of organic-rich, marine black shales, i.e. excellent source intervals accumulated in low-oxygen environments (Peters and Cassa, 1994; Temraz, 2005). Previous work has shown that these intervals are dominated by kerogen of Types II and III, indicating a mixed marine and continental origin with oil-prone characteristics, as also confirmed by Rock-Eval pyrolysis and biomarker analysis (El Nady et al., 2015; Masoud, 2016). Furthermore, vitrine reflectance values (Ro%) range between 0.7 to 1.2%, suggesting that the Khatatba source intervals have reached early to peak oil window maturity in most of the Shushan Basin (Fagelnour et al., 2019). Accordingly, the Khatatba Formation has a high potential for unconventional discoveries of shale gas and tight gas (Younes, 2005; El Diasty, 2015; El Nady et al., 2015 & 2016; Masoud, 2016; Fagelnour et al., 2019).

2.2 Lower Cretaceous source rocks - Alam El-Bueib Formation

Berriasian to Lower Aptian strata are known as the Alam El-Bueib (or Shushan) Formation. They consist of shale, clays, sandstone, and limestone (Ramadan et al., 2016; Makled and Shazly, 2023) (**Fig. 2**). The Alam El-Bueib Formation reaches a maximum thickness of 900 m in the study area, and is related to the last phase of continental rifting in northern Egypt (Bosworth et al., 2008;

Moustafa, 2008; Shehata et al., 2018; Albrkawy et al., 2025). Shale intervals in the Alam El-Bueib Formation contain average TOC values of 2.40 wt.%, making it a good source interval (Alsharhan and Abd El-Gawad 2008) (**Fig. 2**).

2.3 Upper Cretaceous source rocks - Abu Roash-G Member

The Abu Roash Group (Turonian to Cenomanian) comprises seven (7) distinct sub-units, members A-G, in the nearby Abu Gharadiq Basin, where it reaches a maximum thickness of 1,000 m (Khalek et al., 1989). The lower member of this group is known as the Abyad Formation (Abu Roash-G) and comprises carbonates and fine-grained strata (**Fig. 2**). This interval records TOC values between 1.10 and 1.50 wt.%, making it a fair source interval in northern Egypt (Younes, 2012). In contrast, members A and B were completely eroded in the Shushan Basin during Syrian Arc tectonics.

3. Data and Methods

3.1 Seismic data and adopted interpretation workflow

This work uses seismic-reflection profiles covering approximately 450 km² of the Shushan Basin, complemented by wireline, core, and geochemical data from five (5) exploration wells (**Fig. 3**). The seismic data consists of two-way time (twt) post-stack migrated seismic profiles acquired as a 3D seismic cube by Khalda Petroleum Company in 2015 using an onshore acquisition system with geophones arranged in a regular grid to record ground motion. The vertical resolution of Jurassic strata at the depth of interest to this study is 25-40 m, for a frequency bandwidth of 30-45 Hz. Seismic data are sampled at 4 ms intervals, 1501 samples per trace, for a maximum two-way time (twt) depth of 6.0 s. In this work, the seismic data are displayed using the European polarity convention of the Society of Exploration Geophysicists (SEG) whereby positive (red) reflections correspond to a downward increase in acoustic impedance.

All processed seismic data were imported into Petrel® 2023 for seismic interpretation. Check-shot and velocity (V_p) data from wells Amoun-NE-01X and Shams-15, and formation tops taken from five (5) exploratory wells, were then tied to the seismic profiles (**Figs. 3 and 4**). While the gross thicknesses of the mapped Jurassic intervals are expressed in meters in this work, it is important to note that the available velocity data terminate near the top of the Ras Qattara Formation (Lower Jurassic), i.e., sonic logs and check-shot data do not extend into lowermost Jurassic and Triassic strata. To address this limitation, we applied interval velocities derived from the synthetic seismogram modelling of well Amoun NE-ST01X, which contains the most complete wireline logs, whenever necessary (**Fig. 4**). These interval velocities were calibrated against the available check-shot data to ensure consistency and were subsequently used to refine our time-depth conversions. Such an approach improves the accuracy of thickness estimation and structural mapping in the deeper Jurassic successions.

Seismic attribute maps were compiled in this work to aid the interpretation of depositional facies in the study area, at the same time quantifying changes in the internal seismic characters of key stratigraphic intervals (Chopra and Marfurt, 2005). In particular, Root-Mean Square (RMS) amplitude was used to predict lithology, past depositional environments, and hydrocarbon-drilling targets (Taner et. al., 1994; Ajisafe and Ako, 2013). Facies variations were also correlated with petrophysical properties such as porosity and fluid content. This study applied a short window Hilbert transform (three-sample window) to compute RMS amplitude maps and profiles, thus obtaining a high-resolution measure of reflection strength for each stratigraphic interval.

The 3D structural model published in Albrkawy et al. (2025) was used to define the regional structural setting controlling the syn-rift deposition in the Shushan Basin. Adding to this, a new structural model specifically for Middle and Upper Jurassic strata was built using novel stratigraphic information and the formation tops provided by exploration wells. This new structural model became the basis for new 3D facies and petrophysical models concerning the Khatatba Formation (Middle

Jurassic), the most important Jurassic source intervals in the Shushan Basin (see **Supplementary File**).

3.2 Borehole stratigraphic and wireline data

Wireline data obtained from three (3) exploration wells (Amoun-02, Amoun-NE-01X, and Amoun-NE-02) were used to characterise main depositional facies in the Khatatba (Middle Jurassic) and Masajid (Upper Jurassic) Formations (**Fig. 2**). Wireline data of interest to this work comprise gamma-ray (GR), deep resistivity (LLD), shallow resistivity (LLS), bulk density (RHOB), neutron porosity (NPHI), caliper (CALI), photoelectric factor (PEF), formation micro image (FMI), temperature (T), pressure (P), and dipole sonic logs. These logs allowed for the computation of key petrophysical data for Jurassic strata in the Shushan Basin. Neutron-Density (NPHI-RHOB) cross-plots were completed to quantify (and identify) sandstone, siltstone and shale trends in Jurassic syn-rift units that were sampled by the three exploration wells, complementing our seismic attribute and lithological analysis.

Kerogen maturation is a progressive process controlled by temperature and time, impacting the generation of hydrocarbons (Waples, 1994). Therefore, source rock evaluation requires determining vitrinite reflectance (Ro%) as an essential indicator for thermal maturity and the timing(s) of hydrocarbon expulsion (Xianming et al., 2000; Ujii et al., 2004; Hackleyet al., 2020). Vitrinite reflectance (Ro%) data from wells Amoun-NE-01X and Amoun-NE-2 for two of the stratigraphic intervals in the Khatatba Formation (Middle Jurassic), the Upper and the Lower Safa members, were provided by Khalda Petroleum Company, with inherent limitations regarding sample preparation and measurement equipment utilised (**Table 2**). Only a limited number of point measurements were taken per sample, and the reported Ro% values represent mean vitrinite reflectance (**Supplementary File**).

Biochemical analyses provide information on the origin of hydrocarbons based on S1, S2 and TOC estimated from Rock Eval pyrolysis (Kerimov et al., 2017; Hamdy et al., 2021). In this study,

TOC values were not used in isolation to assess source rock quality. Instead, a multi-parameter geochemical approach was adopted by integrating TOC, S1+S2 yields, hydrogen index (HI), T_{max}, and vitrinite reflectance (Ro%). This comprehensive framework allowed for a more robust classification of source potential and thermal maturity, particularly within the Upper Safa member. Typically, native hydrocarbons tend to reflect measurements of S2>S1 and migration indexes (S1/TOC) lower than 1.5. Migrated hydrocarbons show S1>S2 and a S1/TOC higher than 1.5, according to Abrams et al. (2017) and Hamdy et al. (2021).

In a final step, burial and thermal history curves were computed using PetroMod® software by specifically applying the Sweeney and Burnham (1990) vitrinite reflectance model to estimate discrete thermal inputs related to the tectonic phases affecting northern Egypt (**Table 1**). Such a basin modelling approach aimed at predicting the timing of hydrocarbon generation in Jurassic source intervals. Model calibration was achieved by matching calculated Ro% profiles with measured Ro% data and present-day temperature records (**Supplementary File**).

3.3 Geochemical data

Geochemical data were used to delineate Jurassic source intervals in the study area. In detail, core samples from the Upper Safa member (Middle Jurassic) and the Ras Qattara Formation (Lower Jurassic) obtained from well Amoun-NE-01X provided biochemical proxies for Jurassic strata in the Shushan Basin (**Tables 3 and 4**). Rock-Eval pyrolysis data helped to calculate key information such as:

i) Hydrogen index (HI), estimated as S2/TOC and representing the quantity of hydrogen content in organic matter,

ii) Oxygen index (OI), calculated as S3/TOC and representing the quantity of oxygen content in organic matter, and

iii) Production index (PI), defined as S1/(S1+S2) and providing a measure of the hydrocarbon potential in a rock unit (Petersen, 2017; Osli et al., 2018; Vega-Ortiz et al., 2020) (**Tables 3 and 4**). The Rock-Eval pyrolysis and TOC data in this study were provided by Khalda Petroleum Company.

Oil from the Upper and Lower Safa members (Middle Jurassic) sampled from well Amoun-NE-01X were fractionated into saturated, aromatic, and asphaltene compounds (**Table 5**). These oil fractionation data, also obtained from Khalda Petroleum Company, were plotted on the ternary diagram of Peters et al. (2005) and Tissot and Welte (2013) to identify oil types in the study area.

3.4. Porosity models for Jurassic reservoirs

GR and FMI logs acquired in well Amoun-NE-01X were used to investigate porosity types, fluid content and bedding architecture in Upper Jurassic strata. Sonic monopole log data were also used in this work. This method involves measuring the vertical compressional sonic wave (DT_p) along a borehole and is typically used to determine rock properties such as porosity, lithology, and fluid content. Moreover, it can be used to calibrate velocity data derived from check-shot and vertical seismic profiles (VSP) for seismic time-depth conversions (Redaelli et al., 2019) (**Supplementary File**).

Finally, data from Reservoir Description Tool (RDT) tests were analysed for the Lower Safa member at well Amoun-NE-01X as shown in **Supplementary File** and **Tables 6 and 7**. Typically, the results of this test are controlled by the internal character of the drilled rock units, the degree of fracture opening, and the amount of perpendicular stress measured by the RDT tool for any generated fractures (Ma et al., 2017; Wanniarachchi et al., 2018; Bagherzadeh et al., 2021; Trinh et al., 2023).

4. Results

4.1 Seismic interpretation

Seismic interpretation is complemented in this work by detailed attribute analyses and accurate ties to borehole stratigraphic information. The full workflow adopted in this work is shown in **Fig. 5**.

4.1.1 Jurassic seismic stratigraphy and associated syn-rift structures

Seismic horizons were first tied to the formation tops of five (5) exploration wells (**Figs. 6 and 7**). Relevant formation tops include the top Ras Qattara Formation (Lower Jurassic), top Lower Safa member (Middle Jurassic), top Kabrit member (Middle Jurassic), top Upper Safa member (Middle Jurassic), top Zahra member (Middle Jurassic), and top Masajid Formation (Upper Jurassic) (**Figs. 4, 6, and 7**). Hence, exploration wells only reach the upper part of the Lower Jurassic Ras-Qattara Formation in the study area (**Fig. 4**).

Jurassic strata are up to 0.65 s thick (1,300 m) and comprise three (3) main seismic units that correlate with the Ras Qattara, Khatatba and Masajid Formations (**Fig. 6**). The first of these seismic units, corresponding to the Lower Jurassic Ras-Qattara Formation, shows irregular, low-amplitude, and low-frequency internal reflections (**Fig. 6**). It marks the accumulation of coarse-grained clastic sediments throughout the Shushan Basin (Shalaby et al., 2011). The Middle Jurassic Khatatba Formation is a high amplitude interval in seismic data and reveals continuous internal reflections with a maximum thickness of 0.25 s, or 537 m (**Fig. 6**). Internal seismic reflections are associated with alternating shale and sandstone packages, which are common in the Khatatba Formation (Gentzis et al., 2018).

Stratigraphically, the Masajid Formation represents the uppermost Jurassic interval in the Northwest Desert (**Fig. 6**). It is characterised by its moderate to low-amplitude, sub-parallel reflections (**Figs. 6 and 7**). Low-frequency reflections, roughly 0.05 s or 104 m thick, reflect gradual changes in depositional environment, i.e. alternating marine carbonates (oolitic, reefal and dolomitic

limestone) and shales (MA, 1982; Schlumberger, 1984; Dolson et al., 2001; Bakr, 2009; Abdelazeem et al., 2021). The top of the Masajid Formation coincides with an erosional unconformity of regional expression marking a phase of renewed extensional faulting in the Shushan Basin (**Fig. 6**). It relates to continental rifting along the North African continental margin. Such as regional unconformity, dated at the Jurassic-Cretaceous boundary, is recorded all along the SE Mediterranean province, from Lebanon to Libya, and also in southern Europe and Turkey (Schlumberger, 1984; Bosellini and Morsilli, 1997; Tlig, 2015; Vincent et al., 2018; Maksoud et al., 2020; Yousef et al., 2023).

Figures 8 and 9 show two-way-time structural maps for the Jurassic units above. In the study area, tectonic faults range from minor structures that are only a few 100s of meters long, to major normal faults exceeding 10 km (**Figs. 8 and 9**). Four (4) main fault trends, representing the general structural framework of northern Egypt, were interpreted and named the Red Sea (NW-SE), the Aqaba (NNE-SSW), the Tethyan (E-W), and the Syrian Arc (ENE-WSW) trends in Albrkawy et al. (2025) (**Figs. 8 and 9**). The Tethyan (E-W) and Red Sea (NW-SE) trends are predominant in the study area, each comprising 10 faults. Fault displacement along these structures varies from 0.04 to over 0.35 s twt (approximately 80 to 700 m), with the largest throws observed on NW-striking faults in the northern part of the basin. The time-structural maps also show multiple E-W horst and grabens that deepen towards the north (**Figs. 8 and 9**). In contrast, gentle uplift and folding occurs towards the eastern sector of the study area (**Fig. 6c**).

Isochron maps were computed in **Figs. 10 and 11** for the Ras-Qattara (Lower Jurassic), Khatatba (Middle Jurassic), and Masajid (Upper Jurassic) formations to highlight any thickness variations. The Ras Qattara isochron map reveals stratal growth against faults, confirming the importance of Early Jurassic extension in the Shushan Basin. This same extensional pulse is confirmed by borehole correlations across the study area (**Fig. 12**).

Isochron data record an increase in the thickness of Middle Jurassic strata (Khatatba Formation) towards the north (**Fig. 10b**). In parallel, the Khatatba Formation shows significant erosional truncation at its top, with onlapping reflectors occurring above this unit (**Figs. 6 and 7**), Downlapping

reflections occur near its base (**Figs. 6 and 7**). Such downlapping and onlapping terminations, together with the thickness changes recorded in the Khatatba Formation, point out to the development of a prograding sediment wedge in the northern part of the study area. Such an event is interpreted to reflect a gradual regression in sea level during the Middle Jurassic (**Fig. 10b**).

Upper Jurassic strata in the Masajid Formation reveal minor changes in thickness (**Figs. 11 and 12**). The Masajid Formation comprises marine strata over the whole of the Western Desert, thus marking an important transgression maximum.

4.1.2 Seismic attribute analysis

Cenozoic strata record RMS amplitudes greater than 25,000 dB due to sharp increases in acoustic impedance (see red colours in **Fig. 13**). High RMS amplitude strata are often wavy and poorly continuous when in the presence of carbonate intervals such as the Marmarica (Miocene dolomite) and the Mokattam (Paleocene chalk) formations (**Fig. 13**). In contrast, fine- to coarse-grained clastics with no hydrocarbons have RMS amplitudes below 5,000 dB (see blue colours in **Fig. 13**).

High RMS amplitude values in Mesozoic strata are correlated in this work with the presence of saturated carbonate reservoirs and organic-rich shales. This is particularly the case for the Lower Safa (Middle Jurassic clastics) and Kabrit (Middle Jurassic limestone) members. The Masajid Formation (Upper Jurassic limestone) also records high RMS amplitudes (**Fig. 13**). In contrast, coarse-grained strata have relatively low RMS amplitudes, e.g. the Ras Qattara Formation (Lower Jurassic), Upper Alam El-Bueib members (Barremian to Lower Aptian), Kharita Formation (Albian), and Abu Roash C, D, and F members (Turonian) (see blue colours in **Fig. 13**).

4.2 Lithostratigraphic analysis

4.2.1 Petrophysical facies and reservoir characterisation

The upper part of the Ras Qattara Formation was barely drilled but still recognised as comprising thin fine- to coarse-grained clastics (**Figs. 12, 14 and 15a**). Depositional facies recognition for this unit is primarily based on GR and NPHI-RHOB signatures, with the shale interval present at its top suggesting a phase of marine transgression at the end of the Early Jurassic (**Fig. 12**).

The lower part of the Khatatba Formation (Middle Jurassic) correlates with the Lower Safa member and its alternating high and low GR and V_{sh}% readings (**Fig. 12**). This member plots around the sand trend line and shale zone in NPHI-RHOB cross-plots (**Fig. 15b**). It contains good source intervals, as recognised by the significant shale cross-overs on NPHI-RHOB logs (**Fig. 12**). Shale intervals reveal moderate to high deep-resistivity (LLD) readings where the temperature log records 300ºF (148ºC) (**Fig. 12**). Variations in LLD are interpreted to indicate a mixture of fine and coarse-grained intervals with hydrocarbon generating potential.

The Kabrit member, which is also part of the Khatatba Formation, is a limestone interval characterised by its very low GR and V_{sh} % readings and a Photo-Electric Factor (PEF) exceeding 3.14 b/e (**Fig. 12**). NPHI-RHOB cross-plots consequently reveal a distribution of points near the limestone trend line (**Fig. 15c**). The Kabrit member shows high LLD readings, hinting at its excellent reservoir properties (**Fig. 12**). These reservoir properties are inferred from log responses in the absence of core samples.

The Upper Safa member is the thickest sub-unit in the Khatatba Formation, at c. 300 m (**Fig. 14**). This member is composed of alternating cycles of high-to-low GR and V_{sh}%, suggesting the presence of interfingering fine- and coarse-grained clastics (**Figs. 12 and 15d**). High-GR intervals show PEF readings exceeding 5.08 b/e, which correlate with the presence of shale intervals. Low PEF values of less than 1.81 b/e that correlate with low GR and V_{sh}% indicate the presence of sand (**Fig.**

12). Some of the clean sands in the Upper Safa member have high LLD values due to the presence of hydrocarbons in its interior (**Fig. 12**). NPHI-RHOB cross-overs, when combined with high LLD readings, indicate that changes in porosity and formation fluid derive from heterogeneities at reservoir scale.

The Zahra member shows alternating moderate to low GR and V_{sh} % readings, occurring together with intervals with high LLD and PEF, the latter of which are greater than 5.08 b/e (Fig. 11). The NPHI-RHOB cross-plot returns three (3) data clusters between the sandstone trend and the siltstone and shale corners, a character also confirmed by the NPHI-RHOB cross-overs (**Figs. 12 and 15e**). Therefore, the Zahra member comprises medium to coarse sandy intervals that are partly saturated with hydrocarbons. Although lithological information is limited for this member, these petrophysical trends support a degree of heterogeneity in such reservoir intervals.

The Masajid Formation (Upper Jurassic) records low GR and V_{sh}% readings despite the existence of spurious moderate to high values in well Amoun-NE-01X (**Fig. 12**). NPHI-RHOB cross-overs suggest the presence of shale-free zones in its interior (**Fig. 15f**). Low values are also recognised in PEF data; they vary between 3.14 b/e to 5.08 b/e, confirming that the Masajid Formation is mostly composed of carbonates (**Fig. 14**). Cross-plots of NPHI against RHOB denote a concentration of points near the limestone trend, with only a few points near the shale corner (**Fig. 15**). The Masajid Formation also shows high LLD in some intervals. When integrated with supporting petrophysical indicators such as low GR and shale volume values, NPHI-RHOB cross-over behavior, and carbonate lithology from PEF, these high LLD values are interpreted to reflect intervals of shaley limestone partially saturated with hydrocarbons (**Fig. 12**). More importantly, petrophysical analysis reveals differing log facies that can be correlated across the study area, supporting reservoir characterisation in the absence of core validation.

4.2.2 Depositional facies inversion

After completing our seismic and wireline interpretations, the RMS amplitude values computed for the study area were correlated with four (4) pseudo-wells so as to identify lithological changes through the Jurassic units of interest (**Figs. 4 and 13**). Our reverse model of depositional facies shows that carbonate intervals - such as those in the Masajid Formation and Kabrit member – record low to moderate RMS amplitudes between 2,000 and 3,000 (**Fig. 13**). These values are observed even if hydrocarbon-saturated zones occur in their interior, as these are specifically revealed by RMS amplitude readings in excess of 25,000 (**Fig. 13**). Fine-grained clastics with hydrocarbons also show high RMS amplitude readings (≥ 25,000) and markedly contrast with lean coarse-grained sediments recording low RMS amplitude values (≤ 5,000) (**Fig. 15a**).

The RMS amplitude analysis in **Fig. 13** confirms that the Masajid Formation (Upper Jurassic) is dominated by limestone interbedded with thin shales. In contrast, the Zahra member (Middle Jurassic) forms a mix of coarse-grained sediments and patchy siltstone beds. The Upper Safa member (Middle Jurassic) is composed of interfingering shales (potential source intervals), siltstones and sandstones (**Fig. 13**). The Kabrit member (Middle Jurassic) is a limestone with a high hydrocarbon saturation, representing an excellent reservoir in the study area (**Fig. 13**). The fine shales of the Lower Safa member (Middle Jurassic) are very distinctive, reflecting high RMS amplitude readings that are often related to the presence of source intervals (**Fig. 13**). The Ras Qattara Formation (Lower Jurassic) is composed of medium to coarse-grained clastics interbedded with shale in the thin interval drilled in the study area.

4.3 Geochemical character of source rocks

4.3.1 Biogeochemical analysis

The Upper Safa member records TOC values from 1.55 to 3.91 wt.% making it a good source rock (**Table 3**). In contrast, samples from the top of the Ras Qattara Formation (Lower Jurassic) have a low TOC varying from 0.09 to 0.14, indicating its poor character as a source rock (**Table 4**). Once again for the Upper Safa member, source potential (S1+S2) ranges from 1.33 to 3.27 mg $_{HC}/g_{rock}$, while its productivity index S1/(S1+S2) varies from 0.042 to 0.075, confirming the presence of excellent source rocks.

Shales in the uppermost Ras Qattara Formation (Lower Jurassic) reveal a low source potential (S1+S2) ranging from 0.10 to 0.11 mg $_{HC}/g_{rock}$, and a high productivity index (S1/(S1+S2)) varying from 0.2 to 0.36.

Kerogen types in Jurassic strata were determined by plotting hydrogen index (HI) and oxygen index (OI) vs. T_{max} on the van Krevelen diagrams from Kerimov et al. (2017) and Hamdy et al. (2021) (**Fig. 16a**). In parallel, the degree of maturity of Jurassic strata was also estimated from the relationship between PI and T_{max} as shown in **Fig. 16b**. The analysis shows that the Upper Safa member (Middle Jurassic) comprises a mixture of kerogen Types II and III, both of which entered the gas window (**Fig. 16**). In turn, the Ras Qattara Formation (Lower Jurassic) contains poor source intervals with no hydrocarbon generation capacity (**Fig. 16**).

In the study area, both the Upper Safa member (Middle Jurassic) and the Ras Qattara Formation (Lower Jurassic) reveal S2>S1 and S1/TOC ratios of 4 to 42 (**Tables 3 and 4**). Plotting S1 against TOC confirms that hydrocarbons are native to the Shushan Basin and have not migrated from adjacent basins in northern Egypt (**Fig. 17**). Typically, migration index (S1/TOC) rises by increasing thermal maturity to after hydrocarbons expulsion (Smith, 1994; Garry, 2016). The increase in migration index recorded in this work confirms the presence of a heat pulse related to compressional movements

initiated in Late Cretaceous and continuing into the Miocene opening of the Red Sea (Albrkawy et al., 2025). Full biogeochemical data for the Upper Safa member (Upper Jurassic) and Ras Qattara Formation (Lower Jurassic) are summarised in **Table 8**.

4.3.2 Gas chromatography data

Gas chromatography (GC) profiles show distinct n-alkane and biomarker distributions between the Lower and Upper Safa oils, indicating vertical heterogeneity in source-rock intervals. For the Upper Safa member, GC data reveal a high volume of Methylcyclohexane (MCH) at 194,000 cpm, Cyclohexane (CH) at 125,000 cpm, n-C_4 (162,000 cpm), n-C_5 (178,000 cpm), and other light compounds (**Fig. 18**). These values are compared in **Fig. 18** with samples from the Lower Safa member with relatively higher Toluene (TOL) volumes of 138,000 cpm. Such an important contrast in TOL suggests that hydrocarbons in Jurassic strata are generated from different source intervals (Al-Ameri et al., 2016; Qin et al., 2023) (**Supplementary File**).

The full gas chromatography (GC) profile in **Fig. 19**, concerning the Upper Safa member alone, illustrates the hydrocarbon content of n-alkanes (n-C_n), pristane (Pr), and phytane (Ph). It documents for this same unit a high count for n-alkanes of low molecular weight (≤ n-C_7) compared to long-chain normal alkanes (≥ n-C_8). The profile also reveals a high pristane to phytane (Pr/Ph) ratio of 3.57, a low Pr/n-C_{17} of 0.14 and a low Ph/n-C_{18} of 0.04 for Upper Safa strata, confirming that all generated hydrocarbons resulted from a thermal maturation process (see Lotfy et al., 2024) (**Fig. 19**). The GC trace distribution also reveals a significant distribution of homohopane compounds (≥ n-C_{31}), though n-C_{31} has the highest concentration compared to other heavier homohopanes (n-C_{31} > n-C_{32} > n-C_{33} > n-C_{34} > n-C_{35}) (Fig. 23). Such a biomarker fingerprint confirms that hydrocarbons were generated in clay-rich source rocks (Gürgey, 1999).

Based on Thompson (1983), Mango (1994), and Halpern (1995), the GC profile of the Upper Safa member shows a pristane to phytane (pr/ph) fraction of more than three (3) and low distributions

of tricyclic terpanes (n-C_{19} to n-C_{23}), supporting the interpretation that terrigenous organic matter (TOM) was preserved for a long period within Jurassic source rocks (**Fig. 19**). Such a type of organic matter is the main source of the phosphorus, nitrogen and carbon recorded in our data, and is typically derived from strata accumulated in rivers, lakes, or deltaic systems that likely bordered confined marine depocentres (Carroll and Bohacs, 2001; Ogbesejana et al., 2021; Hébert, 2022; Lotfy et al., 2024) (**Fig. 19**).

Oil fractionation ratios for the Upper and Lower Safa members (Middle Jurassic) show these oil samples are highly mature normal crude oil (**Fig. 20**). Highly mature oil develops when organic matter is deeply buried and subjected to sharp increases in temperature and pressure or, instead, experiences tectonic subsidence for a long period of time (Hagemann and Hollerbach, 1986; Fan et al., 2012).

4.4 Reservoir characterisation

4.4.1 Reservoir modelling

Depositional facies models require the compilation of an accurate 3D structural model, so that stratigraphic information is placed under the correct geological context. In this study, the 3D structural framework used for facies interpretation was adopted from Albrkawy et al., (2025), which integrated fault geometry, depth-converted horizons, and well stratigraphic markers to constrain structural relationships across the Shushan Basin. The lithostratigraphic analysis in Section 5 revealed the presence of three (3) fundamental depositional facies in Middle Jurassic units (**Figs. 12 and 14**):

i) Shales, comprising impermeable strata working both as potential source intervals and caprocks,

ii) clastic intervals (sand and siltstone) forming potential reservoirs that are interbedded with shaley strata, and

iii) carbonate rocks that often form prolific reservoirs (**Fig. 12**).

The 3D facies model generated for the Khatatba Formation (Middle Jurassic) reveals an increase in shale concentration towards the north, where the main syn-rift depocentre of the Shushan Basin is located (**Fig. 21a**). These shales are overlain by prograding sands towards the top of the Khatatba Formation (Zahra member) (**Fig. 21a**). Typically, sandstone is the predominant lithology in the Khatatba Formation with its gross volume reaching 45%. Carbonate intervals in the Kabrit member comprise only 7% of the Middle Jurassic Khatatba Formation by gross volume (**Fig. 21a**).

The 3D petrophysical model in **Fig. 21b** confirms the results of our depositional facies models. The V_{sh} model shows that the highest V_{sh} occur in the middle and lower intervals of the Khatatba Formation (**Fig. 21b**). In contrast, the upper part of the Khatatba Formation shows a marked reduction in V_{sh}, highlighting a phase of sediment progradation towards the main basin depocentre, which is located in the north of the study area (**Fig. 21b**).

4.4.2 Porosity types in conventional reservoirs

Carbonate intervals in the Masajid Formation are interbedded by thin shales that are about 0.5 m thick. These shales are identified by their high relatively high electrical conductivity and moderate to high GR values (**Fig. 22**). Generally, the Masajid Formation (Upper Jurassic) is capped by a thick shale interval in the Alam El-Bueib Formation (Berriasian) allowing hydrocarbons to accumulate below the latter, i.e. within Upper Jurassic intervals (**Fig. 22**).

In our analysis, the interval between 3541 m and 3555 m was chosen to represent carbonate reservoirs in the Masajid Formation (Upper Jurassic). This interval shows two (2) main porosity types, fractures and vugs, as shown in Zones 1 and 2 (Z1 and Z2) (**Fig. 22**). In the Masajid Formation, fracture networks are parallel to sub-parallel, as shown in Dynamic Formation Micro-Imager (DFMI)

data (**Fig. 22**). These fractures reflect a moderate to high degree of resistivity in SFMI, and correlate with to very low GR readings (**Fig. 22**).

The Zahra member (Middle Jurassic) also comprises favourable reservoir intervals, namely coarse-grained clastics (sandstones) with low GR and high resistance values in Static Formation Micro-Imager, or SFMI (see Z3 and Z4; **Fig. 23a**). These sandstone intervals are interbedded with shales, which are once again recognised by their high GR and electric conductivity, making them good, local caprocks (**Fig. 23a**). The lower part of the Zahra member (Z4) show fractures that correlate with high resistivity readings, a character suggesting the presence of hydrocarbons. These zones are overlayed by thin shales, which again work as local seals (**Fig. 23a**).

FMI logs only sampled the upper interval of the Upper Safa member (**Fig. 23b**). This interval comprises alternating cycles of fine- and coarse-grained siliclastics, correlated here with cyclic high to low GR readings (**Fig. 23b**). The upper shale interval (Z5) has high electric conductivity and GR values, comprising an effective seal for underlying reservoirs in the Upper Safa member (**Fig. 23b**).

4.4.3 Unconventional pay zones

Data from sonic monopole logs used to determine the petrophysical properties of unconventional pay zones are shown in **Supplementary File**. In **Fig. 24**, five (4) promising zones (Z6 – Z10) are recognised. Z10 and Z9 from the Lower Safa Formation (Middle Jurassic) correlate with moderate to high GR readings and high resistivity readings on PFMI, representing strata with a high shale content that are saturated with hydrocarbons. These zones record a marked anisotropy between fast and slow shear-wave slowness, a character linked to the presence of pervasive, aligned sets of fractures in a likely brittle and heterogeneous formation (Fogal et al., 2002; Plona et al., 2002; Prioul et al., 2007). All in all, these data confirm the Lower Safa member as a potential shale-gas target (**Fig. 24**).

Zones Z7 and Z8 in the Lower Safa member suggest the presence of tight gas sand reservoirs (**Fig. 24**). Their high PFMI values, accompanied by their small anisotropy coefficients and GR readings, relate to a high fluid saturation, with gas present in what is a tight coarse-grained interval. In other words, the anisotropy of filled fractures is always small compared to porous coarse sediments (Shi et al., 2019). Promising intervals such as Z7 are well sealed by impermeable shales and recognised by their low anisotropy coefficients, low FMI readings, and high GR values (**Fig. 24**).

The carbonate-prone Kabrit member (Middle Jurassic) correlates with Zone Z6 and comprises limestones with very low GR readings (**Fig. 24**). Its low anisotropy coefficient suggests the presence of fractures (**Fig. 24**). The Kabrit member is capped by c. 30 m of shales that are part of the Upper Safa member.

4.4.4 Reservoir Description Tool (RDT) tests

The results of shut-in pressure tests in the Lower Safa member show that shale gas reservoirs at depths of 4,074 m, 4,073 m, 4,055 m, 4,053 m, and 4,013 m had a normal response, i.e. hydraulic fracturing operations were carried out without any significant issues (see tests 1, 2, 7, 8, and 13 in **Table 6**). In contrast, the shallowest of shale-gas reservoirs (Z9) denoted supercharged conditions in test 14, likely due to its significant fracturing at a depth of 3,983 m (**Fig. 24**).

Tight gas sands in Z8 were scrutinized in tests 16, 17, and 18 (**Fig. 24 and Table 6**). They show a variation in response between normal, tight, and supercharged conditions, indicating difficulties in fracturing the rock despite the fact that the shallower reservoir interval in Z7 responded normally in test 19 (**Fig. 24 and Table 6**). In contrast, the lower part of the Upper Safa member between 3,820 m and 3,761 m records a normal response when hydraulically fractured (**Fig. 24 and Table 7**).

In conclusion, RDT tests undertaken in Amoun-NE-01X reflect a mix of successful and unsuccessful hydraulic fracturing results for the Lower and Upper Safa members. Nevertheless, most

of shale intervals in the Jurassic strata record a good ability to be hydraulically fractured, a character that may enhance hydrocarbon production.

5. Discussion

5.1 Jurassic syn-rift megasequences

This work led to the definition of seismic megasequences in the Shushan Basin that reflect transgressive and regressive syn-rift depositional cycles (**Fig. 25**). Changes in seismic facies and isochron data reveal three major syn-rift megasequences as follows.

5.1.1 Transgressive megasequence I (Lower Jurassic)

Northern Egypt was affected by a first syn-rift episode that ended in the Early Jurassic, leading to the development of E-W-striking half grabens and horsts (Stampfli et al. 2001; Garfunkel 2004; Bosworth et al. 2008, Bakheit et al, 2014, Albrkawy et al., 2025). Consequently, the Lower Jurassic Ras Qattara Formation grew against E-W faults in the study area. These Lower Jurassic strata are composed of continental coarse-grained clastics eroded from local highs, and thin intervals of marine shales resulting from a gradual marine transgression.

The transgressive period reached its peak at the end of the Early Jurassic and provided algae-rich kerogen preserved in reducing environments to parts of northern Egypt (El Nady et al., 2016; El Atfy et al., 2023) (**Fig. 25a**). However, organic-rich facies are limited in extent and thickness in the Shushan Basin, and their source potential is therefore marginal. This suggests that, although reducing conditions may have developed locally, the Ras Qattara Formation constitutes a weak petroleum

source unit within the overall Jurassic petroleum system as evidenced by its relatively low TOC values between 0.014 and 0.09 wt.%.

5.1.2 Regressive megasequence II (Middle Jurassic)

Middle Jurassic strata are materialised by the Khatatba Formation in the western parts of northern Egypt, and are subdivided into four (4) members in the study area, from bottom to top: the Lower Safa, Kabrit, Upper Safa, and Zahra members (**Fig. 2**). These intervals form the core of the Jurassic petroleum system in the Shushan Basin, comprising key source rocks. The Mid Jurassic regressive cycle documented in this work was accompanied by major sediment influx from source areas to the south, where the Khatatba Formation developed under tidal environment conditions during a post-rift stage (**Fig. 25b**). Such a regressive cycle is documented in borehole data by prograding pulses of fine to coarse-grained strata, which filled the Shushan Basin and other basins in northern Egypt (Abdelhady and Fürsich, 2015; Leila et al., 2022; Ali, 2023). As a result, a prograding sediment wedge was deposited near the northern parts of the study area (**Fig. 25b**). Such a depositional setting provided the Shushan Basin with fine clay organic rich intervals with TOC values ranging from 1.55 to 3.91 wt.%, thus leading to the accumulation of good source intervals in the Khatatba Formation. Source intervals document a good source potential (1.33 to 3.27 mg HC /g rock), and a productivity index of up to 0.075 (**Fig. 16**).

5.1.3 Transgressive megasequence III (Upper Jurassic)

Upper Jurassic strata document a regional marine transgression in northern Egypt (Tassy et al., 2015; Ruban et al., 2019; Albrkawy et al., 2025). In the Shushan Basin, this transgression is marked by the deposition of a retrograding system of shaley marine limestones - the Masajid Formation (**Fig.**

25c). The Late Jurassic is marked by tectonic quiescence and, as a result, minor changes in strata thickness are recorded in this unit (**Fig. 11**).

The Masajid Formation constitutes the main carbonate reservoir of the Jurassic petroleum system. Despite its limited thickness, carbonate intervals with important secondary porosity are present. A low-energy carbonate ramp environment was established at this time, allowing for early diagenesis and local dolomitisation. This improved reservoir quality in some intervals. However, porosity in the Masajid Formation is highly variable and best developed in zones affected by tectonic fracturing, as evidenced by FMI and LLD responses (**Figs. 12 and 22**). The top of the Masajid Formation coincides with a basinwide unconformity that represents the end of the transgressive megasequence III, before the start of a second (Early Cretaceous) syn-rift episode affecting NE Africa (Albrkawy et al., 2025).

5.2 Conventional and unconventional reservoirs and their hydrocarbon retention

5.2.1 Conventional reservoirs

In the Shushan Basin, Lower and Middle Jurassic strata contain a series of clay-rich intervals within the Ras Qattara Formation, and Lower and Upper Safa members (**Figs. 12 and 13**). These intervals preserved terrigenous organic matter (TOM) in low energy environments such as rivers, lakes, or deltaic systems near northern Egypt's palaeo-shoreline, accumulating a mixture of kerogen Types II and III (**Fig. 16**). Above these, Upper and Middle Jurassic strata comprise good carbonate reservoirs (**Fig. 12**). The Masajid Formation is a shaley limestone in most of Egypt's Western Desert and is characterised by fracture systems that were developed during early Cretaceous extension and subsequent tectonic compression (Abdelaziz et al., 2016; Farrag et al., 2022; Albrkawy et al., 2025) (**Fig. 22**). In the study area, the Upper Jurassic Masajid Formation is 106 m thick, on average, and shows significant hydrocarbon saturation. Petrophysical data from the Masajid Formation shows PEF

values ranging between 3.14 and 5.08 b/e, while LLD values are elevated in intervals interpreted as hydrocarbon-bearing. NPHI-RHOB cross-overs indicate the presence of shale-free carbonate facies with localised hydrocarbon saturation (**Figs. 12 and 15**). This fractured carbonate interval is sealed by a significant thickness of shales at the base of the Alam El-Bueib Formation (Berriasian to Lower Aptian). Therefore, Upper Jurassic strata in the Masajid Formation is considered as one of most promising reservoirs in the Shushan Basin.

The Kabrit member (Middle Jurassic) comprises thin limestone intervals varying in thickness between 11 and 18 m (**Figs. 12 and 13d**). It is identified by its very low GR and V_{sh}% values, high LLD responses, and PEF values exceeding 3.14 b/e (**Fig. 12**). NPHI-RHOB cross-overs show a clean carbonate trending close to limestone line, pointing out to a potential conventional reservoir (**Fig. 15c**). In addition, reservoir intervals contain significant fracture systems that were developed over three phases of tectonic movements, from Late Cretaceous to the Miocene (**Fig. 24**). The Kabrit member was likely charged with hydrocarbon from source intervals in the Lower Safa member as confirmed by chromatographic data from oil samples in the Lower and Upper Safa members. These data confirm that hydrocarbons were locally generated as native fluids from two different source intervals (**Figs. 16 and 17**).

5.3.2 Unconventional reservoirs

The Zhara, Upper Safa and Lower Safa members comprise clastic intervals considered in this work as productive tight gas reservoirs (**Figs. 12, 23 and 24**). The Zahra member records a moderate to low GR (< 75 API), moderate V_{sh}% (< 45%) values, a high PEF (> 5.08 b/e) and significant LLD anomalies, correlating with heterolithic sands and silts that are partly saturated with hydrocarbons (**Fig. 12**). Both the Upper Safa and Lower Safa members contain clean sand intervals with low PEF (<1.81 b/e) and high LLD readings, while interbedded shales record high GR values (>100 API),

highlighting their competence as vertical seals (**Fig. 12**). Clastic intervals are locally charged from shales in the Upper and Lower Safa members, and denote significant electric resistance on LLD logs, confirming the presence of hydrocarbon in their interior (**Fig. 12**). Such a character stresses how important is the upper part of the Khatatba Formation (Middle Jurassic) as an unconventional reservoir in northern Egypt (see Farag, 2010; Abdel-Fattah, 2015; Kassab et al., 2020; El-Ghandour et al., 2023).

Shale intervals in the Lower and Upper Safa members of the Khatatba Formation, the main hydrocarbon source intervals in the Shushan Basin, comprise good shale-gas targets, showing developed fracture systems (**Fig. 24**). Most of the Khatatba Formation's tight gas sands and shale gas intervals reveal a good degree of stability to be hydraulically fractured, increasing hydrocarbon recovery.

Based on 3D facies and volume of shale (V_{sh}%) models described in Section 4.1, we show in **Fig. 26** a selected cross-section across the study area that highlights unconventional exploration 'hotspots' in the study area. The cross-section reveals high (V_{sh}%) in its northern part where fine-grained sediments are predominant. This zone is ideal for shale gas exploration where unconventional reservoirs in the Khatatba Formation record formation temperatures of about 160 ºC, allowing kerogens to support local hydrocarbon generation (**Fig. 26**). In contrast, conventional reservoirs in the Masajid and Khatatba Formations are seemingly favourable only in the central and southern parts of the study area. These regions record low V_{sh}% readings and comprise coarse-grained and carbonate strata, lithologies that enhance the vertical and horizontal migration of hydrocarbons allowing for their trapping in horsts and smaller structural highs (**Fig. 26**).

5.3 Thermal and burial histories: Implications for hydrocarbon generation and geothermal potential

One-dimensional (1D) burial models show that Jurassic strata in the Shushan basin experienced two major subsidence phases: an Early Jurassic-Cretaceous rifting event, followed by a later heat

pulse during the Cenozoic (see Bosworth et al., 2008; Moustafa, 2008; Shehata et al., 2018; Albrkawy et al., 2025). Vitrinite reflectance (R_o%) values range between 0.65 and 1.08%, suggesting that Mid Jurassic source intervals in the Khatatba Formation entered the late oil to early gas window (**Figs. 27 and 28; Table 2**). Hydrocarbon generation peaked in the Early to Middle Miocene, coinciding with the opening of the Red Sea (Sarhan and Basal, 2020; Elhossainy et al., 2022). Such a peak in hydrocarbon generation is confirmed by maturity levels (R_o) above > 1.0 and high T_{max} values above 440 ºC from Rock-Eval Pyrolysis tests. The Khatatba Formation is therefore confirmed as the main Jurassic hydrocarbon source rock in the Shushan Basin, having generated hydrocarbons that migrated into adjacent Kabrit and Masajid reservoir intervals. It forms a self-contained petroleum system.

The temperature of Jurassic strata exceeds 150 ºC in pseudo-well 2, where the main Jurassic depocentre is located (**Fig. 28a**). In contrast, the basin shoulder area to the south records temperatures of about 140 ºC in pseudo-well 3 (**Fig. 28b**), dropping to 110 ºC in the center of the study area, over the horst structure where well Amoun-NE-02 was drilled (**Fig. 27b**). These modelled values are consistent with the bottom-hole temperatures from the available exploration wells, which range between 105ºC and 140ºC for the Jurassic succession; elevated heat flow values occur in depocentre areas but are lower over structural highs. Such temperature variations are critical in understanding source-rock maturity, as they confirm that the Upper Safa member has reached peak gas generation conditions in the deepest parts of the Shushan Basin.

Correlation panels for thermal conductivity and formation temperature estimated on PetroMod® show that Jurassic strata have a relatively constant thermal conductivity of about 1.4 W/m/k (**Fig. 29**). This also means that the Middle Jurassic Khatatba Formation overlies porous, siliciclastic Early Mesozoic and Palaeozoic successions with a high thermal conductivity, allowing for heat transfer from basement and magmatic rocks (**Fig. 29**). Kerogen maturation analyses show a Ro% between 1 to 1.08 for the Lower Safa member, while the Upper Safa member records a Ro% that varies from 0.65 to 0.81 (**Table 2**).

Based on the maturation model developed by Sweeney and Burnham (1990), source intervals in the Khatatba Formation (Middle Jurassic) entered the late stage of oil and early stage of gas generation windows in the Late Cretaceous, reaching its hydrocarbon generation peak in the Middle Miocene (**Fig. 30**). Importantly, bottom-hole temperatures are surprisingly high in our models and may relate to the presence of geothermal reservoirs at depth, which are themselves overlain by thick Jurassic shaley successions that extend through northern Egypt (**Figs. 12, 27 and 28**). As documented in geothermal prospects across NW Europe, such as those in the Upper Rhine Graben, temperatures of 130°C-160°C are enough to justify the local production of electricity by geothermal heat when permeability in geothermal reservoirs is accompanied by fracture and fault networks. This is exactly the case of the Soultz, Landau and United Downs geothermal prospects (Vidal and Genter, 2018; Reinecker et al., 2021; Glaas et al., 2021). We therefore evoke in this paper a geothermal energy potential for some of the deeper wells drilled in northern Egypt, and justify the presence of relative high temperatures in the study area to result from: a) the existence of a relatively recent (Cenozoic) magmatic pulse of heat related to Red Sea rifting and ocean opening, and b) the high regional subsidence recorded in the study area during the Early Cretaceous, which continued through the Cenozoic without much effect from Syrian Arc tectonics (**Figs. 27 and 28**). Consequently, Cenozoic magmatic activity is considered in this work to have played a critical role in both source-rock maturation in the Egyptian Western Desert, and also in the potential discovery of new geothermal prospects in deeper Mesozoic strata.

Deposition in the Shushan Basin was mainly controlled by subsidence and eustasy. Later magmatic activity increased regional heat in northern Egypt, allowing the Jurassic source intervals to enter the oil and gas windows (**Figs. 27 and 28**). Starting from the Late Cretaceous, these late heat flow pulses helped the Jurassic kerogen to reach the peak of hydrocarbon generation, with kerogen transformation into hydrocarbons reaching 90% in the Miocene (**Fig. 30**).

6. Conclusions

This study integrates seismic-reflection, borehole and geochemical data to characterise Jurassic petroleum systems in the Shushan Basin, northern Egypt. It confirms the existence of three (3) principal Jurassic syn-rift megasequences that define the stratigraphic framework of the basin's petroleum system: i) a Lower Jurassic retrogressive megasequence I, ii) a Middle Jurassic prograding megasequence II, and iii) an Upper Jurassic retrogressive megasequence III. The main conclusions of this work are as follows:

a) Petrophysical analyses show that Middle Jurassic strata contain two main source intervals (shales); the Lower and Upper Safa members. They constitute the principal Jurassic source rock in the basin. Conventional reservoirs vary between coarse-grained clastic and carbonate intervals, notably the Kabrit and Masajid members, whereas fine clastics comprise promising unconventional targets (tight gas and shale gas).

b) Main source intervals in the Lower and Upper Safa members (Middle Jurassic), together with hydrocarbon-saturated carbonate reservoir intervals such as the Kabrit (Middle Jurassic) and Masajid (Upper Jurassic) members, are accompanied by a significant increase in RMS amplitude readings in seismic data. These amplitude responses can help discerning barren from hydrocarbon-charged intervals.

c) The Lower Jurassic Ras Qattara Formation has poor source-rock potential. In contrast, the Middle Jurassic strata record high Total Organic Carbon (TOC) readings, with kerogen of Types II and III accumulated in favourable conditions for thermal maturation. Source intervals in the Khatatba Formation (Middle Jurassic) reached the oil and gas windows in the Late Cretaceous and a peak hydrocarbon yield during the Miocene.

d) Biogeochemical data for Jurassic strata confirm that trapped hydrocarbons are native fluids that have not experienced horizontal migration from adjacent basins in northern Egypt. They are sourced and trapped locally.

e) Chromatographic analyses confirm that hydrocarbons in the Middle Jurassic strata were generated from terrigenous organic matter (TOM). They were preserved in low energy and clay-rich environments such as rivers, lakes or deltaic systems near the palaeo-shoreline of northern Egypt, favoring the preservation of organic matter.

f) Jurassic strata reveal a secondary porosity system resulting from burial and tectonic compression. These systems enhanced the quality of conventional and unconventional reservoirs in syn-rift Jurassic strata. These same strata also show a good ability for hydraulic fracturing, which may improve the efficiency of hydrocarbon extraction in the Shushan Basin.

In summary, the presence of highly mature normal crude oil in the Shushan Basin can be linked to thermal input from magmatic activity in the Late Cretaceous to Miocene, which followed significant syn-rift basin subsidence in the Early Cretaceous. Given the high formation temperatures recorded in this study, a geothermal option is also feasible for some deeper wells in northern Egypt. This potentially expands the region's economic value beyond conventional and unconventional oil and gas production.

Acknowledgements

The Egyptian Mission Sector has been recognised for its assistance in A. Albrkawy's PhD project. We would like to express our gratitude to the Egyptian General Petroleum Corporation (EGPC) and the Khalda Petroleum Company for providing data on the Amoun and Shams oil fields. Special thanks to Schlumberger for their software support in the 3D Seismic Lab at Cardiff University. We also

appreciate the editorial handling of this manuscript by Petroleum Geoscience, and the constructive comments from Dr. Paul Wilson (Deputy Editor), and reviewers Dr. Ross James Grant and Ms. Dina Hamdy, which helped improve the manuscript.

References

Abd El Halim, M. and Moussad, M., 1992. Western Desert oil and gas field's (A comprehensive overview). *EGPC, ARE, Cairo, Egypt*, pp.45-115.

Abd El-Wahed, A.G. and Anan, T.I., 2016. Detection of sedimentary structural elements using formation micro imager technique, a case study from South Mansoura-1 well, Nile Delta, Egypt. *NRIAG Journal of Astronomy and Geophysics*, *5*(2), pp.413-434. https://doi.org/10.1016/j.nrjag.2016.10.001

Abdelazeem, M., Fathy, M.S. and Gobashy, M., 2021. Magnetometric identification of sub-basins for hydrocarbon potentialities in Qattara Ridge, North Western Desert, Egypt. *Pure and Applied Geophysics*, *178*(3), pp.995-1020. https://doi.org/10.1007/s00024-021-02678-2

Abdelaziz, A., Shahin, W., Mosallam, A., El Gazzar, A., Rezk, A., Abdelfattah, M. and Moukhtar, A., 2016. Challenges and characterization of newly targeted upper Jurassic carbonates, Agiba's Meleiha field, Western Desert, Egypt. In *13th mediterranean offshore conference and exhibition (MOC), Alex, Egypt*. https://www.researchgate.net/publication/301637201_Challenges_and_Characterization_of_Newly_Targeted_Upper_Jurassic_Carbonates_Agiba%27s_Meleiha_Field_Western_Desert_Egypt?enrichId=rgreq-20d5b919a5ca4c0e5dcc13b65284d52e

Abdel-Fattah, M.I., 2015. Impact of depositional environment on petrophysical reservoir characteristics in Obaiyed Field, Western Desert, Egypt. *Arabian Journal of Geosciences*, *8*, pp.9301-9314. https://doi.org/10.1007/s12517-015-1913-5

Abdelhady, A.A. and Fürsich, F.T., 2015. Sequence architecture of a Jurassic ramp succession from Gebel Maghara (North Sinai, Egypt): implications for eustasy. *Journal of Palaeogeography*, *4*(3), pp.305-330. https://www.academia.edu/download/41873631/Sequence_architecture_of_a_Jurassic_ramp20160201-30232-1q9t6lb.pdf

Abrams, M.A., Gong, C., Garnier, C. and Sephton, M.A., 2017. A new thermal extraction protocol to evaluate liquid rich unconventional oil in place and in-situ fluid chemistry. *Marine and Petroleum Geology*, *88*, pp.659-675. https://doi.org/10.1016/j.marpetgeo.2017.09.014

Ajisafe, Y.C. and Ako, B.D., 2013. 3-D seismic attributes for reservoir characterization of "Y" field Niger Delta, Nigeria. *IOSR Journal of Applied Geology and Geophysics*, *1*(2), pp.23-31.

Al-Ameri, T.K., Al-Temimi, A.K. and Zumberge, J., 2016. Assessments of oil characterization, source affinities, and hydrocarbon dynamic of East Baghdad oil fields, Central Iraq. *Marine and Petroleum Geology*, *77*, pp.353-375. https://doi.org/10.3389/feart.2022.1018712

Alberty, M., 1992. Standard interpretation: Part 4. wireline methods. https://archives.datapages.com/data/specpubs/methodo1/data/a095/a095/0001/0150/0180.htm

Albrkawy, A.I., Alves, T.M. and Blenkinsop, T., 2025. Tectono-stratigraphy of the Shushan Basin, Western Desert, Egypt: A window into the evolution of the SE Mediterranean province. *Marine and Petroleum Geology*, *177*, p.107387. https://doi.org/10.1016/j.marpetgeo.2025.107387

Alsharhan, A.S. and Abd El-Gawad, E.A., 2008. Geochemical characterization of potential Jurassic/Cretaceous source rocks in the Shushan Basin, northern Western Desert, Egypt. *Journal of Petroleum Geology*, *31*(2), pp.191-212. https://doi.org/10.1111/j.1747-5457.2008.00416.x

Atlas, D., 1982. *Well logging and interpretation techniques: The course for home study*.

Attiya, A.S., Kassab, M.A., Salem, T.M. and Abbas, A.E., 2023. Source rock evaluation and burial history modeling of the Middle Jurassic Khatatba Formation in the West Kanayes Concession of Matruh Basin, North Western Desert, Egypt. *Egyptian Journal of Chemistry*, *66*(4), pp.71-85. https://doi.org/10.21608/ejchem.2022.132957.5874

Bakheit, A.A., Abdel Aal, G.Z., El-Haddad, A.E. and Ibrahim, M.A., 2014. Subsurface tectonic pattern and basement topography as interpreted from aeromagnetic data to the south of El-Dakhla

Oasis, western desert, Egypt. *Arabian Journal of Geosciences*, *7*, pp.2165-2178. https://doi.org/10.1007/s12517-013-0896-3

Barrier, E., Machhour, L. and Blaizot, M., 2014. Petroleum systems of Syria.Bostick, N.H. and Daws, T.A., 1994. Relationships between data from Rock-Eval pyrolysis and proximate, ultimate, petrographic, and physical analyses of 142 diverse US coal samples. *Organic Geochemistry*, *21*(1), pp.35-49. https://doi.org/10.1016/0146-6380(94)90086-8

Bosworth, W., El-Hawat, A.S., Helgeson, D.E. and Burke, K., 2008. Cyrenaican "shock absorber" and associated inversion strain shadow in the collision zone of northeast Africa. *Geology*, *36*(9), pp.695-698. https://doi.org/10.1130/G24909A.1

Carrie, J., Sanei, H. and Stern, G., 2012. Standardisation of Rock–Eval pyrolysis for the analysis of recent sediments and soils. *Organic Geochemistry*, *46*, pp.38-53. https://doi.org/10.1016/j.orggeochem.2012.01.011

Carroll, A.R. and Bohacs, K.M., 2001. Lake-type controls on petroleum source rock potential in nonmarine basins. *AAPG bulletin*, *85*(6), pp.1033-1053. https://doi.org/10.1306/8626CA5F-173B-11D7-8645000102C1865D

Cheng, J.E., 2020. Petroleum system of Shoushan Basin, Western Desert, Egypt. *Acta Sci. Malay*, *4*(1), pp.1-8. DOI: 10.26480/gbr.01.2020.01.08

Chopra, S. and Marfurt, K.J., 2005. Seismic attributes—A historical perspective. *Geophysics*, *70*(5), pp.3SO-28SO. https://doi.org/10.1190/1.2098670

Chopra, S. and Marfurt, K.J., 2008. Emerging and future trends in seismic attributes. *The Leading Edge*, *27*(3), pp.298-318. https://doi.org/10.1190/1.2896620

Delvaux, D., Martin, H., Leplat, P. and Paulet, J., 1990. Comparative Rock-Eval pyrolysis as an improved tool for sedimentary organic matter analysis. *Organic Geochemistry*, *16*(4-6), pp.1221-1229. https://doi.org/10.1016/0146-6380(90)90157-U

Demirbas, A., Acar, S., Horasan, B.Y. and Alalayah, W.M., 2018. Analysis of petroleum coke from low grade oily sludge of refinery. *Petroleum Science and Technology*, *36*(12), pp.904-909. https://doi.org/10.1080/10916466.2018.1451890

Desert, E.W., 1992. Oil and Gas Fields (A Comprehensive Overview). In *EGPC 11th Petroleum Exploration and Production Conference* (Vol. 431).

Diab, A.I. and Khalil, H.M., 2021. Quantitative assessment of the tight gas reservoirs in the Obaiyed field, Shushan Basin, NW Egypt. *NRIAG Journal of Astronomy and Geophysics*, *10*(1), pp.320-332. https://doi.org/10.1080/20909977.2021.1929745

Dolson, J.C., Boucher, P.J., Siok, J. and Heppard, P.D., 2005. Key challenges to realizing full potential in an emerging giant gas province: Nile Delta/Mediterranean offshore, deep water, Egypt. https://doi.org/10.1144/0060607

Dolson, J.C., Shann, M.V., Matbouly, S., Harwood, C., Rashed, R. and Hammouda, H., 2001. The petroleum potential of Egypt. https://doi.org/10.1306/M74775C23

Dresser Atlas. Bagherzadeh, P., Goshtasbi, K. and Kazemzadeh, E., 2021. Stress-dependence of the permeability, porosity, and compressibility of fractured carbonate rock. *Journal of Porous Media*, *24*(5). Volume 24, Issue 5, 2021, pp. 21-45. https://doi.org/10.1615/JPorMedia.2021027701

EIA/ARI, World Shale Gas and Shale Oil Resource Assessment - Technically Recoverable Shale Gas and Shale Oil Resources: An Assessment of 137 Shale Formations in 41 Countries Outside the United States, iunie 2013.

El Atfy, H., Ghassal, B.I. and Littke, R., 2023. Petroleum source rocks of Egypt: an integrated spatio-temporal palynological and organic geochemical studies within the phanerozoic. In *The Phanerozoic Geology and Natural Resources of Egypt* (pp. 649-674). Cham: Springer International Publishing. https://doi.org/10.1007/978-3-030-95637-0_23

El Dally, N. H., Youssef, M. S., Abdel Aal, M. H., Ismail, A., & Metwalli, F. I. (2023). 3D basin and petroleum systems modeling in Shushan Basin, Western Desert, Egypt. *Modeling Earth Systems and Environment*, *9*(2), 2221-2238. https://doi.org/10.1007/s40808-022-01559-4

El Diasty, W.S., 2015. Khatatba Formation as an active source rock for hydrocarbons in the northeast Abu Gharadig Basin, north Western Desert, Egypt. *Arabian Journal of Geosciences*, *8*, pp.1903-1920. https://doi.org/10.1007/s12517-014-1334-x

El Nady, M.M., 2013. Geothermal history of hydrocarbon generation of wells in the North Western Desert, Egypt. *Energy Sources, Part A: Recovery, Utilization, and Environmental Effects*, *35*(5), pp.401-412. https://doi.org/10.1080/15567036.2010.513276

El Nady, M.M., 2016. Source rock potentiality of middle Jurassic–lower cretaceous of wells, North Western Desert, Egypt. *Energy Sources, Part A: Recovery, Utilization, and Environmental Effects*, *38*(11), pp.1635-1642. https://doi.org/10.1080/15567036.2012.662267

El Nady, M.M., Awad, S.A. and Sharaf, L.M., 2015. Source rock evaluation of selected wells in the North Western Desert, Egypt. *Energy Sources, Part A: Recovery, Utilization, and Environmental Effects*, *37*(20), pp.2151-2162. https://doi.org/10.1080/15567036.2011.608324

El Nady, M.M., Ramadan, F.S., Eysa, E.A. and Said, N.M., 2016. The potentiality of hydrocarbon generation of the Jurassic source rocks in Salam-3x well, North Western Desert, Egypt. *Egyptian Journal of Petroleum*, *25*(1), pp.97-105. https://doi.org/10.1016/j.ejpe.2015.03.007

El Zefzaf, T., El Fattah, M.A., Proett, M.A., Engelman, B. and Bassiouny, A., 2006, September. Formation Testing and Sampling Using an Oval Pad in Al Hamd Field, Egypt. In *SPE Annual Technical Conference and Exhibition?* (pp. SPE-102366). SPE. https://doi.org/10.2118/102366-MS

El-Ghandour, M.M., Abdeldayem, A.L., Soliman, A. and Abu Shady, A., 2023. Reservoir Characterisation of the Jurassic Safa Formation, Shoushan Basin, North Western Desert,

Egypt. *Delta Journal of Science*, *46*(3), pp.144-158. https://doi.org/10.21608/djs.2023.198323.1085

Elhossainy, M.M., El-Shafeiy, M., Al-Areeq, N.M. and Hamdy, D., 2022. Petroleum generation modelling of the Middle-Late Cretaceous sediments in the Abu Gharadig Field, Northwestern Desert, Egypt. *Geological Journal*, *57*(9), pp.3851-3880. https://doi.org/10.1002/gj.4519

Elkhodary, S.T. and Youssef, M.A.S., 2013. Integrated potential field study on the subsurface structural characterization of the area North Bahariya Oasis, Western Desert, Egypt. *Arabian Journal of Geosciences*, *6*, pp.3185-3200. https://doi.org/10.1007/s12517-012-0590-x

El-Shazly, E.M., 1966. Structural development of Egypt. In *14th Annual Meeting, Geological Society of Egypt, Grio* (pp. 31-38).

El-Shorbagy, A.I., Mousa, D.A. and Zein El-Din, M.Y., 2023. Source rock evaluation of Jurassic rock units for Imhotep field, Matruh basin, Western Desert, Egypt. *Egyptian Journal of Geology*, *67*(1), pp.123-134. https://doi.org/10.21608/egjg.2023.200603.1041

Emujakporue, G.O. and Enyenihi, E.E., 2020. Identification of seismic attributes for hydrocarbon prospecting of Akos field, Niger Delta, Nigeria. *SN Applied Sciences*, *2*, pp.1-11. https://doi.org/10.1007/s42452-020-2570-1

Fagelnour, M., Gamil, I., El Toukhy, M., Gharieb, A. and Saad, H., 2019, March. Source rock potentiality, basin modeling, and oil to source correlation in Northern Shushan Basin, Western Desert, Egypt. In *Offshore Mediterranean conference and exhibition* (pp. OMC-2019). OMC. https://doi.org/omc-2019-0876

Fan, Z.Q., Jin, Z.H. and Johnson, S.E., 2012. Gas-driven subcritical crack propagation during the conversion of oil to gas. *Petroleum Geoscience*, *18*(2), pp.191-199. https://doi.org/10.1144/1354-079311-030

Farag, M.I.A.F.I., 2010. Geophysical Reservoir Evaluation of Obaiyed Field, Western Desert, Egypt. https://doi.org/10.14279/depositonce-2626

Farouk, S. and Khalifa, M.A., 2010. Facies tracts and sequence development of the Middle Eocene–Middle Miocene successions of the southwestern Qattara Depression, northern Western Desert, Egypt. *Palaontol Stratigraphie Fazies*, *18*(C536), pp.195-215. https://www.researchgate.net/publication/285678628

Farrag, G., Abd-Allah, A., Bakr, A., Hassan, Z. and El-Shahawy, S., 2022. Hydrocarbon potentiality of the jurassic-lower cretaceous sequence in Abu Sennan area, Abu Gharadig Basin, Egypt. *Arabian Journal of Geosciences*, *15*(17), p.1423. https://doi.org/10.1007/s12517-022-10660-y

Fogal, J., Kessler, C. and Varsamis, G., 2002, September. Application of shear anisotropy from a new generation crossed dipole acoustic tool. In *SPE Annual Technical Conference and Exhibition?* (pp. SPE-77792). SPE. https://doi.org/10.2118/77792-MS

Gaber, G.M., 2022. Evaluation of Sedimentary Basins For Hydrocarbon Exploration Using Aeromagnetic Data, Northwestern Sinai Peninsula, Egypt. https://doi.org/10.21203/rs.3.rs-1910620/v1

Garfunkel, Z., 2004. Origin of the Eastern Mediterranean basin: a reevaluation. *Tectonophysics*, *391*(1-4), pp.11-34. https://doi.org/10.1016/j.tecto.2004.07.006

Garry, P., Atta-Peters, D. and Achaegakwo, C., 2016. source-rock Potential of the Lower Cretaceous sediments in SD-1X well, Ooffshore Tano Basin, South Western Ghana. *Petroleum & Coal*, *58*(4). https://www.vurup.sk/wp-content/uploads/dlm_uploads/2017/07/pc_1_2016_peters_450.pdf

Ghalayini, R., Nader, F.H., Bou Daher, S., Hawie, N. and Chbat, W.E., 2018. Petroleum systems of Lebanon: An update and review. *Journal of Petroleum Geology*, *41*(2), pp.189-214. https://doi.org/10.1111/jpg.12700

Glaas, C., Patrier, P., Vidal, J., Beaufort, D. and Genter, A., 2021. Clay Mineralogy: a signature of granitic geothermal reservoirs of the Central Upper Rhine Graben. *Minerals*, *11*(5), p.479. https://doi.org/10.3390/min11050479

Granot, R., 2016. Palaeozoic oceanic crust preserved beneath the eastern Mediterranean. *Nature Geoscience*, *9*(9), pp.701-705. https://doi.org/10.1038/ngeo2784

Gürgey, K., 1999. Geochemical characteristics and thermal maturity of oils from the Thrace Basin (western Turkey) and western Turkmenistan. *Journal of Petroleum Geology*, *22*(2), pp.167-189. https://doi.org/10.1111/j.1747-5457.1999.tb00466.x

Hackley, P.C., Araujo, C.V., Borrego, A.G., Bouzinos, A., Cardott, B.J., Carvajal-Ortiz, H., Cely, M.R.L., Chabalala, V., Crosdale, P.J., Demchuk, T.D. and Eble, C.F., 2020. Testing reproducibility of vitrinite and solid bitumen reflectance measurements in North American unconventional source-rock reservoir petroleum systems. *Marine and Petroleum Geology*, *114*, p.104172. https://doi.org/10.1016/j.marpetgeo.2019.104172

Hagemann, H.W. and Hollerbach, A., 1986. The fluorescence behaviour of crude oils with respect to their thermal maturation and degradation. *Organic Geochemistry*, *10*(1-3), pp.473-480. https://doi.org/10.1016/0146-6380(86)90047-1

Hakimi, M.H. and Al-Sufi, S.A., 2018. Organic geochemistry investigations of crude oils from Bayoot oilfield in the Masila Basin, east Yemen and their implication for origin of organic matter and source-related type. *Egyptian Journal of Petroleum*, *27*(1), pp.37-54. https://doi.org/10.1016/j.ejpe.2017.01.001

Halpern, H. I. (1995). Development and applications of light-hydrocarbon-based star diagrams. *AAPG Bulletin*, *79*(6), 801-815. https://doi.org/10.1306/8D2B1BB0-171E-11D7-8645000102C1865D

Halsey, J.H. and Gardner, W.C., 1975. Tectonic analysis of Egypt using Earth Satellite data. *Lecture given to Egyptian Petrol Geol Cairo GPC*.

Hamdy, D., El-Bakry, G., El Habaak, G.H. and El-Shafeiy, M., 2021. Characteristics and generation modeling of some source rocks in the South Eastern offshore Mediterranean area, Egypt. *Marine and Petroleum Geology*, *123*, p.104719. https://doi.org/10.1016/j.marpetgeo.2020.104719

Handhal, A.M., Al-Shahwan, M.F. and Chafeet, H.A., 2020. Applications of biomarker and geochemical characterization of crude oil for Mesopotamian basin, Southern Iraq. *Modeling Earth Systems and Environment*, *6*, pp.215-233. https://doi.org/10.1007/s40808-019-00673-0

Hassan, S., Tahoun, S., Darwish, M., Bosworth, W. and Radwan, A.E., 2023. The Albian–Cenomanian boundary on the southern Tethyan margin: Abu Gharadig Basin, Northern Western Desert, Egypt. *Marine and Petroleum Geology*, *154*, p.106334. https://doi.org/10.1016/j.marpetgeo.2023.106334

Hayashi, K. and Sakurai, I., 1989, December. Interpretation of hydraulic fracturing shut-in curves for tectonic stress measurements. In *International Journal of Rock Mechanics and Mining Sciences & Geomechanics Abstracts* (Vol. 26, No. 6, pp. 477-482). Pergamon. https://doi.org/10.1016/0148-9062(89)91424-1

Hébert, A.J., Flamand, A. and Chaillou, G., 2022. Origins and transformations of terrigenous dissolved organic matter in a transgressive coastal system. *Estuarine, Coastal and Shelf Science*, *279*, p.108137. https://doi.org/10.1016/j.ecss.2022.108137

Hillman, E.A., 2023. *Integrating full-bore formation micro-imager (FMI) data for Niobrara Reservoir characterization, Postle area, Wattenberg Field, Colorado, USA*. Colorado School of Mines. https://cardiff.idm.oclc.org/login?url=https://www.proquest.com/dissertations-theses/integrating-full-bore-formation-micro-imager-fmi/docview/2895612958/se-2?accountid=9883

Hunt, J. M. (1995). Petroleum geochemistry and geology (textbook). Petroleum Geochemistry and Geology (Textbook), 2nd ed.; WH Freeman Company: New York, NY, USA.

Ibraheem, I.M., Elawadi, E.A. and El-Qady, G.M., 2018. Structural interpretation of aeromagnetic data for the Wadi El Natrun area, northwestern desert, Egypt. Journal of African Earth Sciences, 139, pp.14-25. https://doi.org/10.1016/j.jafrearsci.2017.11.036

Karimi, S., 2015. *Integrated characterisation of mud-rich overburden sediment sequences using limited log and seismic data: Application to seal risk* (Doctoral dissertation, Durham University). http://etheses.dur.ac.uk/11285/

Kassab, M.A., Abbas, A. and Ghanima, A., 2020. Petrophysical evaluation of clastic Upper Safa Member using well logging and core data in the Obaiyed field in the Western Desert of Egypt. *Egyptian Journal of Petroleum*, *29*(2), pp.141-153. https://doi.org/10.1016/j.ejpe.2020.01.001

Keeley, M.L. and Wallis, R.J., 1991. The Jurassic System in northern Egypt: II. Depositional and tectonic regimes. *Journal of Petroleum Geology*, *14*(1), pp.49-64. https://doi.org/10.1111/j.1747-5457.1991.tb00298.x

Keeley, M.L., 1989. The Palaeozoic history of the western desert of Egypt. *Basin Research*, *2*(1), pp.35-48. https://doi.org/10.1111/j.1365-2117.1989.tb00025.x

Keeley, M.L., 1994. Phanerozoic evolution of the basins of Northern Egypt and adjacent areas. *Geologische Rundschau*, *83*(4), pp.728-742. https://doi.org/10.1007/BF00251071

Kerimov, V.Y., Lapidus, A.L., Yandarbiev, N.S., Movsumzade, E.M. and Mustaev, R.N., 2017. Physicochemical properties of shale strata in the Maikop series of Ciscaucasia. *Solid Fuel Chemistry*, *51*, pp.122-130. https://doi.org/10.3103/S0361521917020057

Khalek, M.A., El Sharkawi, M.A., Darwish, M., Hagras, M. and Sehim, A., 1989. Structural history of Abu Roash district, Western Desert, Egypt. *Journal of African Earth Sciences (and the Middle East)*, *9*(3-4), pp.435-443. https://doi.org/10.1016/0899-5362(89)90027-4

Krupp, E.M., Johnson, C., Rechsteiner, C., Moir, M., Leong, D. and Feldmann, J., 2007. Investigation into the determination of trimethyl arsine in natural gas and its partitioning into gas and condensate phases using (cryotrapping)/gas chromatography coupled to inductively coupled plasma mass spectrometry and liquid/solid sorption techniques. *Spectrochimica Acta Part B: Atomic Spectroscopy*, *62*(9), pp.970-977. https://doi.org/10.1016/j.sab.2007.07.009

Kuss, J., Scheibner, C. and Gietl, R., 2000. Carbonate platform to basin transition along an upper Cretaceous to lower Tertiary Syrian arc uplift, Galala Plateaus, Eastern Desert of Egypt. *GeoArabia*, *5*(3), pp.405-424. https://doi.org/10.2113/geoarabia0503405

Lee, M.Y. and Haimson, B.C., 1989, December. Statistical evaluation of hydraulic fracturing stress measurement parameters. In *International Journal of Rock Mechanics and Mining Sciences & Geomechanics Abstracts* (Vol. 26, No. 6, pp. 447-456). Pergamon. https://doi.org/10.1016/0148-9062(89)91420-4

Leila, M., Yasser, A., El Bastawesy, M. and El Mahmoudi, A., 2022. Seismic stratigraphy, sedimentary facies analysis and reservoir characteristics of the Middle Jurassic syn-rift sediments in Salam Oil Field, north Western Desert, Egypt. *Marine and Petroleum Geology*, *136*, p.105466. https://doi.org/10.1016/j.marpetgeo.2021.105466

Li, Q., Xing, H., Liu, J. and Liu, X., 2015. A review on hydraulic fracturing of unconventional reservoir. *Petroleum*, *1*(1), pp.8-15. https://doi.org/10.1016/j.petlm.2015.03.008

Liu, W., Liao, Y., Jiang, C., Pan, Y., Huang, Y., Wang, X., Wang, Y. and Peng, P.A., 2022. Superimposed secondary alteration of oil reservoirs. Part II: The characteristics of biomarkers under the superimposed influences of biodegradation and thermal alteration. *Fuel*, *307*, p.121721. https://doi.org/10.1016/j.fuel.2021.121721

Lotfy, N.M., Farouk, S., Hakimi, M.H., Ahmad, F., El Shennawy, T., El Nady, M.M., Salama, A. and Shehata, A.M., 2024. Biomarker and isotopic characteristics of Miocene condensates and natural gases, West Delta deep marine concession, Eastern Mediterranean, Egypt. *Scientific Reports*, *14*(1), p.235. https://doi.org/10.1038/s41598-023-50418-4

Ma, X. and Zoback, M.D., 2017. Lithology-controlled stress variations and pad-scale faults: A case study of hydraulic fracturing in the Woodford Shale, Oklahoma. *Geophysics*, *82*(6), pp.ID35-ID44. https://doi.org/10.1190/geo2017-0044.1

Macgregor, D.S. and Moody, R.T., 1998. Mesozoic and Cenozoic petroleum systems of North Africa. *Geological Society, London, Special Publications*, *132*(1), pp.201-216. https://doi.org/10.1144/GSL.SP.1998.132.01.12

Mahdi, T.A., Aqrawi, A.A., Horbury, A.D. and Sherwani, G.H., 2013. Sedimentological characterization of the mid-Cretaceous Mishrif reservoir in southern Mesopotamian Basin, Iraq. *GeoArabia*, *18*(1), pp.139-174. https://doi.org/10.2113/geoarabia1801139

Makled, W.A. and Shazly, T.F., 2023. Inter-basinal Cyclostratigraphic Correlation of Neocomian–Barremian Alam El Buieb Formation in the Northern Part of the Western Desert, Egypt. *Egyptian Journal of Geology*, *67*(1), pp.111-121. https://doi.org/10.21608/egjg.2023.206691.1045

Mango, F.D., 1994. The origin of light hydrocarbons in petroleum: Ring preference in the closure of carbocyclic rings. *Geochimica et Cosmochimica Acta*, *58*(2), pp.895-901. https://doi.org/10.1016/0016-7037(94)90513-4

Mansour, A. and Wagreich, M., 2025. An overview of the Cretaceous oceanic anoxic events in Egypt, southern Tethys. *Geological Society, London, Special Publications*, *545*(1), pp.SP545-2023. https://doi.org/10.1144/SP545-2023-104

Mansour, A., Gentzis, T., El Nady, M.M., Mostafa, F. and Tahoun, S.S., 2020. Hydrocarbon potential of the Albian-early Cenomanian formations (Kharita-Bahariya) in the North Western Desert,

Egypt: a review. *Journal of Petroleum Science and Engineering*, *193*, p.107440. https://doi.org/10.1016/j.petrol.2020.107440

Mansour, A., Wagreich, M., Gentzis, T., Ocubalidet, S., Tahoun, S.S. and Elewa, A.M., 2020. Depositional and organic carbon-controlled regimes during the Coniacian-Santonian event: First results from the southern Tethys (Egypt). *Marine and Petroleum Geology*, *115*, p.104285. https://doi.org/10.1016/j.marpetgeo.2020.104285

Mansour, A., Wagreich, M., Gier, S., Gentzis, T., Kloetzli, U., Tahoun, S.S. and Elewa, A.M., 2021. Climate variability and paleoceanography during the Late Cretaceous: Evidence from palynology, geochemistry and stable isotopes analyses from the southern Tethys. *Cretaceous Research*, *126*, p.104831. https://doi.org/10.1016/j.cretres.2021.104831

Masoud, A.A., Abu Shady, A.M.N., Abdeldayem, A. and El Sherief, M., 2016. Three-Dimensional Hydrocarbon Potentiality Modeling of the Source/Reservoir Rocks of the Alam El Bueib and Khatatba Formations, Shoushan Basin, North Western Desert, Egypt. *Delta Journal of Science*, *37*(2), pp.142-154. https://journals.ekb.eg/article_139932_0ac6151aaea0a9186458624ba05639d0.pdf

Meshref, W.M., 1995. Well evaluation conference of Egypt. *Schlumberger Technical Editing Services, EGPC, Egypt*, p.87.

Montadert, L., Nicolaides, S., Semb, P.H. and Lie, Ø., 2014. Petroleum systems offshore Cyprus. Moustafa, A.R., 2008. Mesozoic-Cenozoic basin evolution in the northern Western Desert of Egypt. *Geology of East Libya*, *3*, pp.29-46.

Moustafa, A.R., 2013. Fold-related faults in the Syrian Arc belt of northern Egypt. *Marine and Petroleum Geology*, *48*, pp.441-454. https://doi.org/10.1016/j.marpetgeo.2013.08.007

Nader, F.H., 2011. The petroleum prospectivity of Lebanon: an overview. *Journal of Petroleum Geology*, *34*(2), pp.135-156. https://doi.org/10.1111/j.1747-5457.2011.00498.x

Ogbesejana, A.B., Bello, O.M., Ali, T., Uduma, U.A., Kabo, K.S. and Akintade, O.O., 2021. Geochemical significance of tricyclic and tetracyclic terpanes in source rock extracts from the Offshore Niger Delta Basin, Nigeria. *Acta Geochimica*, *40*(2), pp.184-198. https://doi.org/10.1007/s11631-020-00422-6

Osli, L.N., Shalaby, M.R. and Islam, M.A., 2018. Characterization of source rocks and depositional environment, and hydrocarbon generation modelling of the Cretaceous Hoiho Formation, Great South Basin, New Zealand. *Petroleum & Coal*, *60*(2), p255-275. 22p. https://web.p.ebscohost.com/abstract?site=ehost&scope=site&jrnl=13353055&AN=130292250&h=fchHhTwoHt3jTWwQP17RJrWWRB6%2b5OAGqGTrOqkHlNmfMmgzxfDVbIBAvgXnlPM62sQMLj9XXuT7vbYpwqW0og%3d%3d&crl=c&resultLocal=ErrCrlNoResults&resultNs=Ehost&crlhashurl=login.aspx%3fdirect%3dtrue%26profile%3dehost%26scope%3dsite%26authtype%3dcrawler%26jrnl%3d13353055%26AN%3d130292250

Patterson, D. and Tang, X.M., 2001. Shear wave anisotropy measurement using cross-dipole acoustic logging: an overview. *Petrophysics-The SPWLA Journal of Formation Evaluation and Reservoir Description*, *42*(02).

Peters, K.E. and Cassa, M.R., 1994. Applied source rock geochemistry. https://doi.org/10.1306/M60585C5

Peters, K.E., Walters, C.C. and Moldowan, J.M., 2005. *The biomarker guide* (Vol. 1). Cambridge university press.

Petersen, H., 2017. Source Rocks, Types and Petroleum Potential. In *The Role of Organic Petrology in the Exploration of Conventional and Unconventional Hydrocarbon Systems: Geology: Current and Future Developments: Volume 1* (pp. 104-130). Bentham Science Publishers.

Plona, T.J., Kane, M.R., Sinha, B. and Walsh, J., 2002, October. Evaluating stress-induced anisotropy and mechanical damage from cross-dipole sonic data using dispersion analysis. In *SPE/ISRM Rock Mechanics Conference* (pp. SPE-78233). SPE. https://doi.org/10.2118/78233-MS

Prioul, R., Donald, A., Koepsell, R., Marzouki, Z.E. and Bratton, T., 2007. Forward modeling of fracture-induced sonic anisotropy using a combination of borehole image and sonic logs. *Geophysics*, *72*(4), pp.E135-E147. https://doi.org/10.1190/1.2734546

Ramadan, F.S., El Nady, M.M., Eysa, E.A. and Mahdy, S.A., 2016. Isopach, lithofacies changes, and source rocks chracteristics of Khatatba and Alam El Bueib formations of some wells in North East Western Desert, Egypt. *Petroleum Science and Technology*, *34*(23), pp.1920-1928. https://doi.org/10.1080/10916466.2016.1238931

Reda, M., Fathy, M. and Gawad, E.A., 2022. Comprehensive 3D reservoir modelling and basin analysis: an insight into petroleum geology to re-evaluate the hydrocarbon possibilities in the Siwa Basin, North-Western Desert, Egypt. *Geological Journal*, *57*(4), pp.1600-1616. https://doi.org/10.1002/gj.4362

Redaelli, M., Victor, R.A., Beneduzi, C.F. and Batista, P.D., 2019. Algorithm for processing dispersive waves from dipole sonic tool.

Reinecker, J., Gutmanis, J., Foxford, A., Cotton, L., Dalby, C. and Law, R., 2021. Geothermal exploration and reservoir modelling of the United Downs deep geothermal project, Cornwall (UK). *Geothermics*, *97*, p.102226. https://doi.org/10.1016/j.geothermics.2021.102226

Rider, M.H., 1986. The geological interpretation of well logs.

Routledge. Sarhan, M.A. and Basal, A.M.K., 2020. Total organic carbon content deduced from resistivity-porosity logs overlay: a case study of Abu Roash formation, Southwest Qarun field, Gindi Basin, Egypt. *NRIAG Journal of Astronomy and Geophysics*, *9*(1), pp.190-205. https://doi.org/10.1080/20909977.2020.1736761

Ruban, D.A., Sallam, E.S. and Wanas, H.A., 2019. Middle–Late Jurassic sedimentation and sea-level changes on the northeast African margin: A case study in the Khashm El-Galala area, NE

Egypt. *Journal of African Earth Sciences*, *156*, pp.189-202. https://doi.org/10.1016/j.jafrearsci.2019.04.008

Said, R., 2017. Cenozoic. In *The geology of Egypt* (pp. 451-486).

Scheeder, G., Weniger, P. and Blumenberg, M., 2020. Geochemical implications from direct Rock-Eval pyrolysis of petroleum. *Organic Geochemistry*, *146*, p.104051. https://doi.org/10.1016/j.orggeochem.2020.104051

Schlumberger (1984). Well evaluation conference (WEC), Egypt. Schlumberger Middle East, 201.

Segev, A., Sass, E. and Schattner, U., 2018. Age and structure of the Levant basin, Eastern Mediterranean. *Earth-Science Reviews*, *182*, pp.233-250. https://doi.org/10.1016/j.earscirev.2018.05.011

Segev, A., Sass, E. and Schattner, U., 2025. Volcano-sedimentary response to a mantle plume decay: A case study from the Eastern Mediterranean margin. *Geoscience Frontiers, 16,* 102161. https://doi.org/10.1016/j.gsf.2025.102161

Shafiabadi, M., Kamkar-Rouhani, A., Riabi, S.R.G., Kahoo, A.R. and Tokhmechi, B., 2021. Identification of reservoir fractures on FMI image logs using Canny and Sobel edge detection algorithms. *Oil & Gas Science and Technology–Revue d'IFP Energies nouvelles*, *76*, p.10. https://ogst.ifpenergiesnouvelles.fr/10.2516/ogst/2021023

Shafiezadeh, M., Ziaee, M. and Tokhmchi, B., 2015. A new approach towards precise planar feature characterization using image analysis of FMI image: case study of gachsaran oil field well no. 245, southwest of Iran.

Shehata, A.A., El Fawal, F.M., Ito, M., Abdel Aal, M.H. and Sarhan, M.A., 2018. Sequence stratigraphic evolution of the syn-rift Early Cretaceous sediments, West Beni Suef Basin, the Western Desert of Egypt with remarks on its hydrocarbon accumulations. *Arabian Journal of Geosciences*, *11*, pp.1-18. https://doi.org/10.1007/s12517-018-3688-y

Shi, W., Wang, X., Shi, Y., Feng, A., Zou, Y. and Young, S., 2019. Application of dipole array acoustic logging in the evaluation of shale gas reservoirs. *Energies*, *12*(20), p.3882. https://doi.org/10.3390/en12203882

Smith, J.T., 1994. Petroleum system logic as an exploration tool in a frontier setting. https://doi.org/10.1306/M60585C2

Stampfli, G.M., 2001. Permo-Mesozoic evolution of the western Tethyan realm: the Neo-Tethys/East-Mediterranean connection. Pre-Tethyan memoir 6: pre-Tethyanrift/wrench basins and passive margins. *Int. Geol. Correl. Prog.*, *369*, pp.51-108.

Strating, E.H.H., Amin, S., Samiee, R.A., Shanab, M.A., Ebied, M., Samaie, A.A. and Ali, N.M., 2005, June. Developing the Obaiyed Tight Gas/Condensate Field, Egypt–A Case Study. In *SPE Europec featured at EAGE Conference and Exhibition?* (pp. SPE-94106). SPE. doi: https://doi.org/10.2118/94106-MS

Sweeney, J.J. and Burnham, A.K., 1990. Evaluation of a simple model of vitrinite reflectance based on chemical kinetics. *AAPG bulletin*, *74*(10), pp.1559-1570. https://doi.org/10.1306/0C9B251F-1710-11D7-8645000102C1865D

Taner, M.T., Schuelke, J.S., O'Doherty, R. and Baysal, E., 1994. Seismic attributes revisited. In *SEG technical program expanded abstracts 1994* (pp. 1104-1106). Society of Exploration Geophysicists. https://doi.org/10.1190/1.1822709

Tang, X. and Chunduru, R.K., 1999. Simultaneous inversion of formation shear-wave anisotropy parameters from cross-dipole acoustic-array waveform data. *Geophysics*, *64*(5), pp.1502-1511. https://doi.org/10.1190/1.1444654

Tang, X.M. and Cheng, C.H.A., 2004. *Quantitative borehole acoustic methods* (Vol. 24). Elsevier.

Tassy, A., Crouzy, E., Gorini, C., Rubino, J.L., Bouroullec, J.L. and Sapin, F., 2015. Egyptian Tethyan margin in the Mesozoic: Evolution of a mixed carbonate-siliciclastic shelf edge (from Western

Desert to Sinai). *Marine and Petroleum Geology*, *68*, pp.565-581. https://doi.org/10.1016/j.marpetgeo.2015.10.011

Teama, M.A., Kassab, M.A., Cheadle, B.A., Mesbah, M.A., Mohamed, I.F. and El-Din, E.S., 2018. 3D seismic and formation micro-imager (FMI) integrated study to delineate depositional pattern of Abu Madi (Upper Miocene) clastic reservoir rocks in El-Wastani gas field, onshore Nile Delta, Egypt. *Egyptian journal of petroleum*, *27*(4), pp.747-758. https://doi.org/10.1016/j.ejpe.2017.11.003

Temraz, M.G.M.A., 2005. Mineralogical and geochemical studies of carbonaceous shale deposits from Egypt. https://doi.org/10.14279/depositonce-1173

Thompson, K.F., 1983. Classification and thermal history of petroleum based on light hydrocarbons. *Geochimica et Cosmochimica Acta*, *47*(2), pp.303-316. https://doi.org/10.1016/0016-7037(83)90143-6

Thompson, K.F.M., 1979. Light hydrocarbons in subsurface sediments. *Geochimica et Cosmochimica Acta*, *43*(5), pp.657-672. https://doi.org/10.1016/0016-7037(79)90251-5

Thompson, K.F.M., 1988. Gas-condensate migration and oil fractionation in deltaic systems. *Marine and Petroleum Geology*, *5*(3), pp.237-246. https://doi.org/10.1016/0264-8172(88)90004-9

Tissot, B.P. and Welte, D.H., 2013. *Petroleum formation and occurrence*. Springer Science & Business Media.

Trabelsi, K., Espitalié, J. and Huc, A.Y., 1994, June. Characterization of extra heavy oils and tar deposits by modified pyrolysis methods. In *European symposium on Heavy Oil Technologies in a Wider Europe, Proceedings* (pp. 30-40).

Trinh, N.Q., Hagen, S.A., Strømsvik, H., Larsen, T. and Grøv, E., 2023. Two New Methods for Defining Shut-In Pressure in Hydraulic Fracturing Tests. *Rock Mechanics and Rock Engineering*, *56*(4), pp.3055-3076. https://doi.org/10.1007/s00603-022-03212-z

Ujiie, Y., Sherwood, N., Faiz, M. and Wilkins, R.W., 2004. Thermal maturity and suppressed vitrinite reflectance for Neogene petroleum source rocks of Japan. *AAPG bulletin*, *88*(10), pp.1335-1356. https://doi.org/10.1306/05030403035

Vega-Ortiz, C., Beti, D.R., Setoyama, E., McLennan, J.D., Ring, T.A., Levey, R. and Martínez-Romero, N., 2020. Source rock evaluation in the central-western flank of the Tampico Misantla Basin, Mexico. *Journal of South American Earth Sciences*, *100*, p.102552. https://doi.org/10.1016/j.jsames.2020.102552

Vidal, J. and Genter, A., 2018. Overview of naturally permeable fractured reservoirs in the central and southern Upper Rhine Graben: Insights from geothermal wells. *Geothermics*, *74*, pp.57-73. https://doi.org/10.1016/j.geothermics.2018.02.003

Wanniarachchi, W.A.M., Ranjith, P.G., Perera, M.S.A., Rathnaweera, T.D., Zhang, D.C. and Zhang, C., 2018. Investigation of effects of fracturing fluid on hydraulic fracturing and fracture permeability of reservoir rocks: An experimental study using water and foam fracturing. *Engineering Fracture Mechanics*, *194*, pp.117-135. https://doi.org/10.1016/j.engfracmech.2018.03.009

Wescott, W.A., Atta, M., Blanchard, D.C., Cole, R.M., Georgeson, S.T., Miller, D.A., O'Hayer, W.W., Wilson, A.D., Dolson, J.C. and Sehim, A., 2011. PS Jurassic Rift Architecture in the Northeastern Western Desert, Egypt.

Xianming, X., Wilkins, R.W.T., Dehan, L., Zufa, L. and Jiamu, F., 2000. Investigation of thermal maturity of lower Palaeozoic hydrocarbon source rocks by means of vitrinite-like maceral reflectance—a Tarim Basin case study. *Organic Geochemistry*, *31*(10), pp.1041-1052. https://doi.org/10.1016/S0146-6380(00)00061-9

Younes, M.A., 2005. Petroleum geochemistry and potential source rock correlation in the Shushan Basin, north Western Desert, Egypt. *Petroleum science and technology*, *23*(5-6), pp.507-536. https://doi.org/10.1081/LFT-200031092

Younes, M.A., 2012. *Hydrocarbon potentials in the northern Western Desert of Egypt* (pp. 23-46). INTECH Open Access Publisher.

Yousef, M., Moustafa, A.R. and Bosworth, W., 2023. Structural and tectonostratigraphic evolution of Matruh Basin, northern Western Desert, Egypt: An example of an inverted rift basin. *Journal of African Earth Sciences*, *203*, p.104958. https://doi.org/10.1016/j.jafrearsci.2023.104958

Youssef, M.M., 2003. Structural setting of central and south Egypt. https://doi.org/10.2113/49.Suppl_1.1

Zhang, S., Creaser, R.A., Pell, J. and Stasiuk, V., 2014. Discovery of organic-rich black shale xenolith from kimberlite on the Hall Peninsula, Nunavut and its implication for petroleum potential in Cumberland Sound. *Bulletin of Canadian Petroleum Geology*, *62*(3), pp.125-131. https://doi.org/10.2113/gscpgbull.62.3.125

Zheng, Y., Tang, X. and Patterson, D.J., 2009, June. Identifying stress-induced anisotropy and stress direction using cross-dipole acoustic logging. In *SPWLA Annual Logging Symposium* (pp. SPWLA-2009). SPWLA.

Figure and Table captions

Fig. 1. Map of the study area showing the structural zones that compose northern Egypt together with the names and boundaries of major sedimentary basins. The map also shows isopach readings for the Khatatba Formation (Middle Jurassic). The map is modified from Schlumberger (1984), EGPC (1992), Meshref and EGPC (1995), EIA/ARI (2013) and Albrkawy et al. (2025).

Fig. 2. Stratigraphic panel for the Shushan Basin revealing lithostratigraphic units and main tectonic stages recorded in the SE Mediterranean region (modified from Schlumberger (1984) and Albrkawy et al. (2025)).

Fig. 3. Basemap of the study area showing the interpreted seismic and borehole data from the Shushan Basin. The interpreted time-domain seismic data set consists of 24 seismic profiles, striking N-S and E-W, and six (6) arbitrary lines, extracted from a 3D seismic volume. A combination of wireline data and well tops obtained from five (5) exploration wells were acquired in the Shushan Basin up to the top of the Ras Qattara Formation (Lower Jurassic). Four (4) pseudo-wells were also modelled in this work to improve the depositional facies and petrophysical modelling, as well as to compare thermal and burial curves with the exploration wells located in the center of the basin.

Fig. 4. Synthetic seismogram computed for well Amoun-01 tied to seismic arbitrary line-01 (see **Fig. 2** for location). Well-to-seismic ties are accurate for horizons such as the top Masajid Formation, Zahra member, Upper Safa member, Kabrit member, Lower Safa member, and Ras Qattara Formation. These seismic horizons are also confirmed by significant changes in interval velocity, and correlate with formation tops in well completion reports.

Fig. 5. Workflow followed in this work to analyse Jurassic syn-rift strata and their related petroleum systems in the Shushan Basin.

Fig. 6. Interpreted seismic profiles across the Shushan Basin. (a) and (b) show a series of normal faults in the central part of the study area. (c) Denotes gentle uplift and folding near reactivated normal faults located in the eastern part of the study area. The seismic profiles also show the regional dip of the basin to the north, which is accompanied by an increase in strata thickness in the same direction. A prograding sediment wedge is identified in the main depocentre within the Middle Jurassic Khatatba Formation (see zoomed-in section in **Fig. 7**).

Fig. 7. Zoomed-in sections and corresponding insets of (a) crossline 14924, and (b) crossline 15065 (**Figs. 2 and 6**). The seismic profiles reveal a series of prograding sediment wedges in the Khatatba Formation (Middle Jurassic) deposited during a major regression in sea level.

Fig. 8. TWT structural maps for (a) the top of the Ras Qattara Formation (Middle Jurassic) and (b) the top of the Khatatba Formation (Middle Jurassic). The maps reveal the Shushan Basin as dipping towards the north where a main Jurassic depocentre is located. The southern part of the study area coincides with the basin shoulder. A local low is recognised towards the east as a result of local subsidence.

Fig. 9. TWT structural map of the top of Masajid Formation (Upper Jurassic). The map reveals four (4) distinct fault trends in the study area: NW-SE, NNE-SSW, ENE-WSW, and E-W. At this time in the syn-rift development of the basin, a central horst was formed and delimited by normal faults in the middle of the study area.

Fig. 10. Isochron maps for the (a) Ras Qattara Formation (Upper Jurassic), and (b) Khatatba Formation (Middle Jurassic). The Ras Qattara Formation reveals a significant increase in strata thickness (growth) against most of faults, confirming its development during a main syn-rift stage. Growth of Lower Jurassic strata is mainly recorded at border of the central horst, where E-W (Tethyan trend) and NNE-striking (Aqaba trend) faults are observed. The Middle Jurassic Khatatba Formation shows a moderate increase in thickness towards the north, where prograding sediment wedges are detected in seismic data (see **Figs. 6 and 7**).

Fig. 11. Isochron map for the Masajid Formation (Upper Jurassic) revealing it as a relatively thin unit with minor changes in thickness. The Masajid Formation is associated with a period of tectonic quiescence in the Shushan Basin.

Fig. 12. Correlation panel for key Jurassic stratigraphic units in the Shushan Basin. The panel highlights the lateral changes in depositional facies and petrophysical properties recorded between exploration wells. Both the Upper and Lower Safa members comprise shales with potential for hydrocarbon generation, as discussed in the text based on new lithological and geochemical data. The Middle Jurassic strata shown in this panel are topped by a shaley

limestone interval (Masajid Formation) that forms a good reservoir interval in the Shushan Basin.

Fig. 13. RMS amplitude profile computed from (a) seismic arbitrary line 2, and (b) seismic arbitrary line 3, which are shown in **Fig. 2**. High RMS amplitudes (≥25,000) are recoded in the Lower Safa member (Middle Jurassic), the Alam El-Bueib Formation (Barremian-Berriasian), and the Abu Roash G member (Turonian), correlating with the main Mesozoic source intervals in northern Egypt. RMS amplitude data discriminates between key petroleum elements in the Lower Safa member (Middle Jurassic), i.e. it recognises source from reservoir intervals. The Kabrit member (Middle Jurassic) and Masajid Formation (Upper Jurassic) are also identified as carbonate reservoirs.

Fig. 14. Lithostratigraphic correlation panels for (a) reverse models interpreted in three (3) exploration wells, and (b) forward models predicting the stratigraphy of the Jurassic strata at the location of four (4) pseudo wells correlated with RMS amplitude data.

Fig. 15. Neutron porosity (NPHI) vs. bulk density (RHOB) cross-plots powered by gamma ray (GR) readings in Amoun-NE-01X well. The method shown, modified from Alberty (1992), was used to estimate the main lithofacies in the (a) Ras Qattara Formation (Lower Jurassic), (b) the Lower Safa member (Middle Jurassic), (c) Kabrit member (Middle Jurassic), (d) Upper Safa member (Middle Jurassic), (e) Zahra member (Middle Jurassic), and (f) Masajid Formation (Upper Jurassic). Jurassic strata in the Shushan Basin reveals a combination of fine- to coarse-grained clastic intervals and carbonates. Siltstone and shales predominate in the Middle Jurassic Khatatba Formation.

Fig. 16. Van Krevelen diagrams modified from Kerimov et. al (2017) and Hamdy et al. (2021) showing the projected Rock Eval pyrolysis results for core samples in the Upper Safa member (well Amoun-NE-01X) and Ras Qattara Formation (well Shams-15). (a) Jurassic strata in the Shushan Basin contains a mixture of kerogens type II and III as shown in the

upper graph. (b) Plots of Tmax against PI reveals that the Upper Safa member entered the oil and gas windows. The samples collected for the Ras Qattara Formation suggest it did not generate any hydrocarbons.

Fig. 17. Modified cross-plot from Hunt (1995) representing TOC vs. S1 ratios for the Upper Safa member (Middle Jurassic) and the Ras Qattara Formation (Lower Jurassic). The results confirm that hydrocarbons in both the Lower and Middle Jurassic strata are native to the study area.

Fig. 18. Gas chromatogram (CG) windows for light hydrocarbons compounds of n-alkanes (≤ n-C_7), alkenes (MCH), cycloalkanes (CH), aromatics (TOL), and other compounds for oil samples in the Upper and Lower Safa members in well Amoun-NE-01X (**Fig. 2**). The CG profile reveals a general increase in condensate gases in the Upper Safa member oil samples, compared to the Lower Safa member.

Fig. 19. Full gas chromatographic (GC) profile and calculated fractions derived by Thompson (1983), Mango (1994), and Halpern (1995) for oil samples obtained from well Amoun-NE-01X, Upper Safa member (**Fig. 2**). The GC analysis shows a high concentration of light compounds (≤ n-C10).

Fig. 20. Diagram of gross hydrocarbon composition defining the type of crude oil based on saturated hydrocarbons (SAT%), aromatic hydrocarbons (ARO%), and Non-Saturates and Oxygen (NSO%) ratios. The diagram shows that the Upper and the Lower Safa members (Middle Jurassic) of the Shushan Basin contain high mature crude oil. Diagram modified from Peters et al. (2005) and Tissot and Welte (2013).

Fig. 21. (a) Depositional facies, and (b) volume of shales (V_{sh}%) models for the Middle Jurassic Khatatba Formation. These 3D models reveal a north-prograding depositional system where the coarse-grained sediment was driven from local footwall and structural highs in the southern and central parts of the study area. This coarse-grained sediment was deposited

over finer-grained marine strata in the northern part of the Shushan Basin where its main depocentre was located in the Middle Jurassic.

Fig. 22. Formation Micro-Images (SFMI and DFMI) and gamma ray (GR) logs obtained from well Amoun-NE-01X when crossing the Masajid Formation (Upper Jurassic). The data reveal two types of secondary porosity in the study area: vugs in Z1 and fractures as in Z2. Both of these porosity types generate good reservoir intervals interbedded with thin shale, which work as local cap rocks.

Fig. 23. Formation Micro-Images (SFMI and DFMI) and gamma ray (GR) logs for the Zahra and Upper Safa members (Middle Jurassic) drilled by well Amoun-NE-01X. The FMIs image bedding planes dipping to the SSE in alternating fine and coarse-grained intervals. Fine-grained intervals such as Z5 show high conductivity and GR readings, comprising good seals for permeable pay zones such as Z3 and Z4.

Fig. 24. Wireline data showing fast and low shear waveforms and acoustic slowness (DT_{SF} and DT_{SS}), anisotropy coefficients, together with formation micro-image (PFMI), and gamma ray (GR) logs, in well in Amoun-03. The data shown concerns the Middle Jurassic Khatatba Formation. Data interpretation shows four (4) distinct reservoirs (Z6 to Z9) that occur in the Lower Safa and Kabrit members. They both have shaley cap rock intervals.

Fig. 25. Geological models summarizing the paleo-depositional environments and related depositional facies in the Shushan Basin during the (a) Early Jurassic, (b) Middle Jurassic, and (c) Late Jurassic. The model denotes three (3) depositional megasequences related to changes in relative eustasy and subsidence during continental rifting.

Fig. 26. Cross-sections across the Shushan Basin extracted from the 3D facies and volume of shale (V_{sh}%) models in Fig. 15: a) Main stratigraphic facies and lateral distribution, and b) Variations in the volume of shale through the Khatatba and Masajid Formations. These cross-sections reveal an increase in the volume of shales in the northern parts of the study

area where unconventional reservoirs (shale gas and tight-gas sands) are likely to occur. The central and southern parts reflect a low volume of shale, i.e. sand is predominant, comprising zones with promising clastic and carbonate reservoirs.

Fig. 27. Burial and thermal history models for three (3) production wells located in the Shushan Basin (**Fig. 3**). The models show evidence for multiple phases of source rock maturation affecting the Jurassic strata. The Shushan Basin records three (3) main episodes of tectonic subsidence started in Palaeozoic and extended to the Early Cretaceous. The Jurassic strata recorded a substantial increase in temperature from the Late Cretaceous, which lasted until the Miocene. In particular, wells Amoun-NE-2 and Amoun-NE-01X record sharp late Paleogene-early Miocene thermal pulses in (b) and (c).

Fig. 28. Burial and thermal history models for the three (3) pseudo wells shown in Fig. 2. The graphs reveal an increase in formation temperature where local depocentres are recognised (see **Figs. 8 and 9**). Jurassic strata record temperature exceeding 150 ºC (302 ºf), which reflects good conditions for source rock maturation.

Fig. 29. Thermal conductivity and formation temperature data for the study area. a) The panels highlight a decrease in formation temperature in the central parts of the basin, where a basin horst is located (see **Figs. 8 and 9**). (b) Thermal conductivity of the Middle Jurassic Khatatba Formation is approximately constant at about 1.5 W/m/k, above older strata with relatively high thermal conductivity values exceeding 2.2 W/m/k. These panels justify the significant increase in Khatatba Formation's temperatures recorded towards the northern parts, where its main depocentre is located.

Fig. 30. Burial model for well Amoun-NE-01X projected against (a) kerogen transformation ratio and (b) vitrinite reflectance. Transformation ratios show that shale intervals of the Khatatba Formation started to generate hydrocarbons in the Late Cretaceous, reaching a peak in the

Miocene. Vitrinite reflectance (R_o%) data document changes between 1 to 1.08 R_o% in the Khatatba Formation, confirming its present-day position in the oil and early gas windows.

Table 1: Parameters used in the compilation of the PetroMod® burial and thermal models analysed in this work.

Table 2. Vitrinite reflectance measurements for the Upper and Lower Safa members as sampled in wells Amoun-NE-01X and Amoun-NE-2.

Table 3. Total organic carbon and Rock-Eval pyrolysis results for core samples acquired from the Upper Safa member (Middle Jurassic), well Amoun-NE-01X.

Table 4. Total organic carbon and Rock-Eval pyrolysis results for core samples taken from the Ras Qattara Formation (Lower Jurassic), well Shams-15.

Table 5. Medium-pressure liquid chromatography (MPLC) results for the Lower and Upper Safa members, well Amoun-NE-01X.

Table 6. Results of Reservoir Description Tool (RDT) tests ran for the Lower Safa member (Middle Jurassic), well Amoun-NE-01X.

Table 7. Results of Reservoir Description Tool (RDT) tests ran for the Upper Safa member (Middle Jurassic), well Amoun-NE-01X.

Table 8. Biogeochemical data for Jurassic shale intervals in the Shushan Basin.

Figures

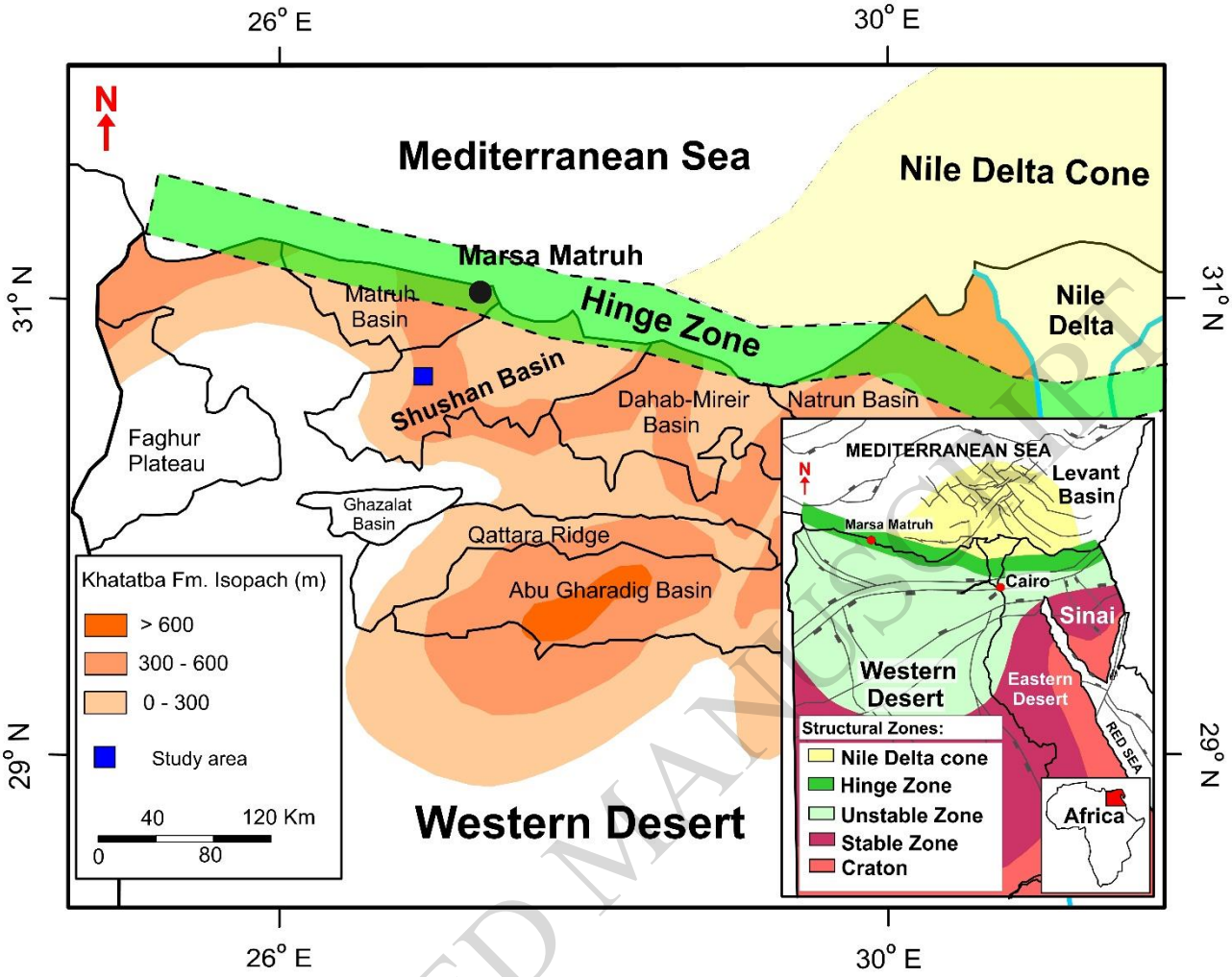

Fig. 1.

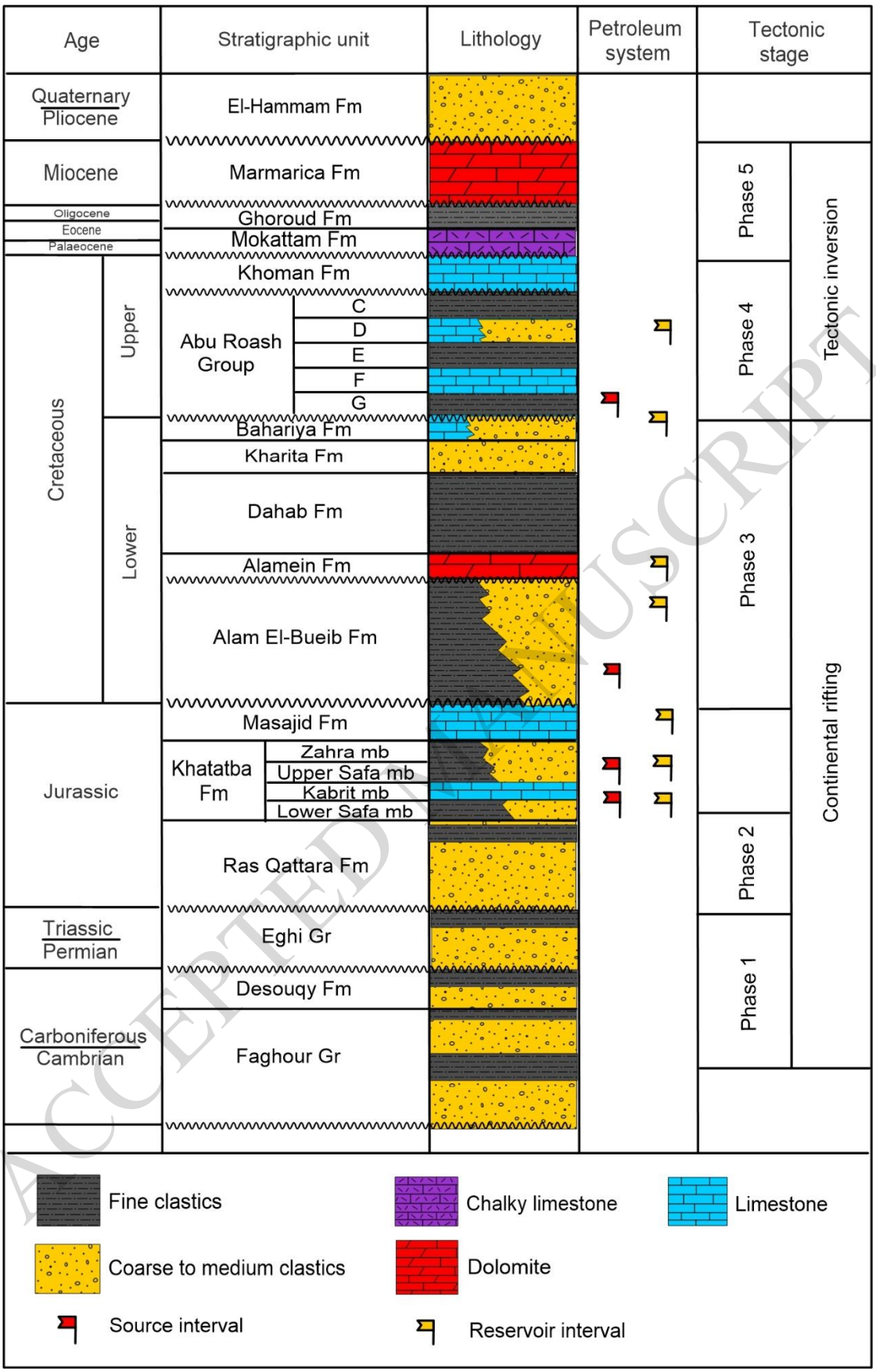

Fig. 2

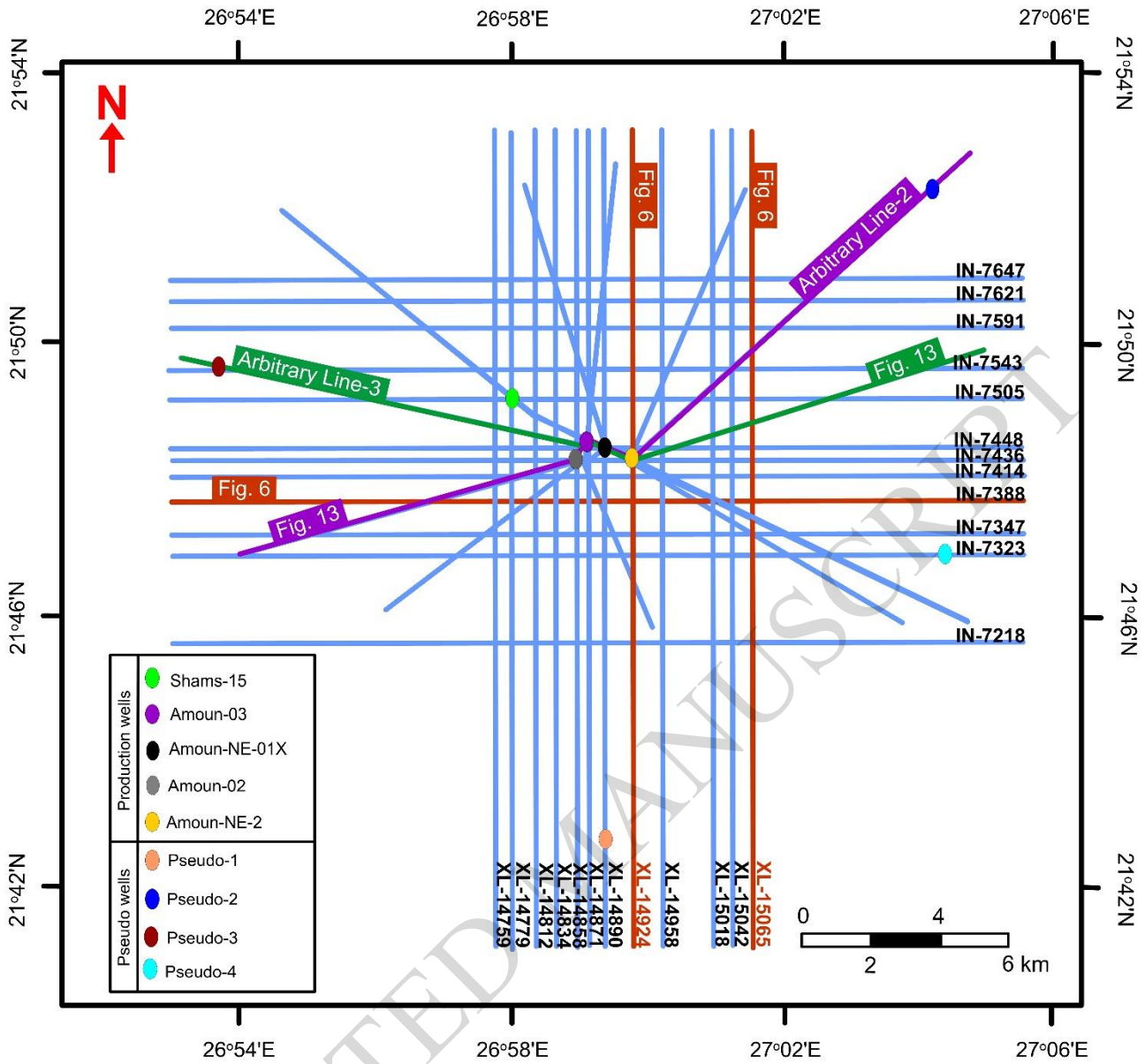

Fig. 3.

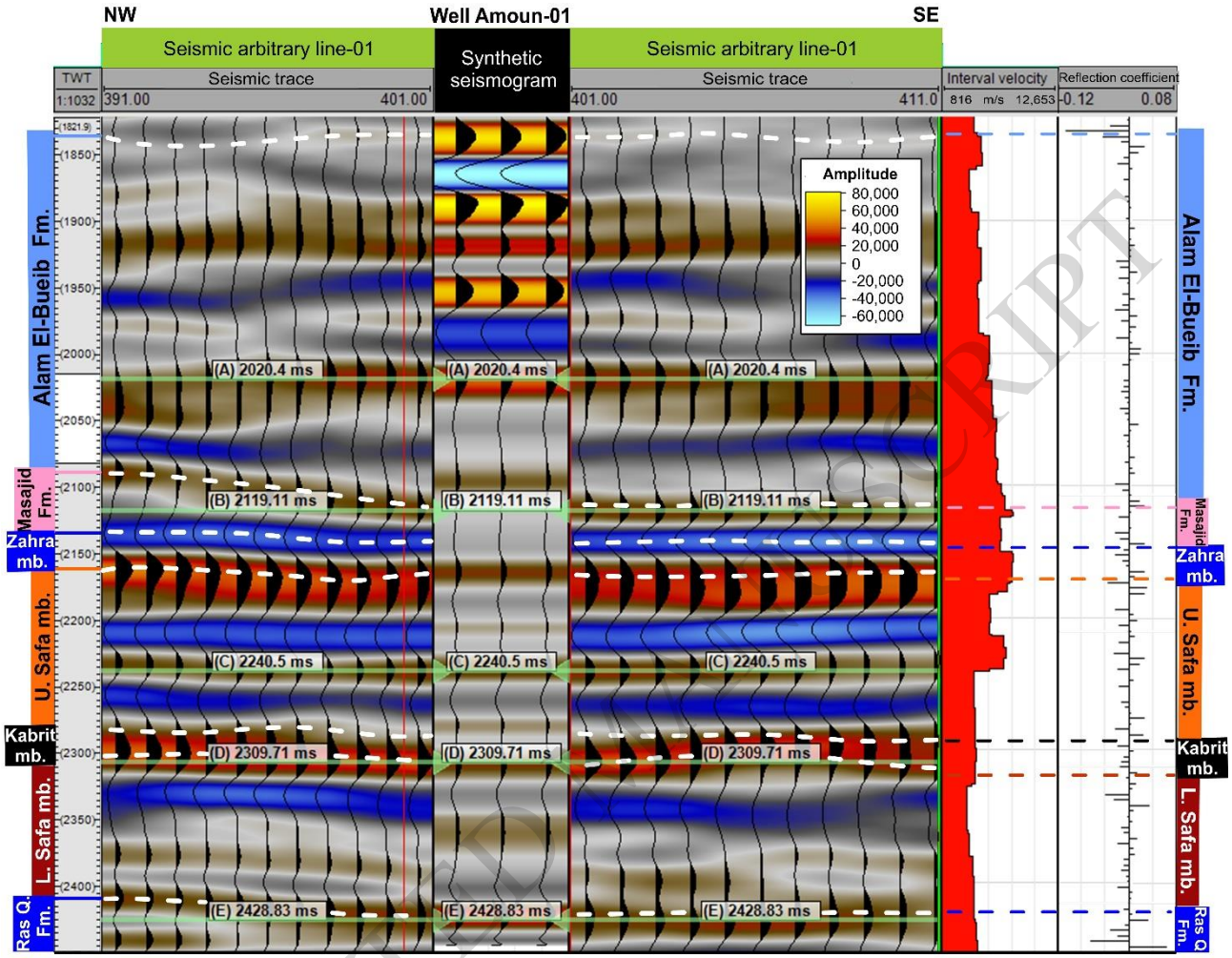

Fig. 4.

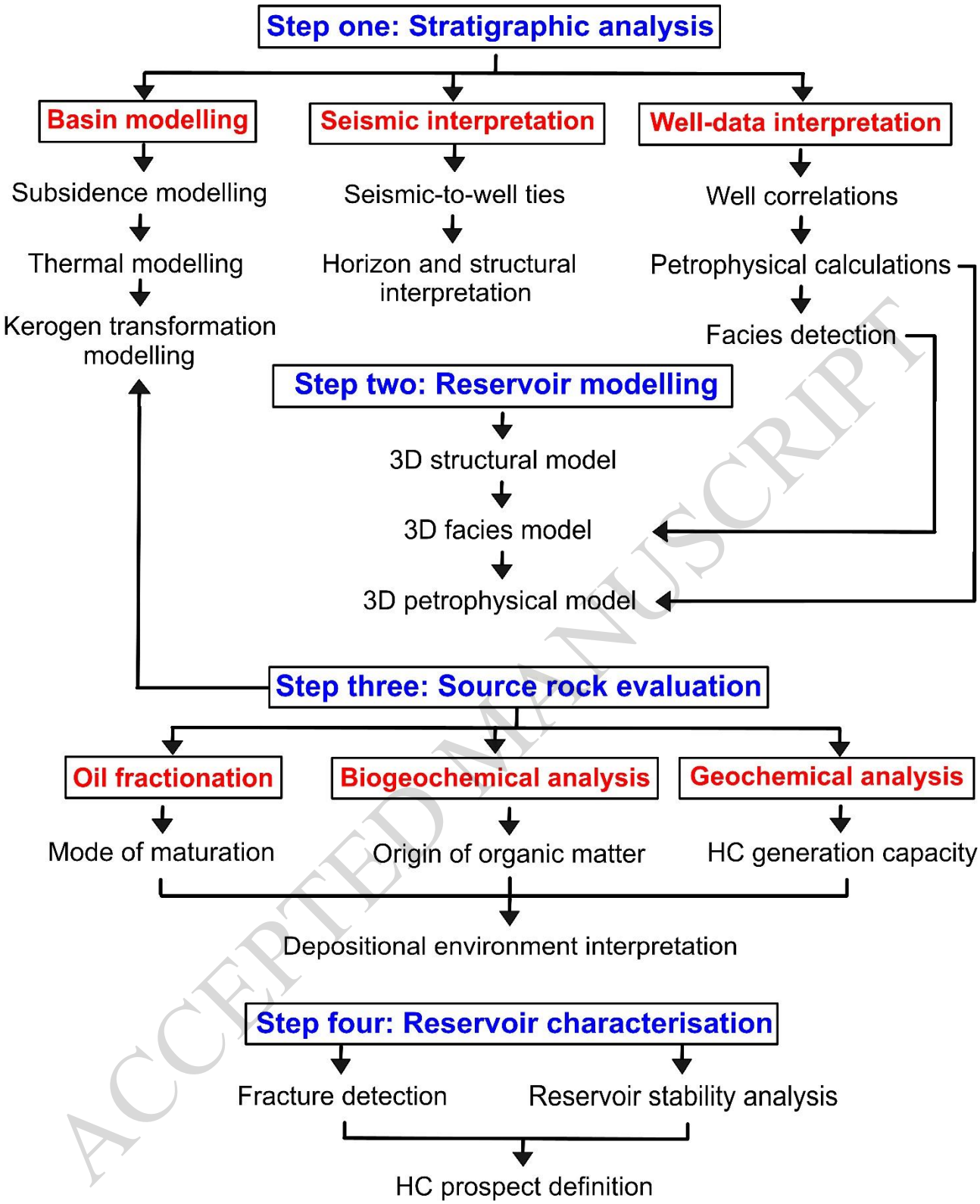

Fig. 5.

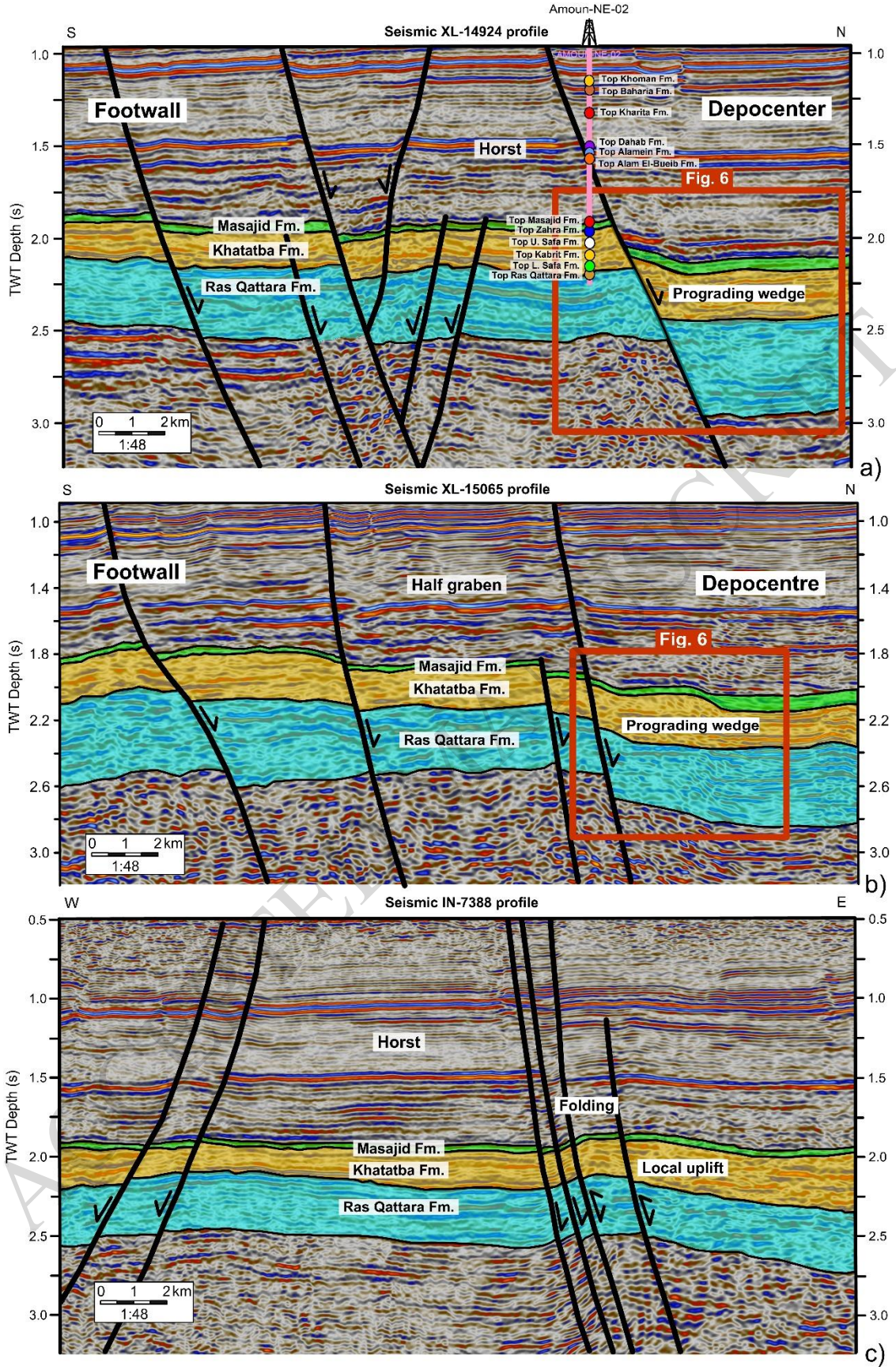

Fig. 6.

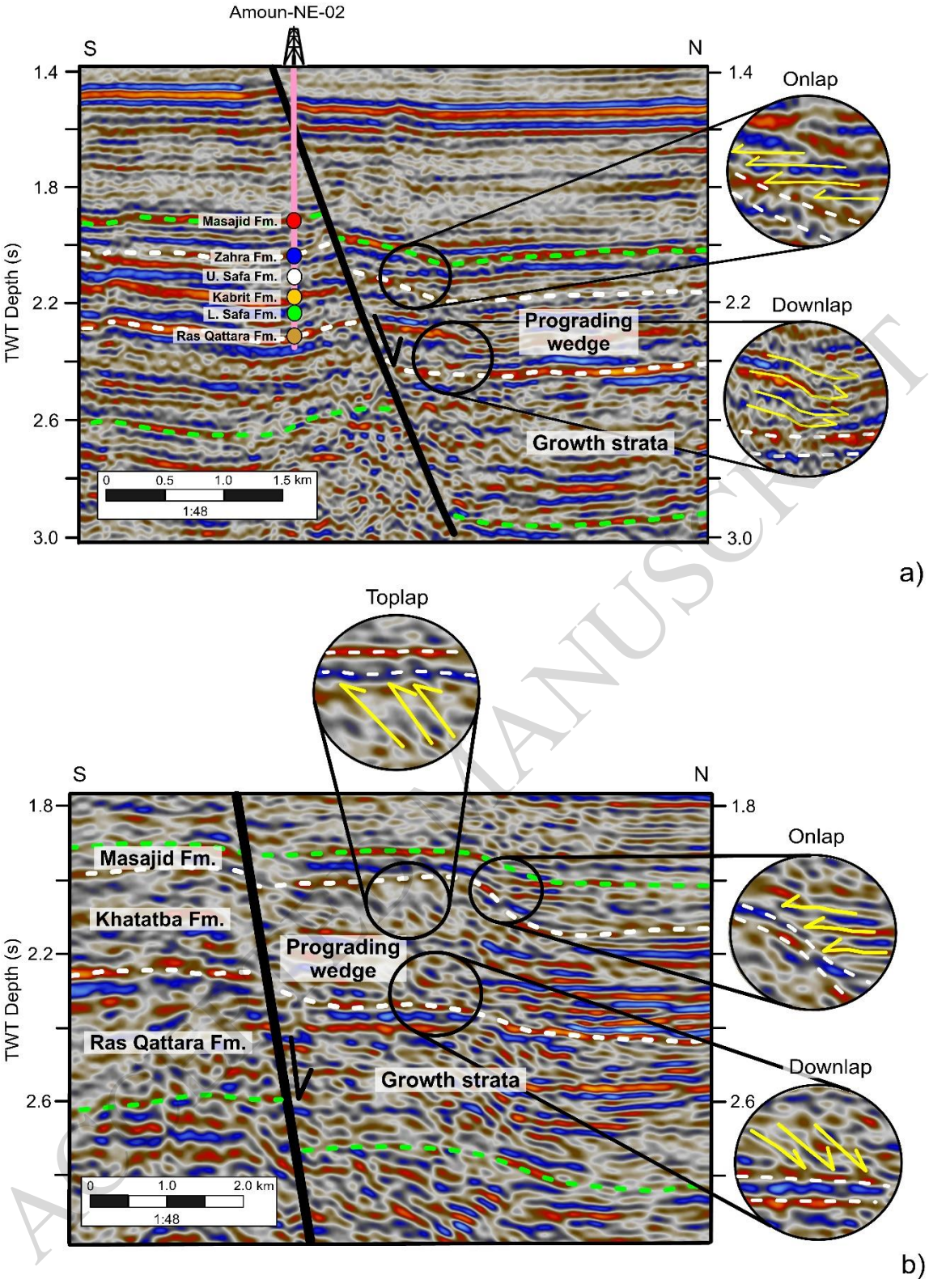

Fig. 7.

TWT structural map of the top Ras Qattara Formation (Lower Jurassic)

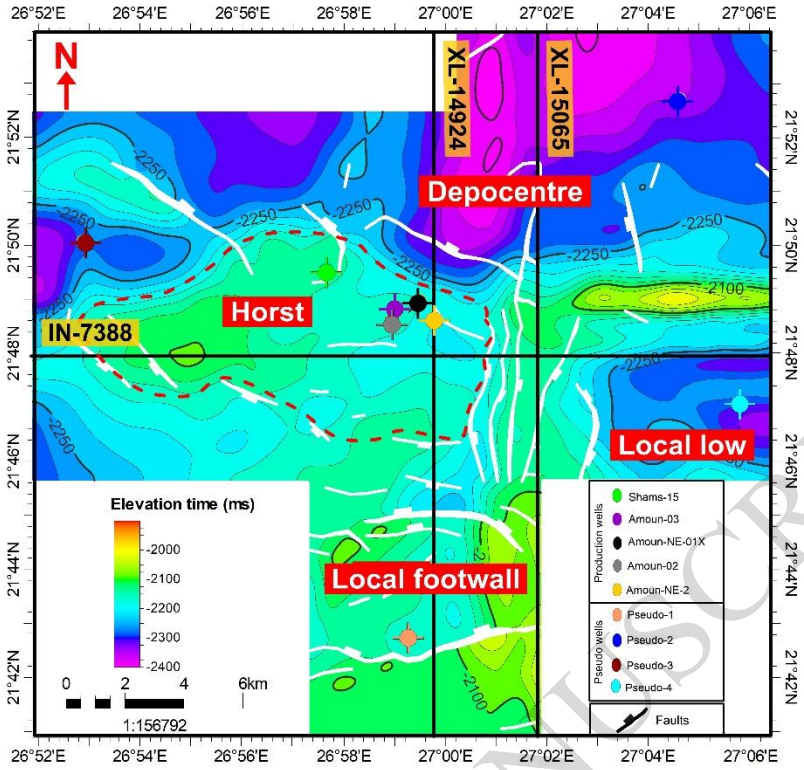

a)

TWT structural map of the top Khatatba Formation (Middle Jurassic)

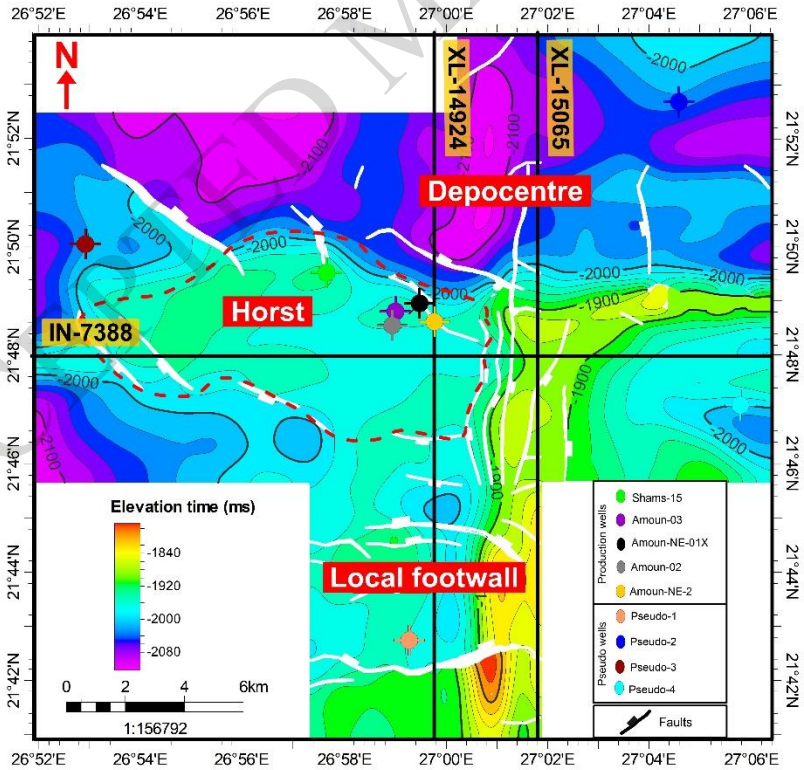

b)

Fig. 8.

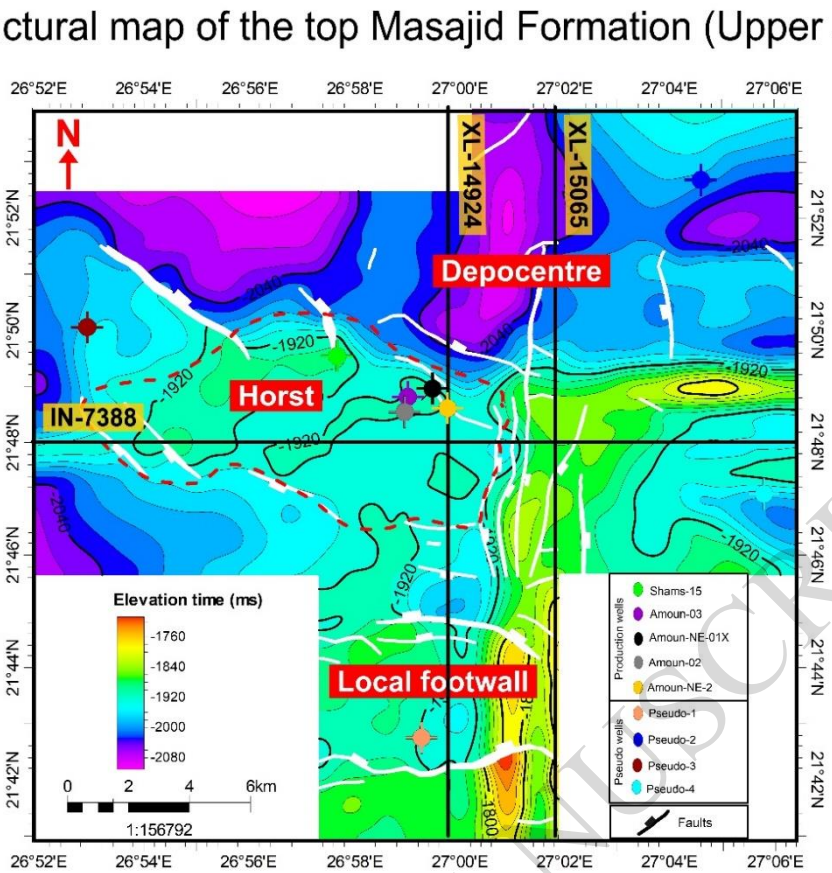

Fig. 9.

Isochron map of the Ras Qattara Formation (Lower Jurassic)

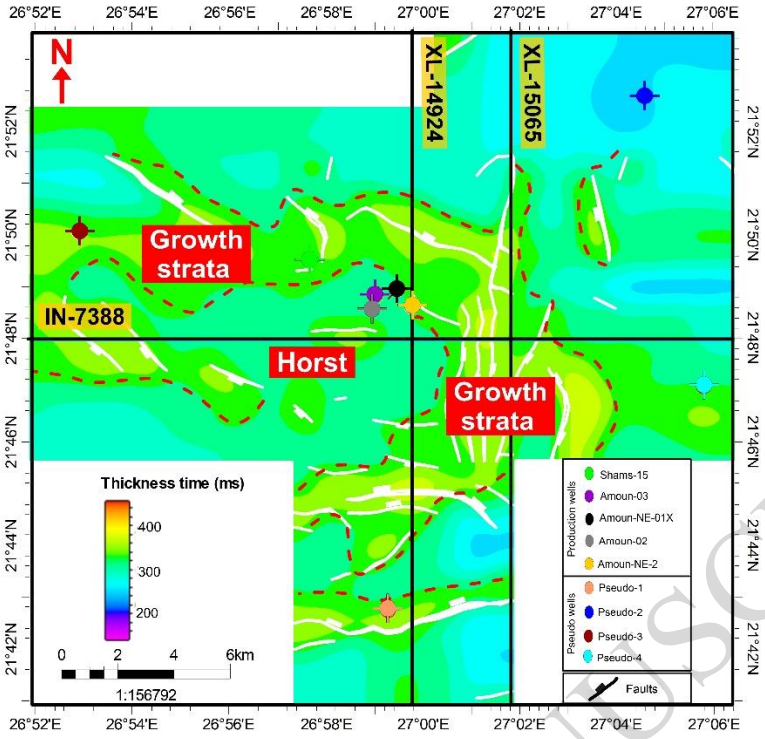

a)

Isochron map of the Khatatba Formation (Middle Jurassic)

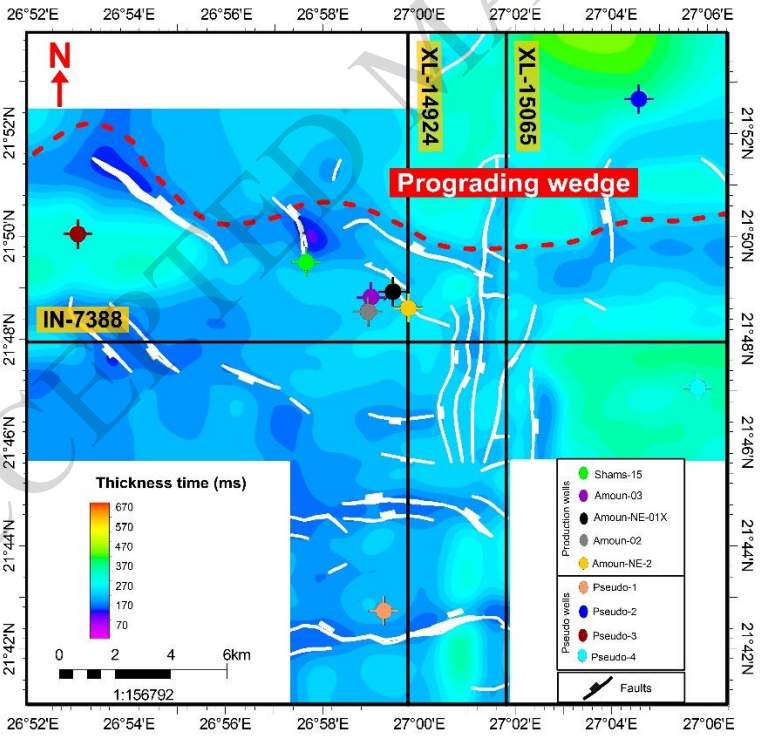

b)

Fig. 10.

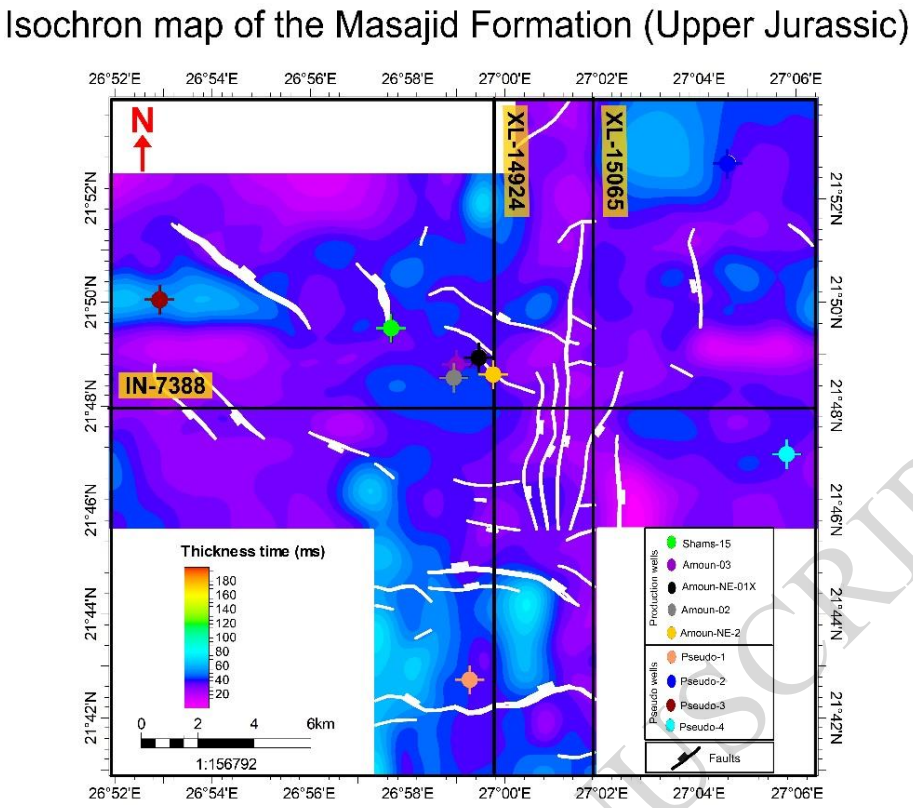

Fig. 11.

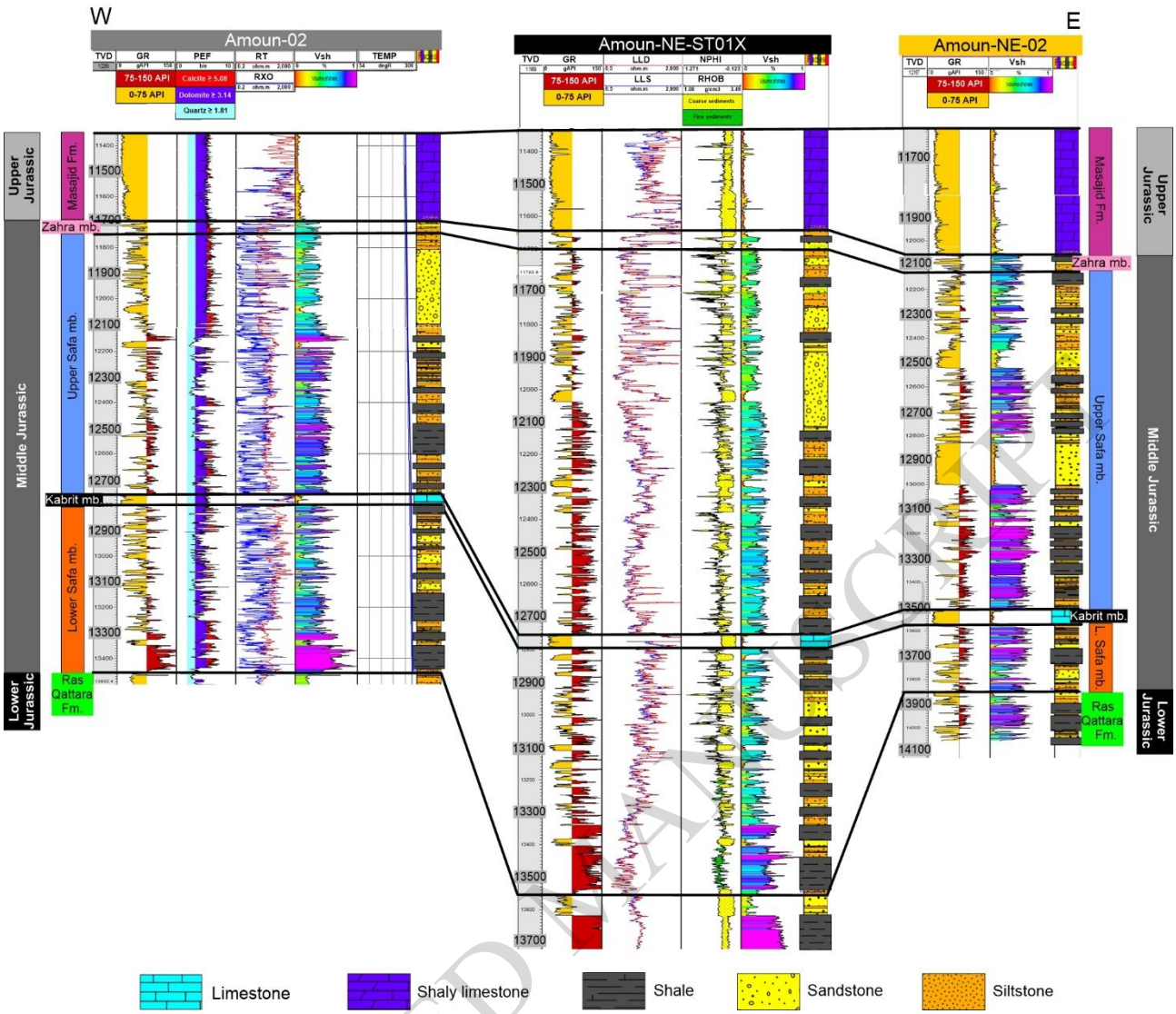

Fig. 12.

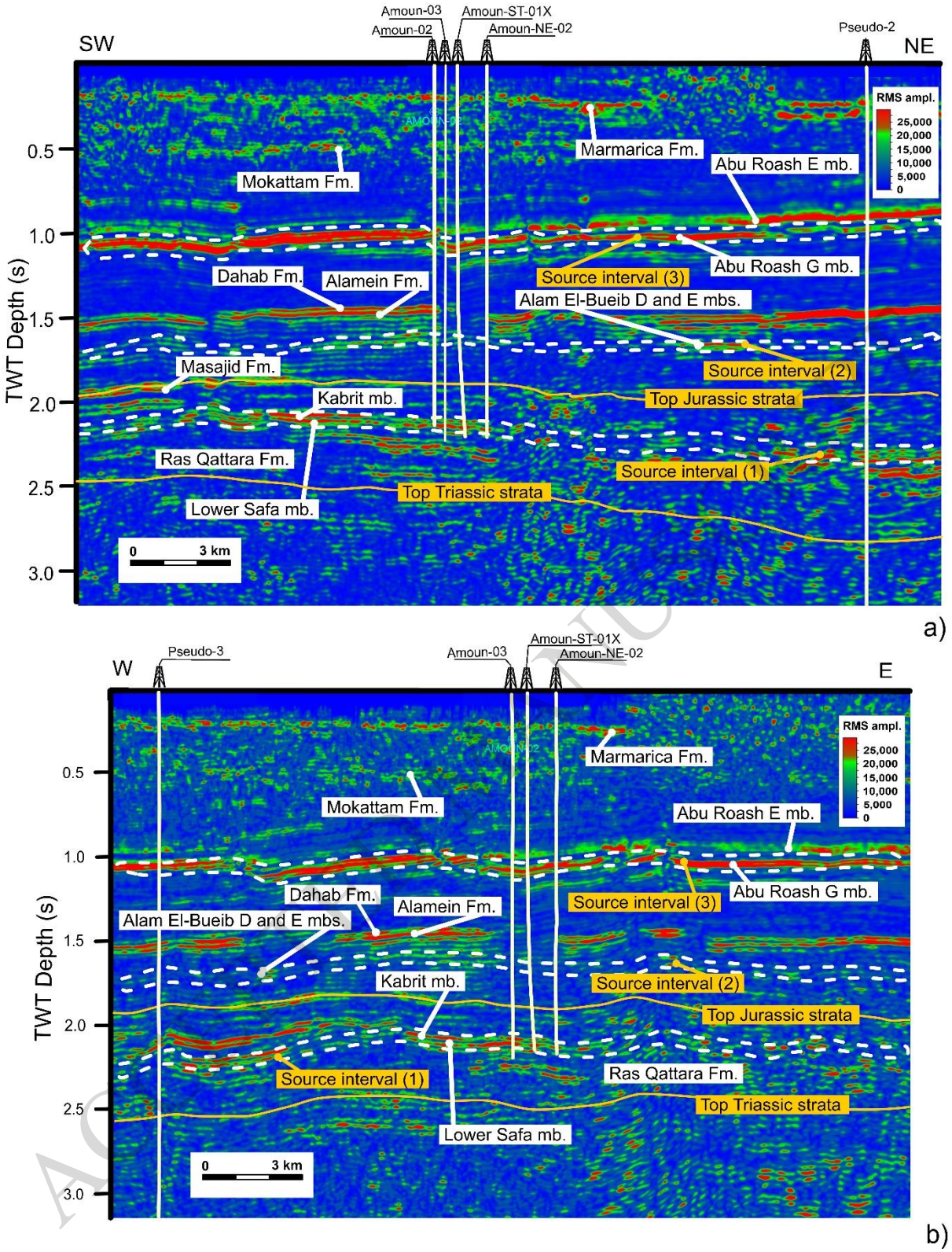

Fig. 13.

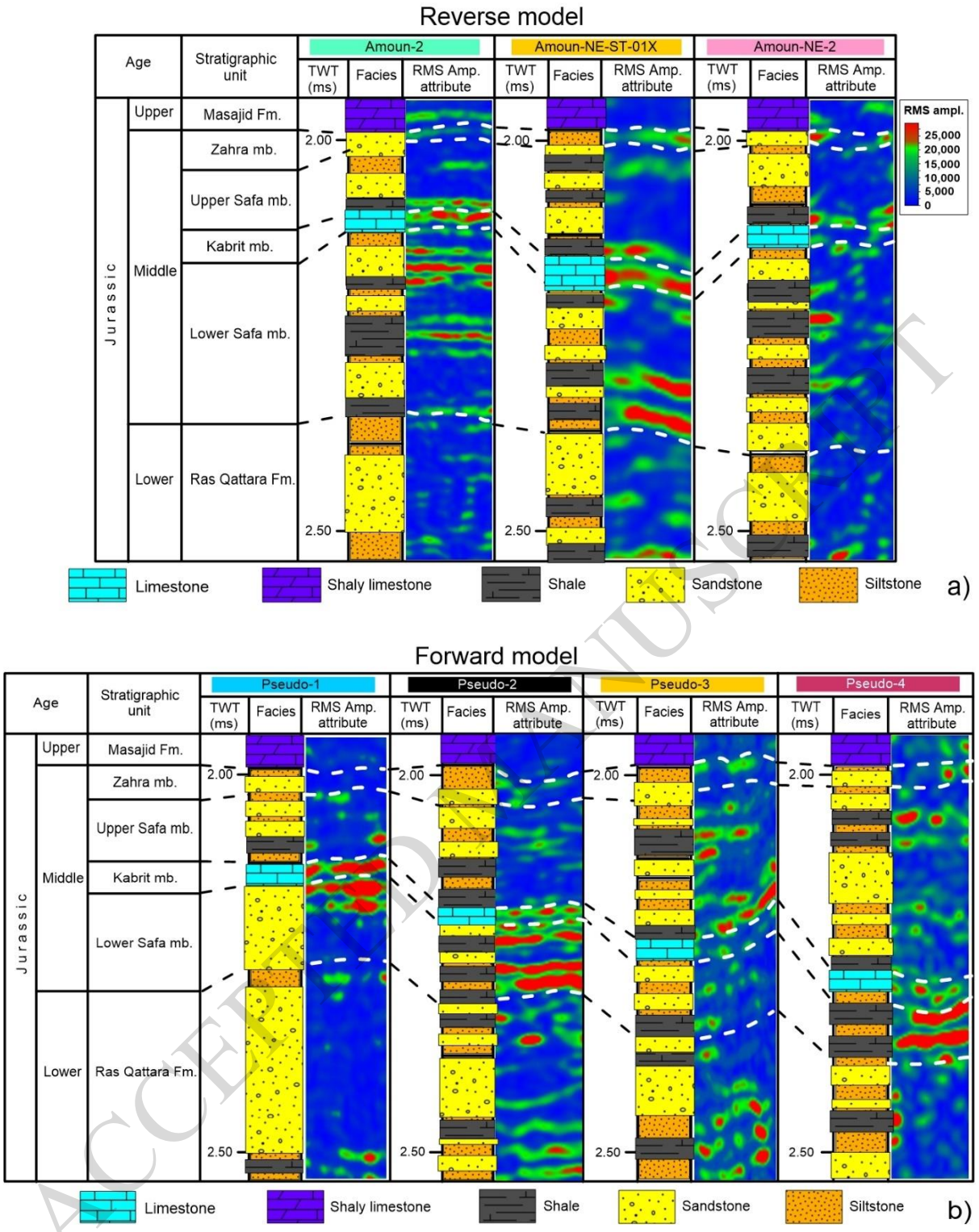

Fig. 14.

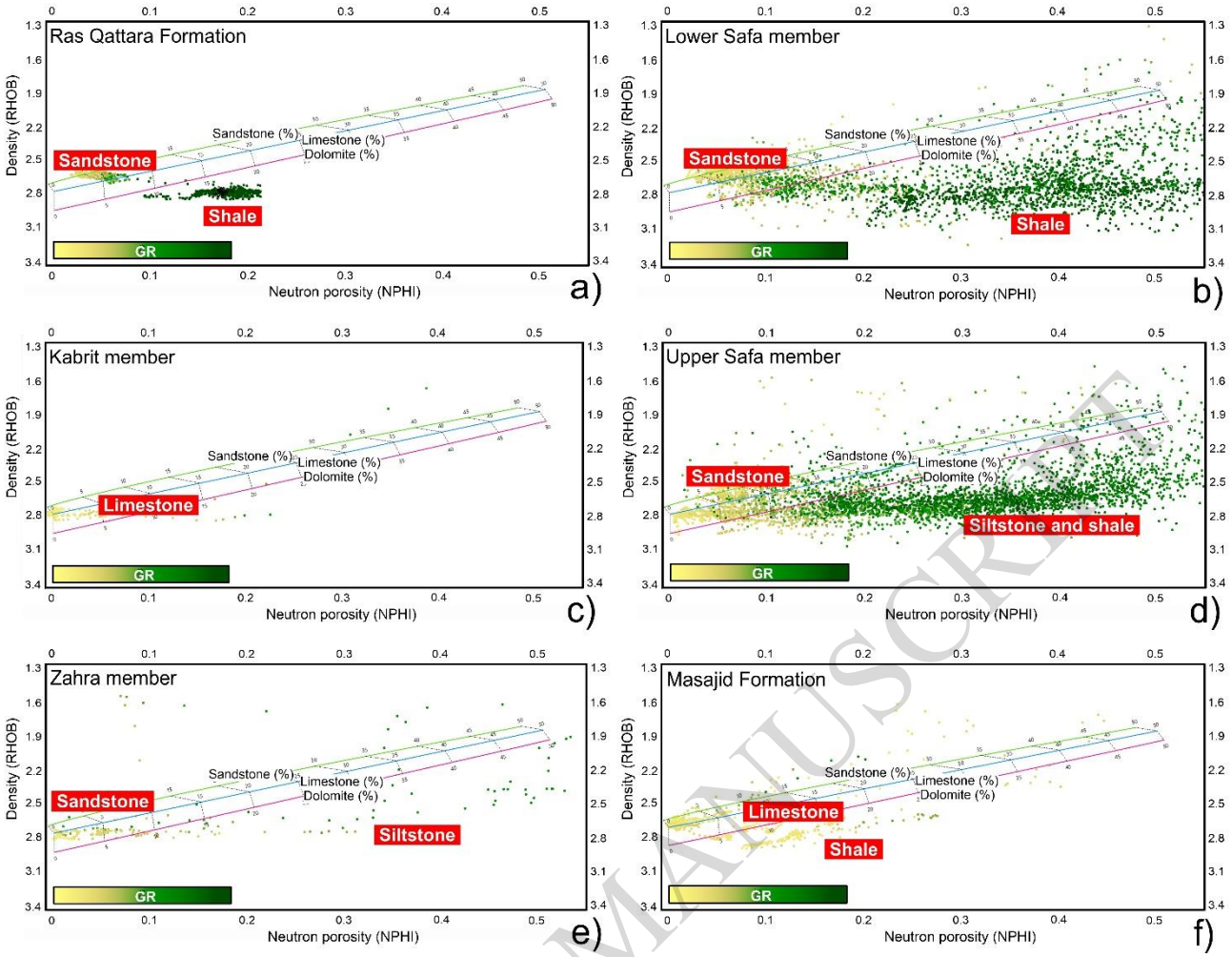

Fig. 15.

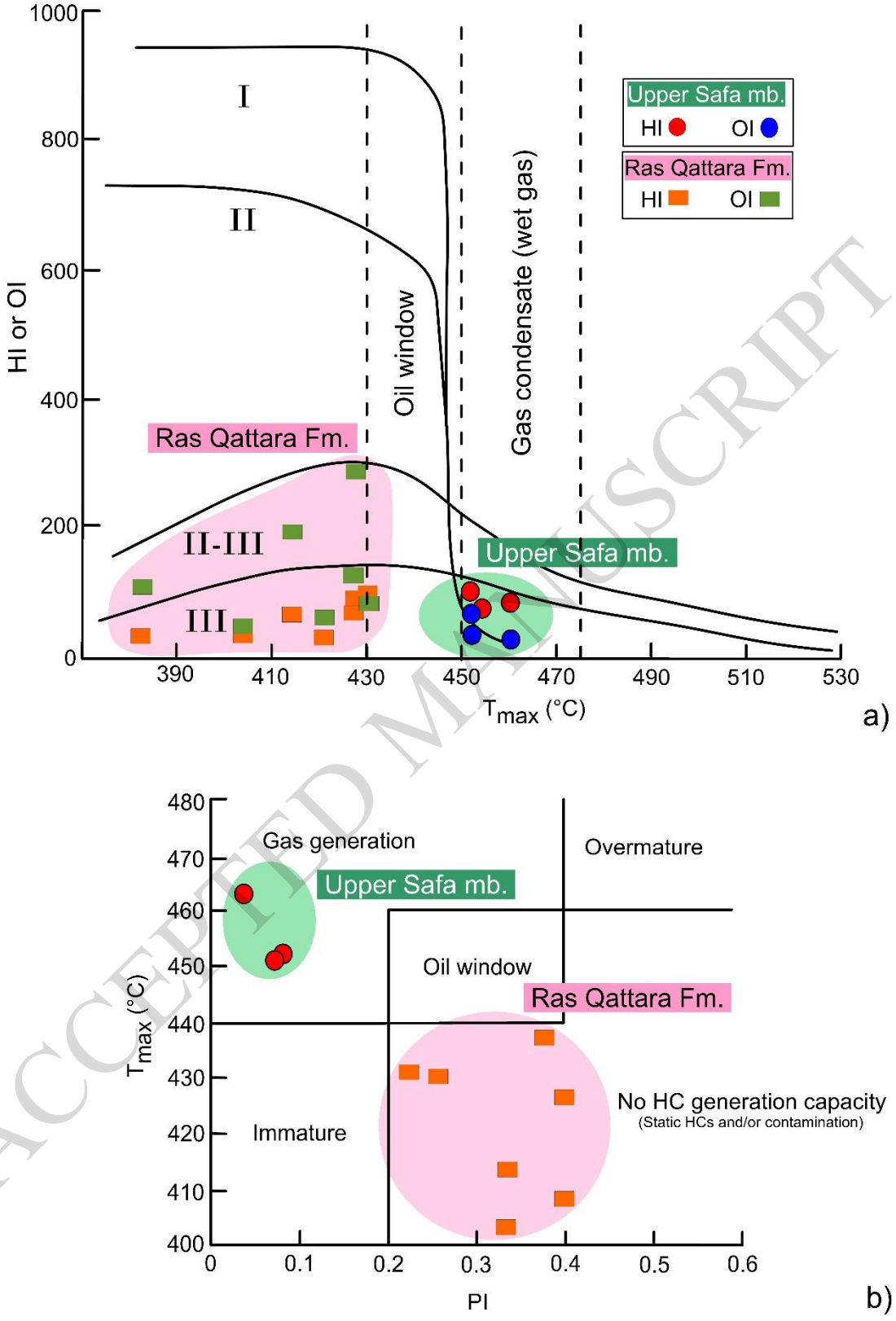

Fig. 16.

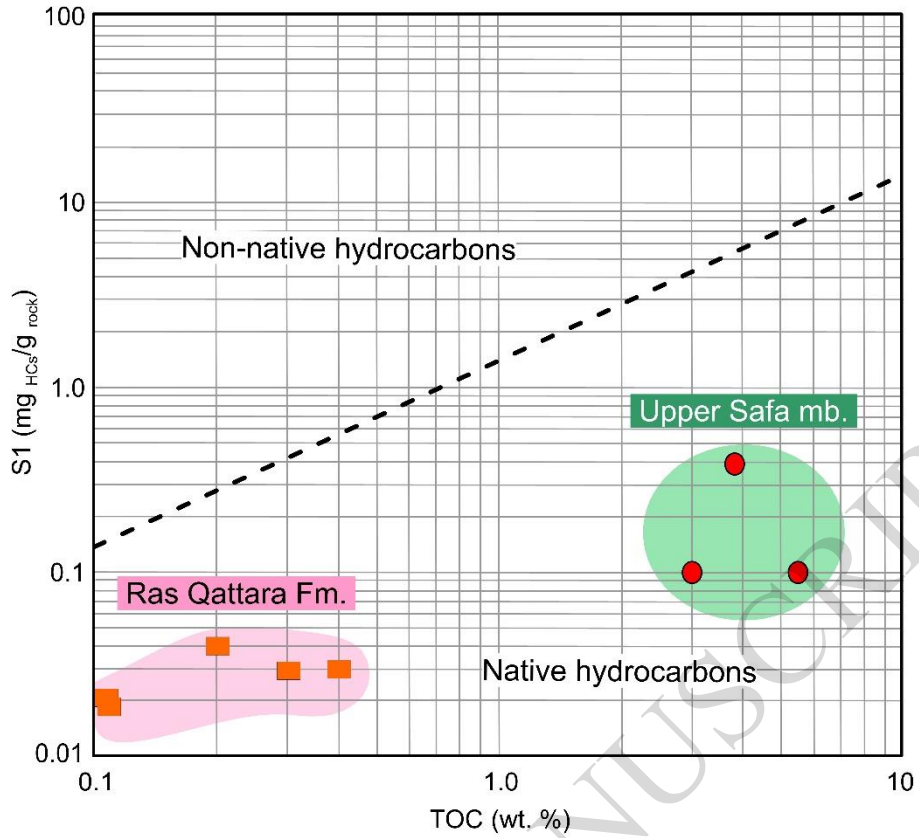

Fig. 17.

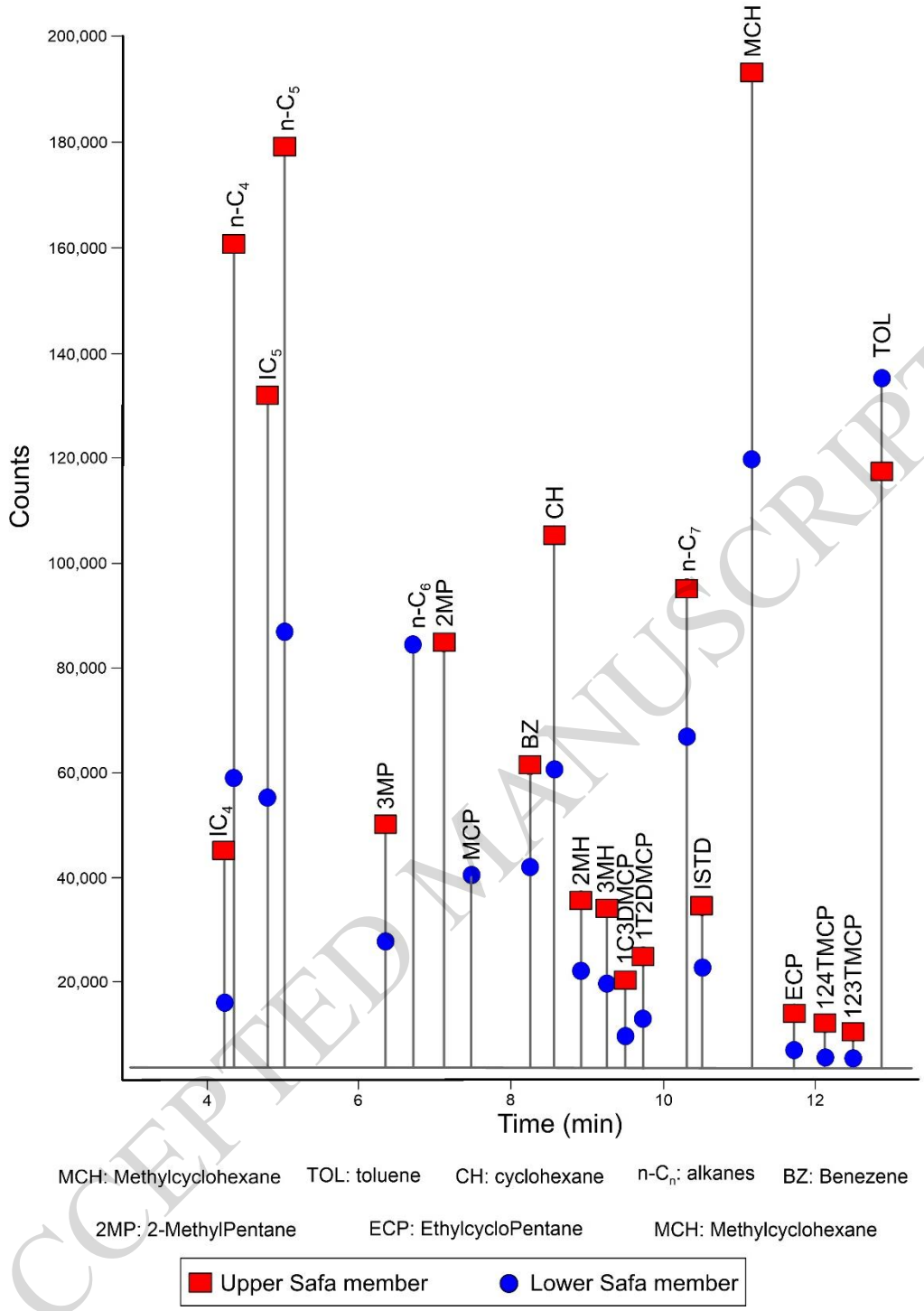

Fig. 18

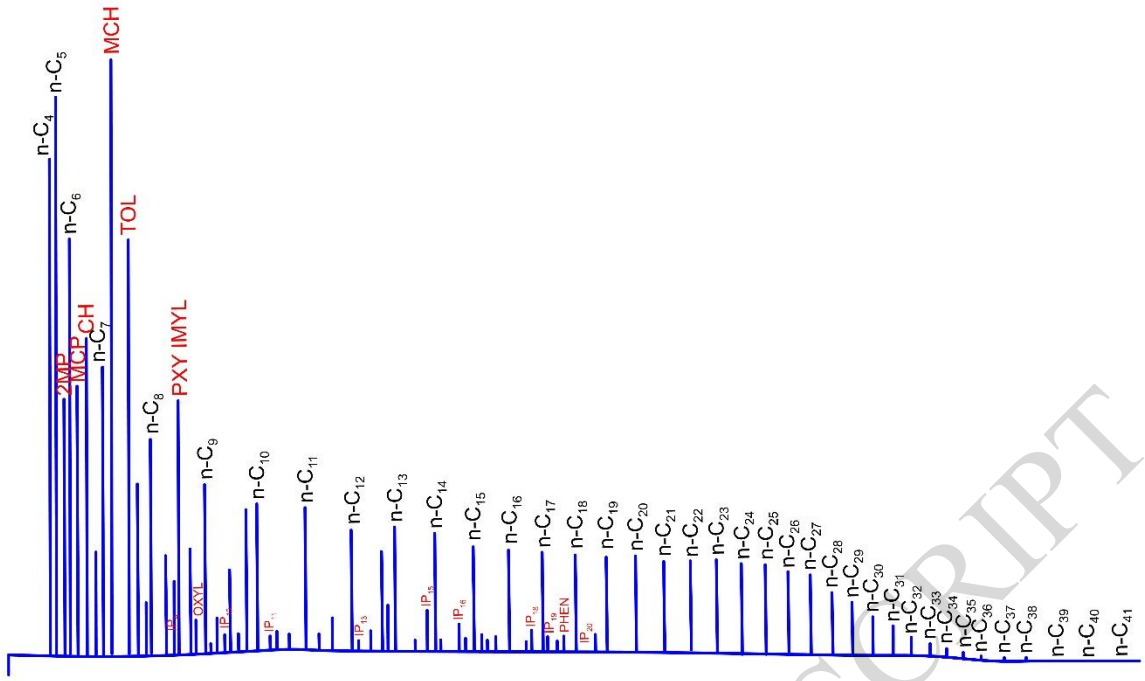

WGC parameters	
Pristane/Phytane	3.57
Pristane/n-C_{17}	0.14
Phytane/n-C_{18}	0.04
n-C_{18} /n-C_{19}	0.04
n-C_{17} /n-C_{29}	1.93
CPI Marzi-4	1.02
Normal Paraffins	33.90
Isoprenoids	2.00
Cycloparaffins	10.30
Branched (iso-) Paraffins	6.30
BTX aromatics	8.40
Resolved unknowns	38.60

Thompson, 1983	
A. BZ/n-C_6	0.47
B. TOL/n-C_7	1.80
C. $(n\text{-}C_6+n\text{-}C_T)/(CH+MCH)$	0.60
I. Isoheptane Value	1.14
F. n-C_7/MCH	0.39
U. CH/MCP	1.28
R. nC7/2MH	3.20
S. n-C6/22DMB	66.80
H. Heptane Value	17.16
MCH/n-C_7	2.54
mpXYL/n-C_8	1.97

Mango, 1994	
P_1	14.73
P_2	8.75
P_3	2.43
$5N_1$	4.71
N_2	5.39
$6N_1$	63.99
K_1	1.16
K_2	0.62
$5N_1/6N_2$	0.07
P_3/N_2	0.45
ln(24DMP/23DMP)	-0.40

Halpern, 1995	
Tr_1	28.20
Tr_2	15.67
Tr_3	4.41
Tr_4	4.90
Tr_5	9.31
Tr_7	2.30
Tr_8	3.70
C_1	0.09
C_2	0.44
C_3	0.29
C_4	0.06
C_5	0.12

Fig. 19.

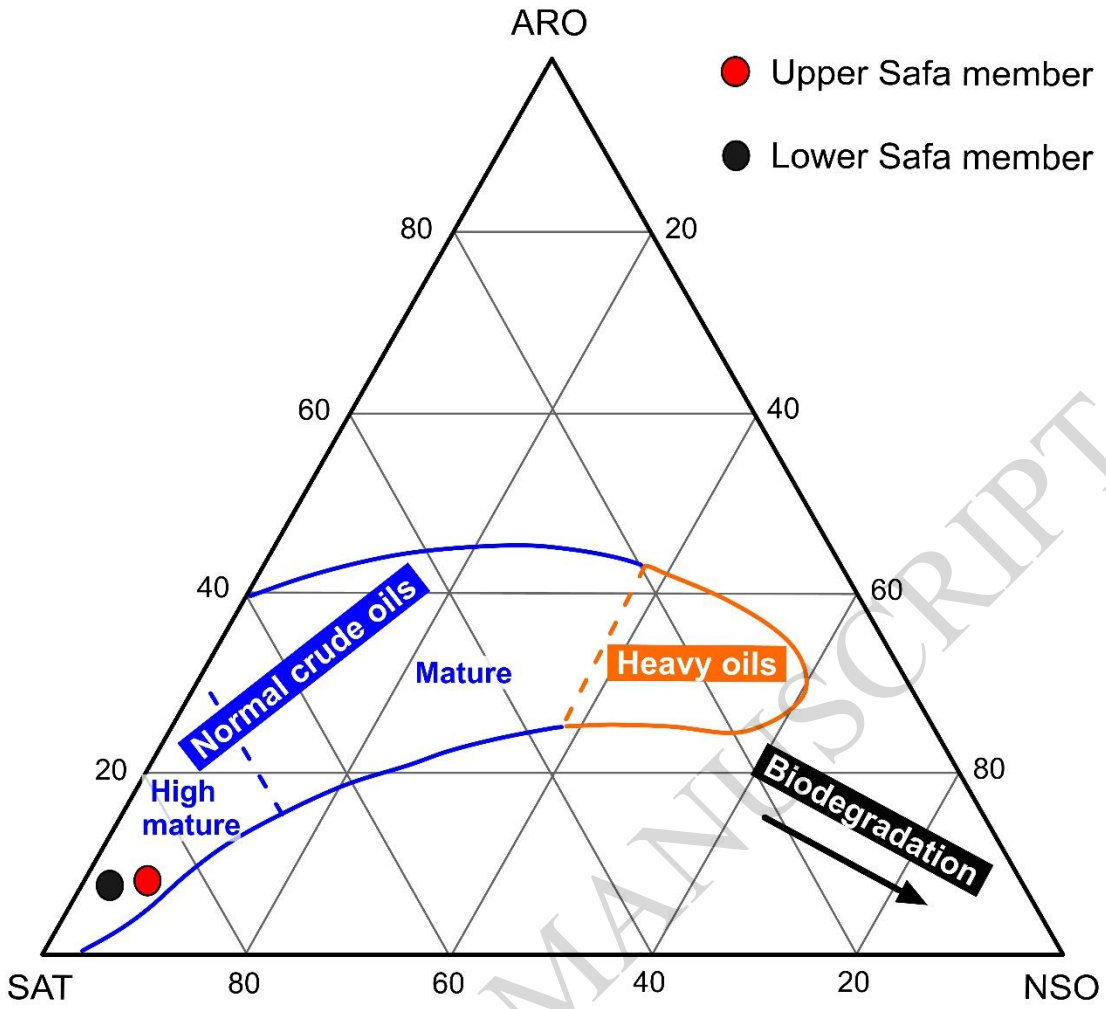

Fig. 20.

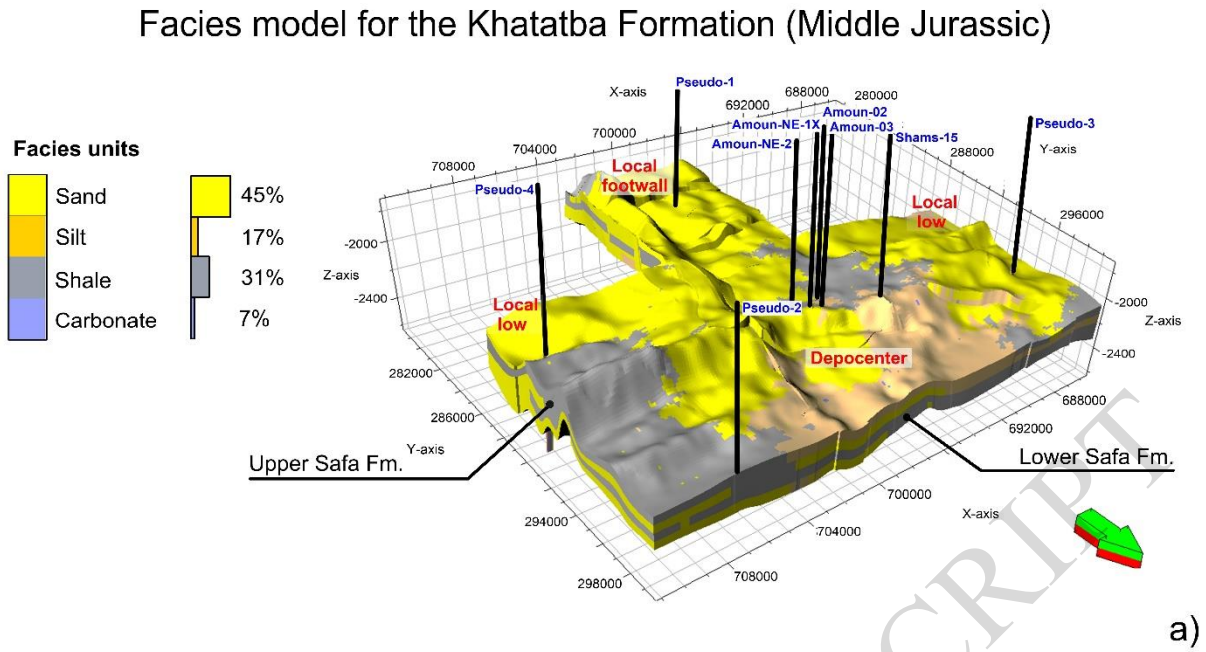

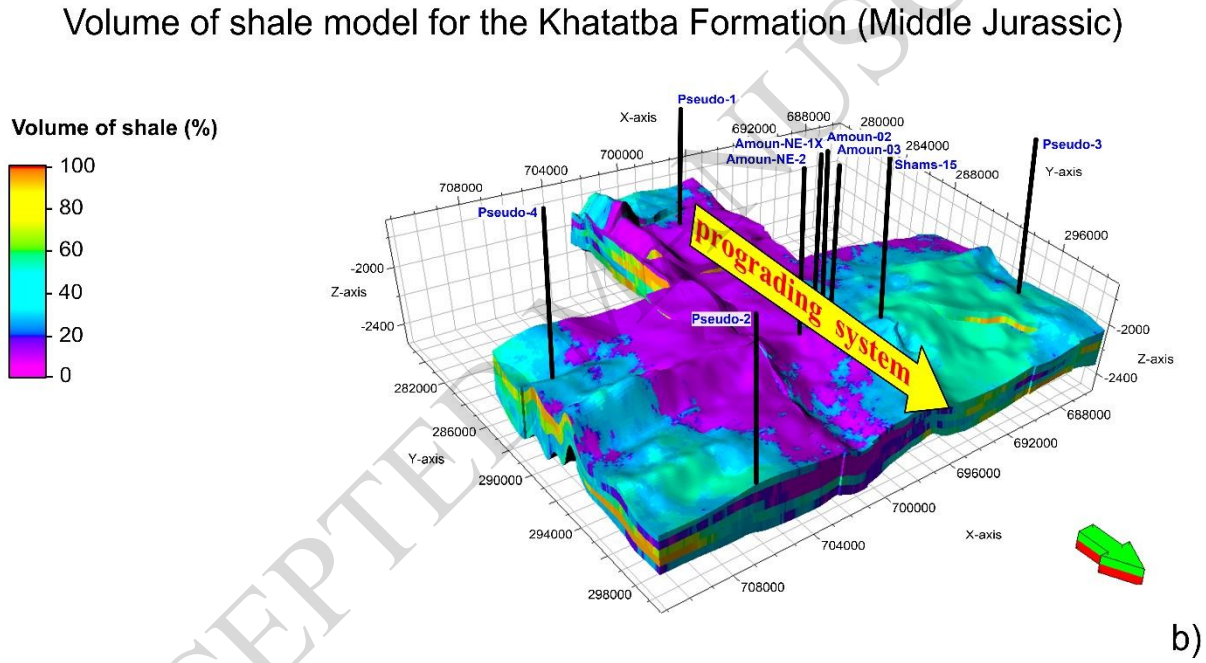

Fig. 21.

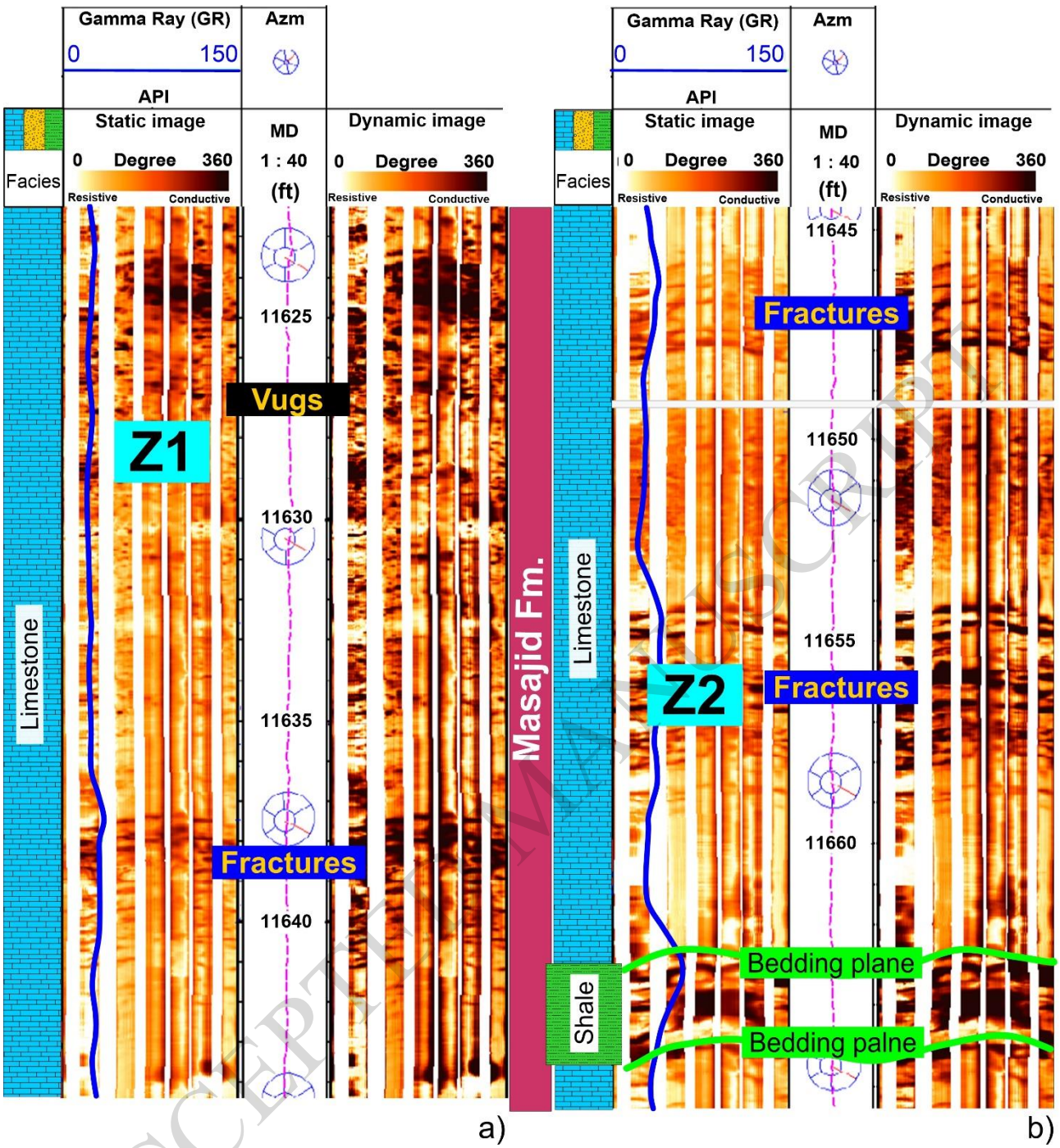

Fig. 22.

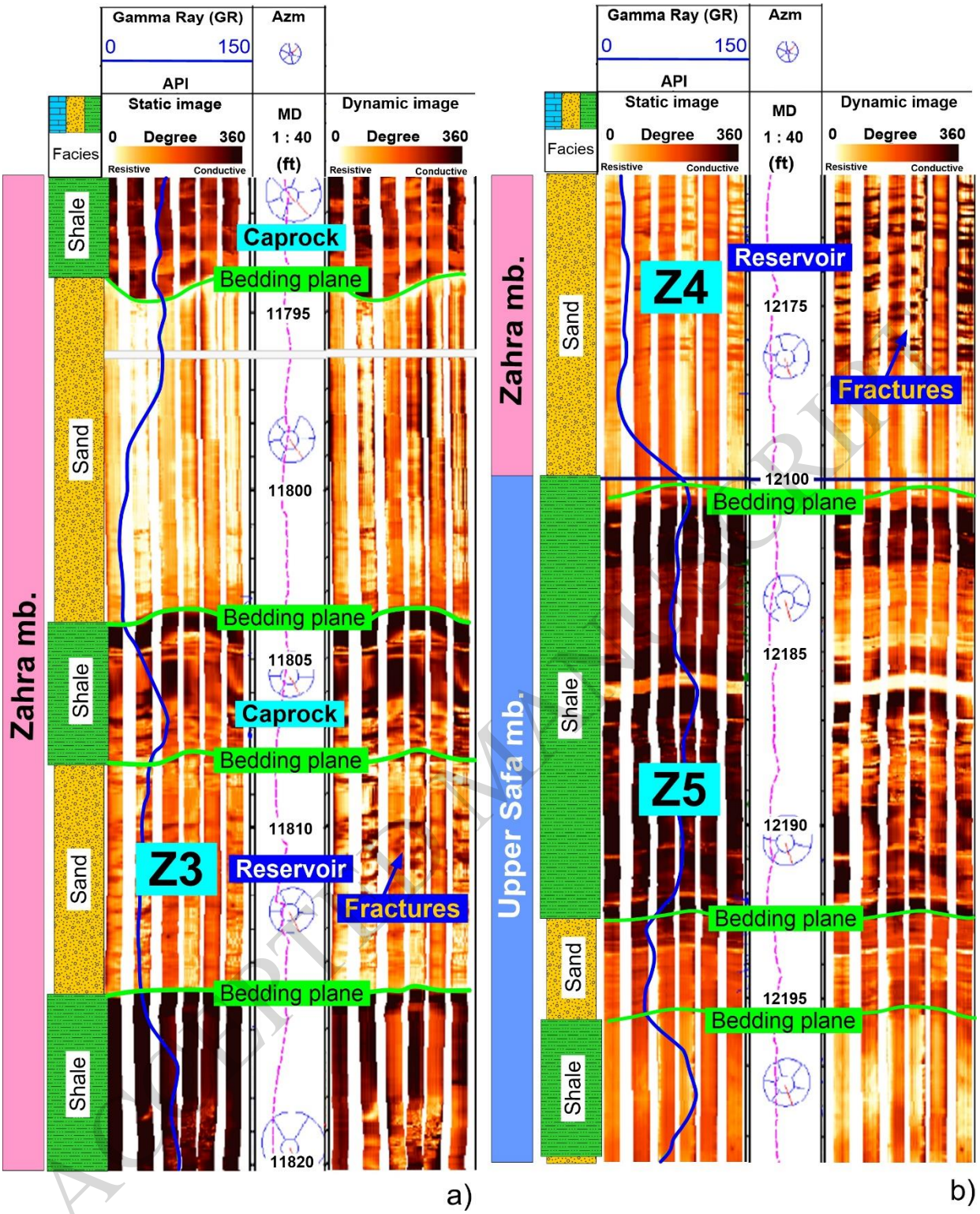

Fig. 23.

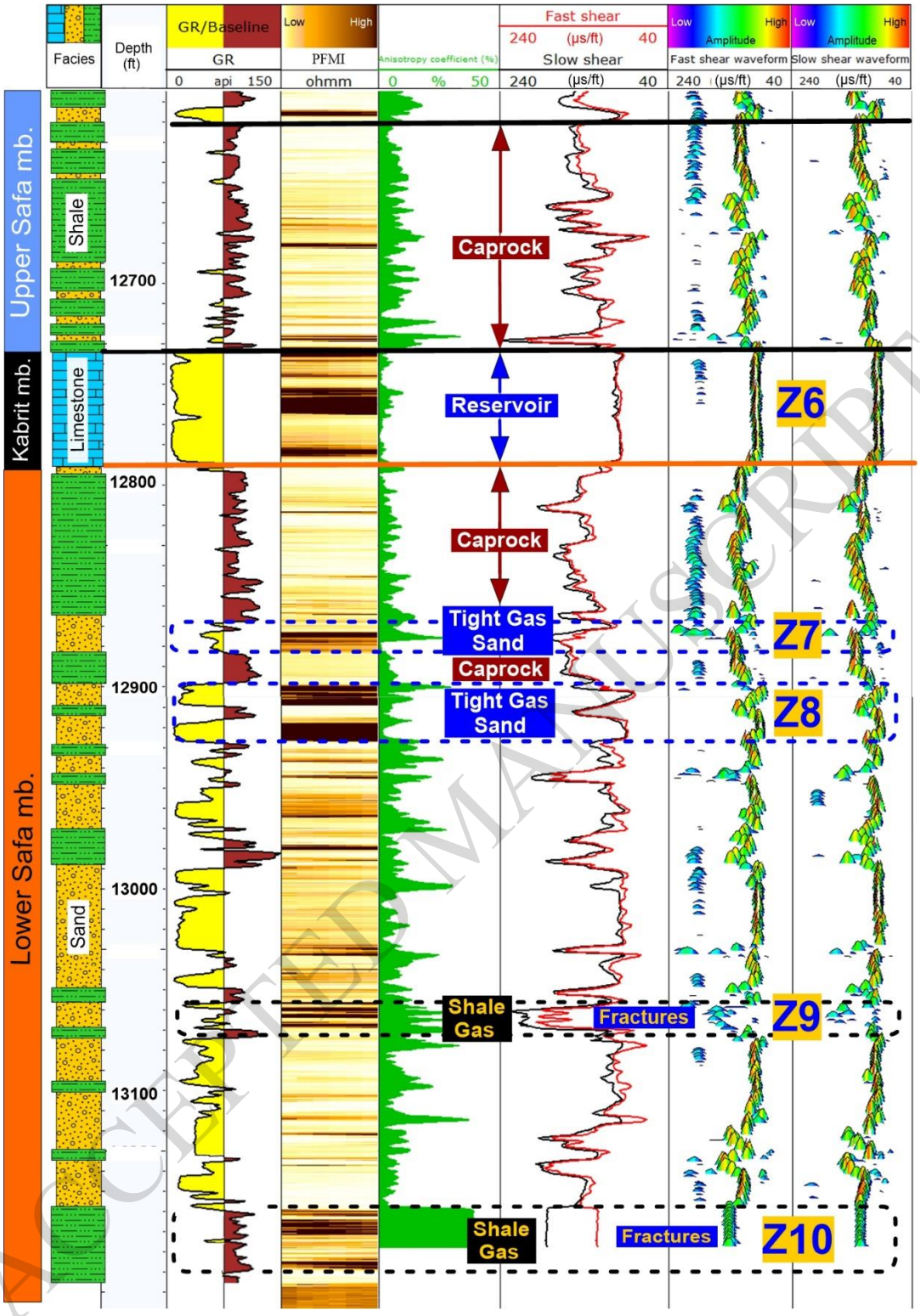

Fig. 24.

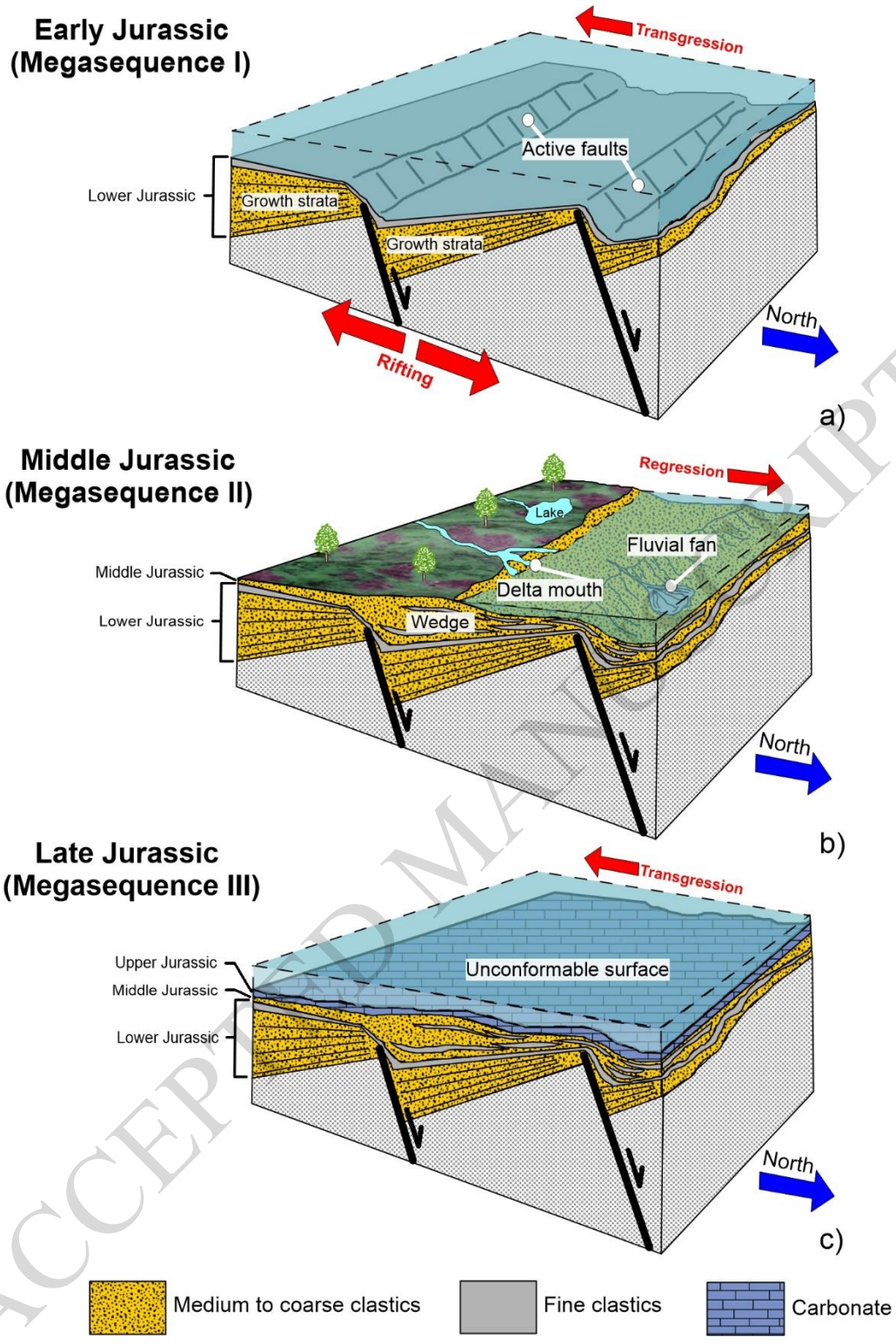

Fig. 25.

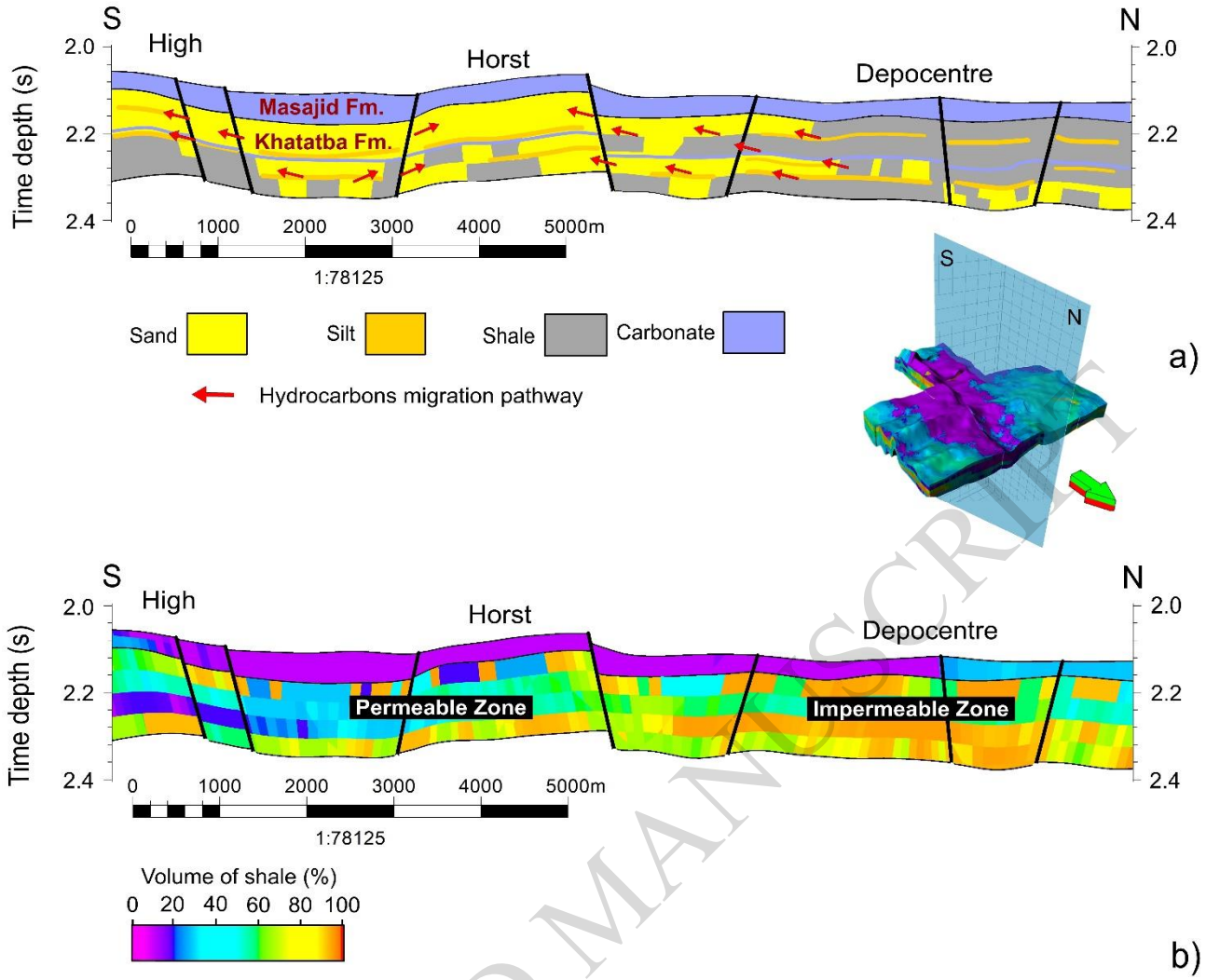

Fig. 26.

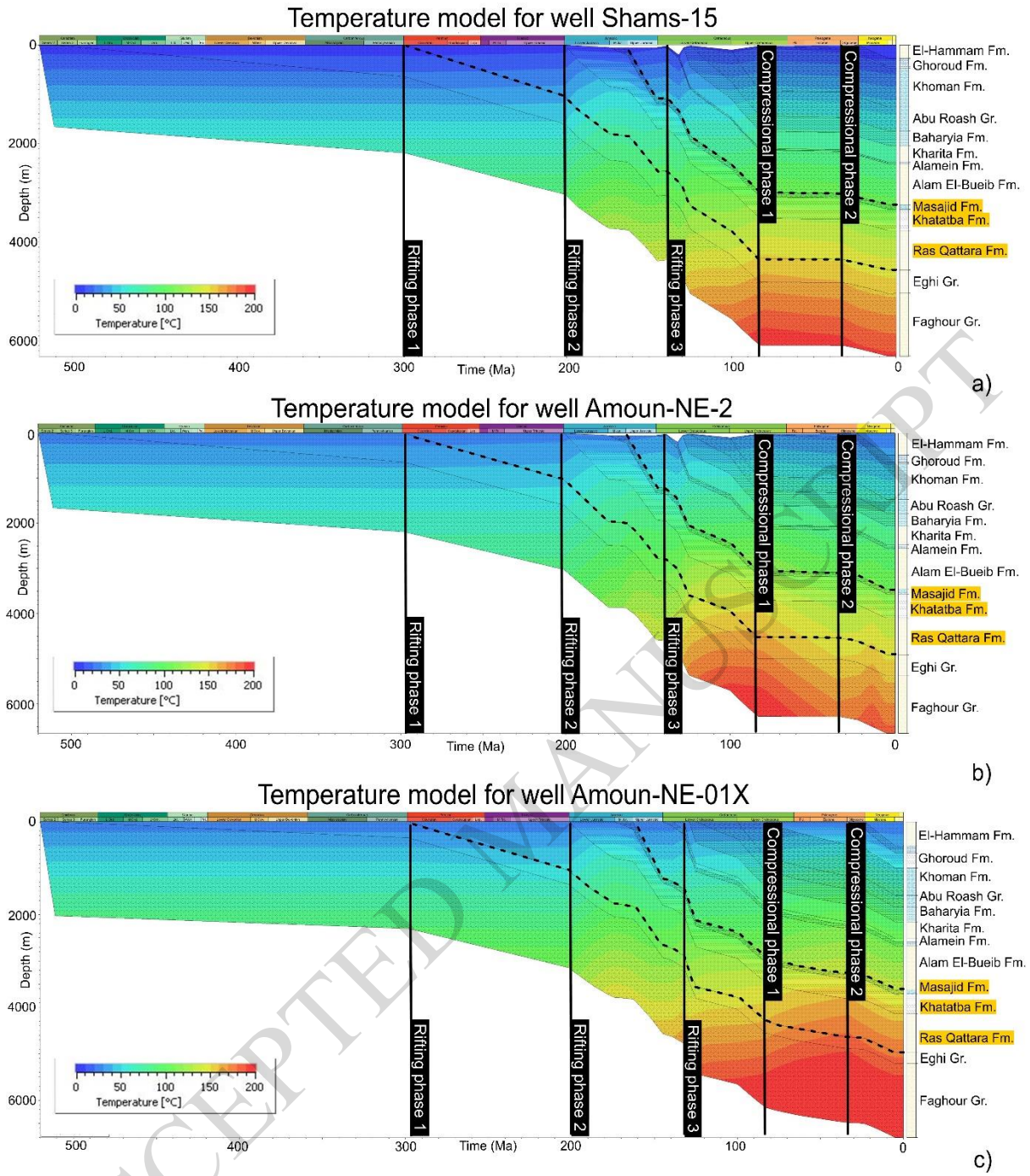

Fig. 27.

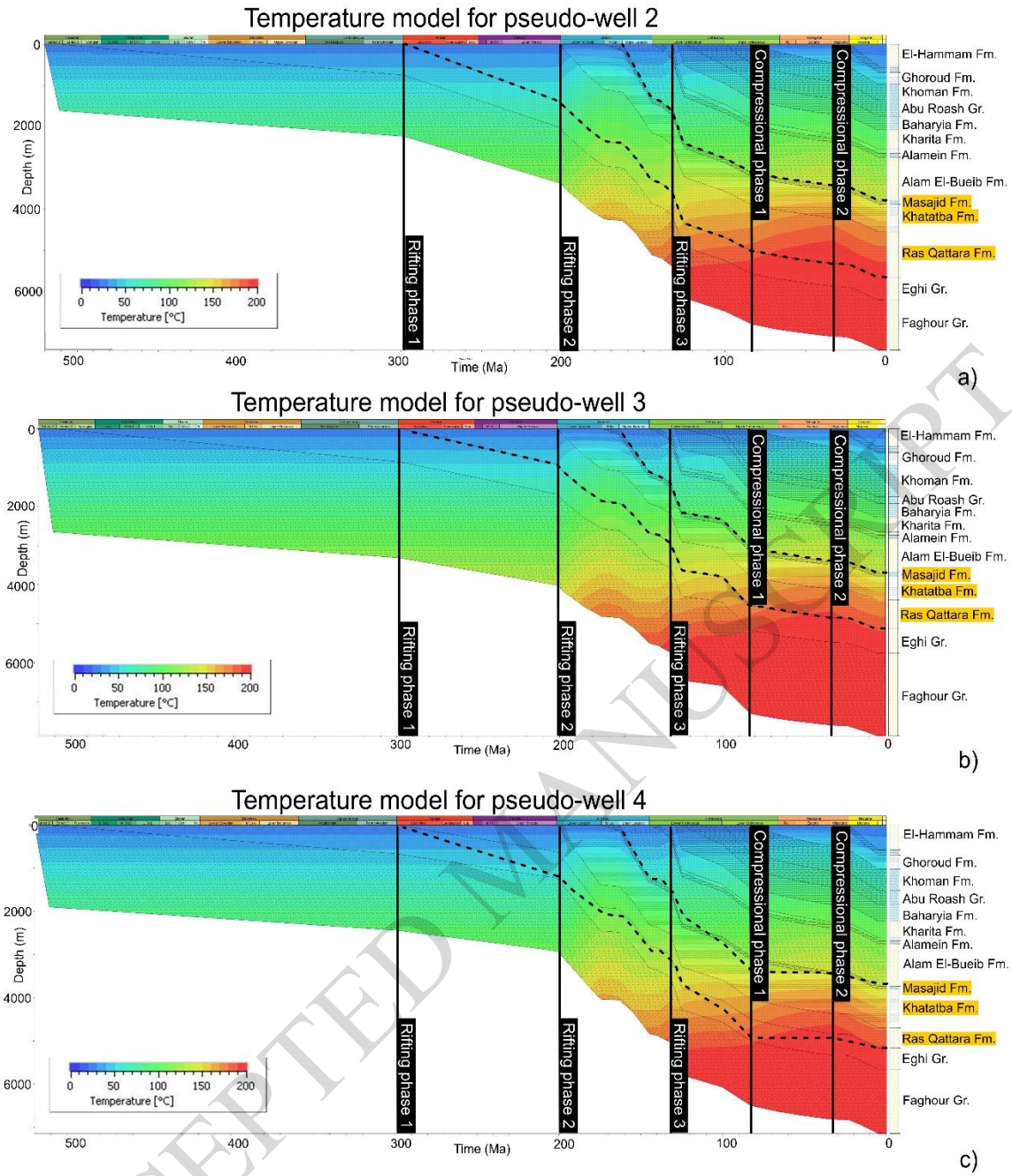

Fig. 28.

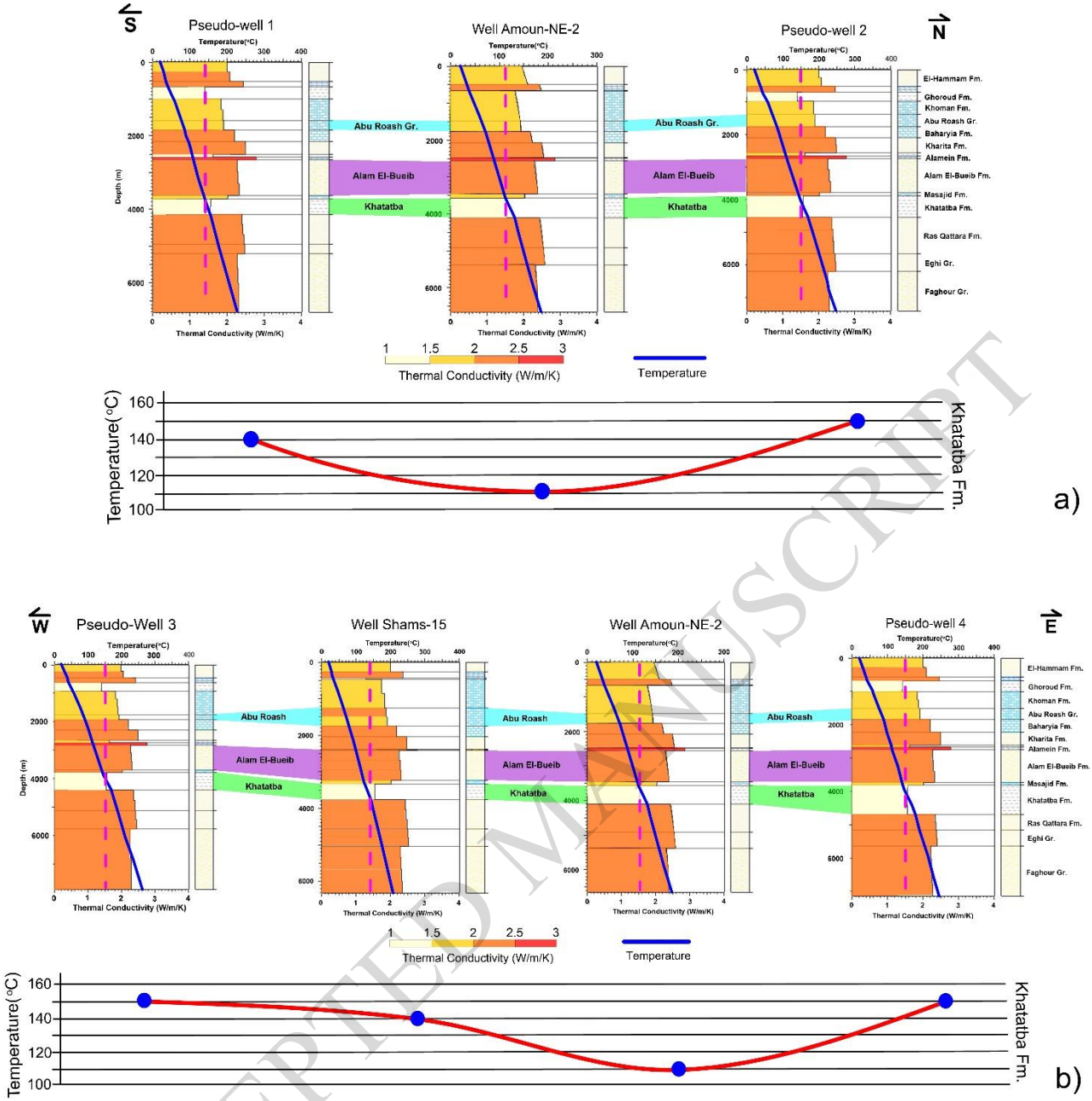

Fig. 29.

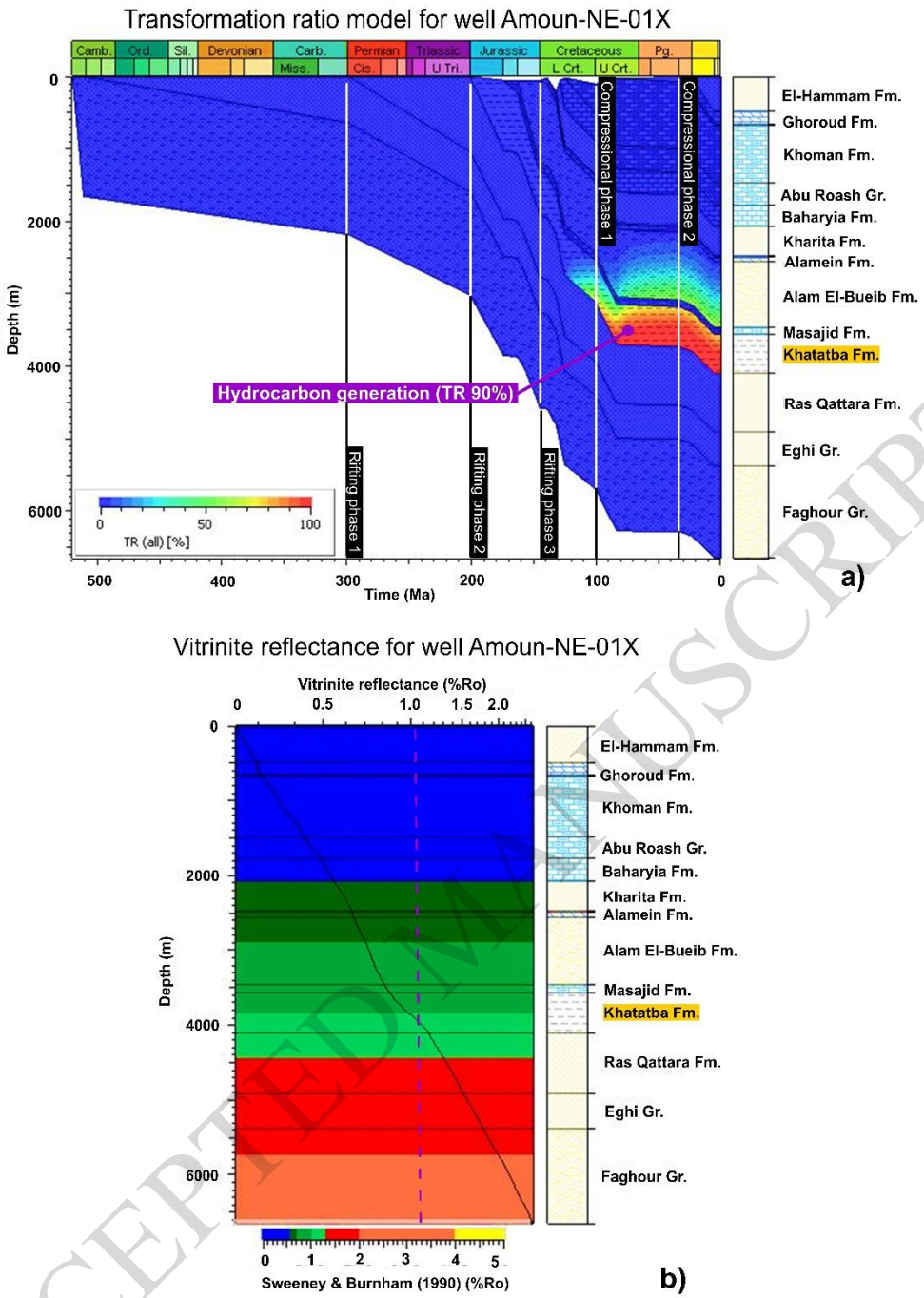

Fig. 30.

Table 1: Parameters used in the compilation of the PetroMod® burial and thermal models analysed in this work.

Initial lithospheric thickness	126 km
Initial crustal thickness	33 km
Water density	1030 kg m^{-3}
Average crustal density	2780 kg m^{-3}
Mantle density (0°C)	3330 kg cm^{-3}
Mantle potential temperature	1333°C
Thermal expansion coefficient	3.1x10^{-5} K^{-1}
Thermal diffusivity	8.0x10^{-7} m^2 s^{-1}
Mantle thermal conductivity	3.138 W m^{-1} K^{-1}
Crustal thermal conductivity	2.700 W m^{-1} K^{-1}
Age of syn-rift extension	Late Triassic-Early Jurassic to Early Cretaceous
Beta (β) factor	1.25
Basement lithology	Granitic rocks
Kinetics	Sweeney and Burnham (1990) – type II kerogen
TOC	3.91
HI	80

Table 2. Vitrinite reflectance measurements for the Upper and Lower Safa members as sampled in wells Amoun-NE-01X and Amoun-NE-2.

Lower Safa Formation (well Amoun-NE-01X)		Upper Safa Formation (well Amoun-NE-2)	
Depth (m)	Vitrinite reflectance (%)	Depth (m)	Vitrinite reflectance (%)
3,904	1	3,843	0.65
3,913	1.05	3,855	0.69
3,925	1.08	3,867	0.69
		3,880	0.78
		3,892	0.75
		3,910	0.78
		4,020	0.75
		4,102	0.78
		4,117	0.81

Table 3. Total organic carbon and Rock-Eval pyrolysis results for core samples acquired from the Upper Safa member (Middle Jurassic), well Amoun-NE-01X.

Depth (m)	TOC wt. %	S1 mg/g	S2 mg/g	S3 mg/g	T_{max}	HI	OI	S1/TOC	PI
3,773	3.91	0.14	3.13	1.07	462	80	27	4	0.04
3,825	1.31	0.10	1.23	0.84	453	94	64	8	0.08
3,895	1.55	0.10	1.39	0.70	454	90	45	6	0.07

Table 4. Total organic carbon and Rock-Eval pyrolysis results for core samples taken from the Ras Qattara Formation (Lower Jurassic), well Shams-15.

Depth (m)	TOC wt. %	S1 mg/g	S2 mg/g	S3 mg/g	T_{max}	HI	OI	S1/TOC	PI
4,045.6	0.14	0.03	0.08	0.16	429	56	113	21	0.27
4,049.8	0.09	0.02	0.08	0.27	430	88	297	22	0.20
4,063.8	0.13	0.03	0.06	0.13	384	48	104	24	0.33
4,094.6	0.09	0.03	0.06	0.09	413	69	103	34	0.33
4,099.2	0.12	0.04	0.06	0.19	405	49	156	33	0.40
4,102.3	0.12	0.04	0.06	0.14	426	49	115	33	0.40
4,109.9	0.07	0.03	0.05	0.19	433	71	268	42	0.38

Table 5. Medium-pressure liquid chromatography (MPLC) results for the Lower and Upper Safa members, well Amoun-NE-01X.

Fm.	Sample type	Sample weight	SAT weight	ARO weight	NSO Weight	ASPH weight	SAT %	ARO %	NSO %	ASPH %	Total recovery %
U. Safa	Oil	0.0731	0.0422	0.0180	0.0042	0.0002	85.50	11.65	2.72	0.13	100
L. Safa	Oil	0.0799	0.0514	0.0148	0.0020	0.0009	88.59	9.54	1.29	0.58	100

Table 6. Results of Reservoir Description Tool (RDT) tests ran for the Lower Safa member (Middle Jurassic), well Amoun-NE-01X.

Test no.	Depth (m)	Hydrostatic press.		Shut in press. (psi)	Temp. (ºF)	Volume (cc)	Mobility	Comments	Zone
		Before	After						
1	4,074.5	7021.0	7021.0	5724.6	267	50	0.602	Normal test	
2	4,073.6	7020.0	7020.0	5723.7	269	50	1.210	Normal test	
3	4,072.4	7019.0	7019.0	N/A	273	50	N/A	Tight	
4	4,071.2	7018.0	7017.0	5861.4	271	70	N/A	Not stabilized	
5	4,057.4	6995	6995	N/A	N/A	N/A	N/A	No seal	
6	4,056.5	6993	6993	N/A	267	N/A	N/A	No seal	
7	4,055.3	6990	6990	5691.3	271	60	0.115	Normal test	
8	4,053.8	6988	6988	5566.2	272	90	3.240	Normal test	
9	4,020.6	6933	6933	N/A	268	30	N/A	Tight	
10	4,020	6931	6931	N/A	269	40	N/A	Tight	
11	4,017.8	6929	6929	N/A	268	40	N/A	No seal	
12	4,011.1	6917	6917	6908.3	271	60	N/A	Super charged	
13	4,013.6	6916	6916	5753.4	271	70	17.000	Normal test	Z10
14	3,983.4	6871	6871	6772.4	268	70	N/A	Super charged	Z9
15	3,982.2	6869	6869	6220.7	270	80	N/A	Not stabilized	
16	3,937.7	6846	6846	5947.9	266	75	23.600	Normal test	Z8
17	3,937.1	6845	6845	N/A	269	656	N/A	Tight	Z8
18	3,934.3	6843	6843	6038.7	269	20	N/A	Super charged	Z8
19	3,923.3	6842	6842	5954.6	271	60	5.920	Normal test	Z7
20	3,903.2	6838	6838	5953.8	269	50	7.270	Normal test	

Table 7. Results of Reservoir Description Tool (RDT) tests ran for the Upper Safa member (Middle Jurassic), well Amoun-NE-01X.

Test no.	Depth (m)	Hydrostatic press.		Shut in press. (psi)	Temp. (F)	Volume (cc)	Mobility	Comments
		Before	After					
21	3,820	6603	6603	N/A	258	10	N/A	Tight
22	3,816	6598	6597	N/A	259	10	N/A	Tight
23	3,805.7	6580	6579	5182	258	50	3.320	Normal test
24	3,803.2	6575.0	6576.0	N/A	260	10	N/A	Tight
25	3,796.8	6565.0	6564.0	5262.6	259	60	12.400	Normal test
26	3,795.9	6563.0	6563.0	5260.9	261	80	92.900	Normal test
27	3,792.6	6561.0	6560.0	5260.8	261	50	10.300	Normal test
28	3,792.6	6558	6558	5258.6	261	100	52.200	Normal test
29	3,788.6	6552	6552	6399	260	40	N/A	Super charged
30	3,767.6	6518	6518	N/A	255	10	N/A	Tight
31	3,761.2	6508	6506	5259.7	257	100	33.000	Normal test

Table 8. Biogeochemical data for Jurassic shale intervals in the Shushan Basin.

Biogeochemical parameters	Upper Safa member (Middle Jurassic)	Ras Qattara Formation (Lower Jurassic)
TOC %	1.55 - 3.91 wt.% (very Good)	0.09 - 0.14 wt.% (poor)
Source potential (S1+S2)	1.33 - 3.27 mg HC /g rock (very good)	0.10 - 0.11 mg HC /g rock (poor)
Productivity index (S1/(S1+S2))	0.042 - 0.075 (low)	0.2 - 0.36 (high)
Maturity	Mature (gas window)	Immature (no HC generation capacity)
Origin	S2>S1 (native fluids)	
Migration index (S1/TOC)	4 - 42 (thermal maturation)	